Netherlands Journal of Geosciences

Original Article

Cite this article: Rimbaud E. Lapperre et al. Fault-zone hydraulic conductivity distribution in unconsolidated sediments: insights from a trench study across the Peel Boundary Fault Zone, the Netherlands. *Netherlands Journal of Geosciences*, Volume 105, e12686. https://doi.org/10.70712/NJG.v105.12686

Received: 19 April 2025
Revised: 18 April 2026
Accepted: 28 April 2026
Published: 25 June 2026

Keywords
anisotropy; fault hydrogeology; grain size distribution; permeability; rift system

Corresponding author:
Rimbaud (E.) Lapperre,
Email: r.e.lapperre@vu.nl

Supplementary material:
The supplementary material for this article can be found at https://doi.org/10.70712/NJG.v105.12686.

Fault-zone hydraulic conductivity distribution in unconsolidated sediments: insights from a trench study across the Peel Boundary Fault Zone, the Netherlands

Rimbaud E. Lapperre[1], Victor F. Bense[2], Cornelis Kasse[1], Jelle T. Buma[3], Ronald Harting[3] and Ronald T. van Balen[1,3]

[1]Department of Earth Sciences, VU University Amsterdam, Amsterdam, the Netherlands; [2]Wageningen University & Research, Wageningen, the Netherlands; [3]TNO – Geological Survey of the Netherlands, Utrecht, the Netherlands

Abstract

In the subsurface, the faults of the Peel Boundary Fault Zone, part of the Roer Valley Rift System in the Netherlands, Germany, and Belgium, often act as fault-parallel conduits and fault-perpendicular barriers for groundwater flow. However, our understanding of the conduit–barrier architecture of these faults remains limited. This study addresses this gap by presenting a detailed overview of the spatial variation in hydraulic conductivity and anisotropy, based on 161 collected samples, resulting in 150 measurements of saturated hydraulic conductivity (K_{sat}) and total porosity (P_{total}), and 151 measurements of median grain size (*GS*) from a trench site near Uden, the Netherlands. The results indicate that K_{sat} values across the fault range by almost four orders of magnitude, from 0.004 to 32.1 m day^{-1}. Within this range, the fault exhibits the lowest horizontal (0.01–3.6) and vertical (0.004–7.1) K_{sat} values. Compared to the fault, values in the foot-wall damage zone (horizontal: 1.4–22.6 and vertical: 0.08–18.4) are significantly higher for both orientations, whereas in the hanging-wall damage zone (horizontal: 2.0–22.7 and vertical: 1.8–9.5), all values are higher, but only the horizontal values reach statistical significance. These findings indicate that the conduit–barrier effect of faults in unconsolidated sediments extends to the near surface. Hydraulic conductivity largely correlates positively with median *GS* but shows little to no overall correlation with total porosity (P_{total}). This trench study also reveals that the near-surface conduit–barrier architecture and hydraulic conductivity distribution is likely to evolve over geological timescales due to ongoing hydrogeological processes and fault activity. Such insight has the potential to contribute to future approaches for protecting and restoring fault-related seepage areas known as 'wijstgronden'.

Introduction

Faults significantly impact groundwater flow in both unconsolidated and lithified sedimentary rocks (Antonellini & Aydin 1994; Babiker & Gudmundsson, 2004; Bense et al., 2003a, 2003b; Bense & Person, 2006; Bense & Van Balen, 2004; Scibek, 2020; Sheldon et al., 2023). They often act as poorly permeable zones, forming lateral barriers due to reduced permeability perpendicular to the fault zone (e.g. Caine et al., 1996; Scibek et al., 2016; Lapperre et al., 2019, 2022). Simultaneously, enhanced along-fault permeability can make faults serve as preferential pathways (conduits) for groundwater flow along the fault (Anderson & Bakker 2008; Bense & Person, 2006; Bense et al., 2013).

In general, the conduit–barrier architecture of faults is inferred through various methods, including hydrogeological field studies (Bense et al., 2003a; Kettermann et al., 2016; Lapperre et al., 2022), modelling (Anderson & Bakker, 2008; Bakker, 2006; Bense & Person, 2006; Haneberg, 1995), the simultaneous interpretation of multiple fault characteristics using triangular diagrams (Aubert et al., 2021), analyses of hydrothermal characteristics (Bense et al., 2008, 2013), and assessments of groundwater composition (Broers et al., 2021; Cook et al., 2022; Gumm et al., 2016). However, these approaches primarily provide information on regional scales and lack detailed field analyses of fault-permeability distribution in unconsolidated sediments. Given the scarcity of field measurements, the inferred fault-permeability values are mainly applicable to regional studies and are insufficient for explaining near-fault hydrogeological phenomena such as fault-related seepage. Moreover, the deduced values frequently tend to either over- or underestimate actual fault-permeability values (Lapperre et al., 2022).

This study, based on an extensive set of field samples, examines the distribution of fault-zone permeability perpendicular to (horizontal) and along (vertical) the fault in an unconsolidated lithological setting. In this context, permeability refers more broadly to the intrinsic capacity of the porous subsurface to transmit groundwater, while saturated hydraulic conductivity is used to quantify permeability through measurements. The findings are compared with larger-scale values inferred from regional studies. This analysis enhances our understanding of cross-fault groundwater-level steps (Lapperre et al., 2022), the upward seepage of groundwater and its associated higher groundwater temperatures on the upstream (foot-wall) side of faults (Bense, 2004; Bense & Kooi, 2004; Bense et al., 2008), iron (hydr)oxide precipitation on the downstream (hanging-wall) side, and the occurrence of sand volcanoes in cross-fault watercourses. The broader implications of these findings extend to other rift systems with similar unconsolidated (soft) sedimentary conditions.

In late 2018, a trench was excavated west of the village of Uden in the Netherlands to study near-fault hydrogeology and to collect undisturbed field samples. This trench location is situated across one of the faults of the Peel Boundary Fault Zone (PBFZ) (Figure 1) and is characterized by the presence of fault-related topographic offset of ~1–2 m, seepage of iron-rich groundwater, a shallow groundwater table on the foot wall, and an average cross-fault groundwater-level step of almost 2 m (Lapperre et al., 2025). Undisturbed field samples were collected from this trench to prepare laboratory samples for measuring horizontal and vertical saturated hydraulic conductivity (K_{sat}), total porosity (P_{total}), and grain size (GS) distribution.

A better understanding of permeability distribution in unconsolidated (soft) sediments could contribute to the future development of effective restoration measures for fault-related seepage areas known as 'wijstgronden' and to the refinement of groundwater models by incorporating field-based values, their directional variability (anisotropy), and their variation with distance from the fault in deformed (fault-affected) and undeformed (non-affected) sediments.

Setting

The Roer Valley Rift System

The Roer Valley Rift System (RVRS) is a seismically active rift system in the southern part of the Netherlands, extending into adjoining areas in Belgium and Germany (Michon et al., 2003; Michon & Van Balen, 2005; Van Balen et al., 2005, 2019, 2021, 2024). The central part of this rift system, the Roer Valley Graben (RVG), is bounded by the Feldbiss Fault Zone (FFZ) to the southwest and the PBFZ to the northeast. The PBFZ delineates the boundary between the uplifting Peel Block and the subsiding Roer Valley Graben (Figure 2a). The current faulting phase of this rift system began at the Oligocene–Miocene boundary and is ongoing (Michon et al., 2003; Michon & Van Balen, 2005; Van Balen et al., 2005). The central Roer Valley Graben is subsiding substantially faster than the adjoining Campine Block and Peel Block in this region (Houtgast & Van Balen, 2000; Van Balen et al., 2005). The ongoing fault activity in this part of the rift system (Figure 2a) is evidenced both by large, surface rupturing earthquakes during the Late Glacial (Van Balen et al., 2019) as well as smaller, non-surface rupturing earthquakes in modern times

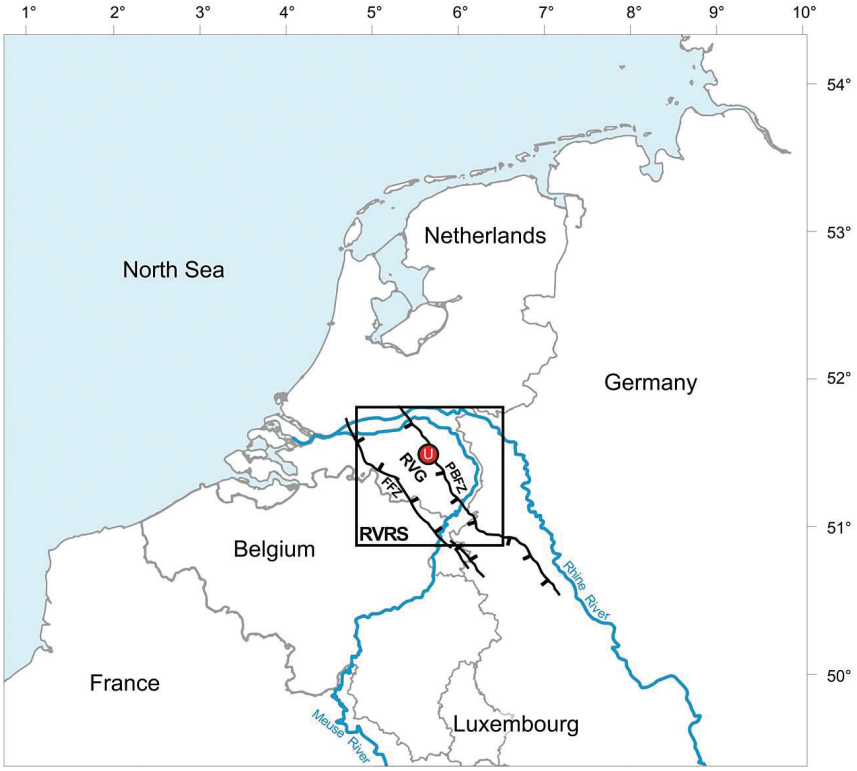

Figure 1. The Roer Valley Rift System (RVRS) consists of the Roer Valley Graben (RVG), flanked by the Peel Boundary Fault Zone (PBFZ) to the northeast and the Feldbiss Fault Zone (FFZ) to the southwest. The red U marks the location of the Uden trench site. The map uses a geographic coordinate system (latitude-longitude). Modified from van Balen et al. (2019) and Lapperre et al. (2022).

https://doi.org/10.70712/NJG.v105.12686

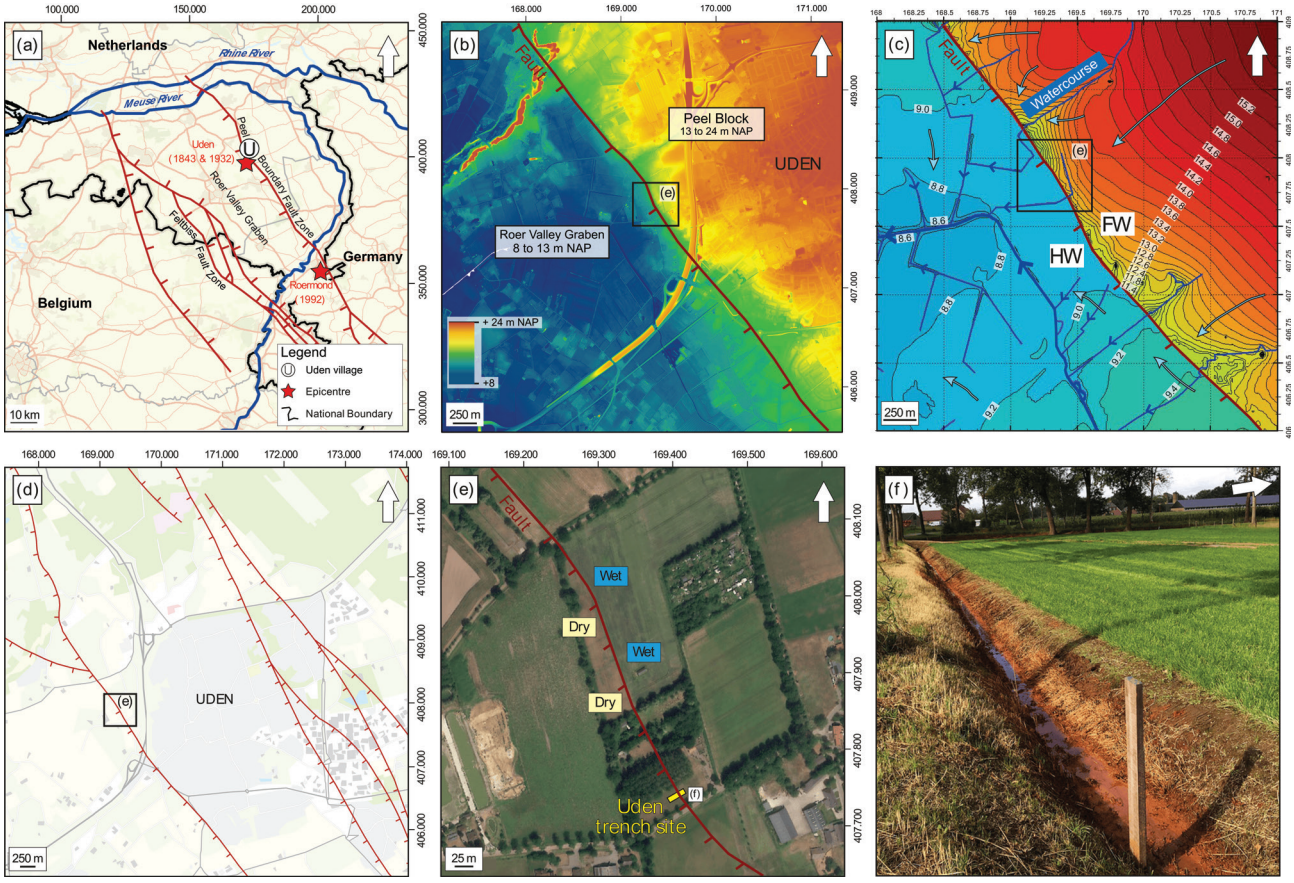

Figure 2. Location of the study area, Uden trench site and overview figures. Coordinate system is the Dutch National Grid (RD). (a) The village of Uden (U) along with the epicentres of earthquakes near Uden (1843 and 1932) and near Roermond (1992) marked by the red stars; (b) Digital elevation model (Actueel Hoogtebestand Nederland [AHN], 2022) indicating the location of the fault; (c) Overview of the phreatic groundwater-level isohypses pattern (m NAP), assuming an impermeable fault, represented by a hydraulic resistance (c-value) of 1 *10^7 days. The variation in groundwater-flow direction (blue arrows) is inferred from the calibrated steady-state regional groundwater model GRAM3.0 from Water Authority Aa en Maas; (d) Multiple faults extending in a northwest–southeast direction, part of the Peel Boundary Fault Zone; (e) Abrupt soil moisture contrast visible on satellite imagery (NSO, 2023), from wet (dark coloured surface, groundwater at or near the surface) to dry (light coloured surface, groundwater sloping away from the fault to depths of several metres), and the location of the Uden trench site; and (f) One of the trench-adjacent watercourses, oriented perpendicular to the fault, displaying a distinctive orange-to-brown discolouration due to iron (hydr)oxide precipitation. The locations of (e) is indicated in (b), (c) and (d), and the location of (f) is indicated in (e).

(KNMI, 2024; near Uden in 1843, ML 4.8, in 1932, ML 5.0, and near Roermond in 1992, ML 5.8). The larger events have resulted in the formation of fault scarps in the landscape. Due to regional variations in displacement rates and the effects of erosion and/or blanketing by younger sedimentary deposits, the scarps exhibit height differences mostly in the range of 1–3 m (Figure 2b).

The subsurface lithology of the Uden region is characterized by unconsolidated, mostly sandy sediments of Pleistocene age. The coarser sediments, primarily deposited by the Meuse River, are overlain by mostly fine-grained local-fluvial, lacustrine, and aeolian sands (Schokker et al., 2005). On elevated areas, such as the Peel Block, the coarser sediments are present at depths of only a few metres, covered by relatively thin layers (1–3 m) of fine-grained deposits. Within the subsiding RVG, coarser sediments are found at greater depths, overlain by fine sediments with a maximum thickness of ~35 m (Schokker et al., 2005; Westerhoff et al., 2008). At fault locations, lithologies with different *GS* and associated contrasting permeabilities are juxtaposed. The displacement of the top of the coarser sediments at fault locations ranges from ~1–2 to ~10 m.

The geological and morphological setting significantly influences hydrology (Figure 2c), with regional surface and groundwater flow in permeable unconsolidated sandy sediments being largely topography-driven (Lapperre et al., 2019). At fault locations, where lateral (~horizontal) groundwater flow is often impeded, and along-fault (~vertical) flow is enhanced, wet areas (locally known as 'wijstgronden') with shallow groundwater tables occur in the elevated foot walls. Deeper groundwater tables are found in the lower-lying hanging walls. These abrupt-level changes are identified as cross-fault groundwater-level steps. Additionally, surface-water runoff through watercourses follows topography, draining elevated landscape parts (foot walls) and infiltrating lower-lying areas (hanging walls).

Local-scale hydrogeology

Around Uden, multiple northwest–southeast-oriented faults associated with the PBFZ (Figure 2) are present, with the Uden trench site situated at the westernmost of these faults (Figure 2d). The fault locations are indicated in the Digital Geological Model of the Netherlands DGM v2.2 (Hummelman et al., 2019a) and can often be identified in the field through fault-related phenomena, such as the presence of scarps, sudden changes in lateral soil moisture (Figure 2e), and crop marks, demarcating cross-fault groundwater-level steps. When the fault-related seepage is rich in iron (hydr)oxide, watercourses turn orange upon oxidation

https://doi.org/10.70712/NJG.v105.12686

(Figure 2f), also serving as a marker for the nearby presence of faults. The mean cross-fault groundwater-level step at the trench location, based on groundwater-level monitoring (2018–2023) in a cross-fault piezometer array, is 1.83 m (Lapperre et al., 2025). An abrupt shift in the groundwater table is also observed at other fault locations, resulting from a reduced permeability within the fault zone (Lapperre et al., 2019).

A cross section of the subsurface at the trench location (Figure 3a), composed from the national hydrogeological model REGIS II v2.2.2 (Hummelman et al., 2019b) and the geological model GeoTOP v1.6 (Stafleu et al., 2023), reveals the fault's position and the layering of unconsolidated sandy to gravelly lithologies. These lithologies (Figure 3b) are grouped into the Boxtel Formation, consisting mainly of finer-grained local fluvial and aeolian deposits, and the Beegden Formation, comprising coarser-grained Meuse River deposits. These formations overly deeper fluvial and marine deposits. Horizontal saturated hydraulic conductivities (K_h) inferred from the regional-scale REGIS II model (Hummelman et al., 2019b) range from 5 to 10 m day^{-1} for finer-grained deposits (105–300 µm) and from 50 to 100 m day^{-1} for coarser-grained deposits (210–2,000 µm) (Figure 3b). Vertical saturated hydraulic conductivities (K_v) are not included for these sandy hydrogeological units, nor are hydraulic properties of fault zones.

Trench scale

Building on the previously described regional and local setting, the trench site at Uden is examined to assess fault-zone hydrogeology more closely. The following description presents geological and hydrogeological information previously documented by Van Balen et al. (2024), providing context for the analyses presented in this study at the trench scale.

The Uden trench, located across one of the faults of the PBFZ, measures 25 m in length, 8 m in width, and 2.5 m in depth. In both trench walls, the fault, numerous adjoining minor faults, different sedimentary deposits and their stratification, a man-made channel, an unconformity and iron (hydr)oxide precipitation are present (Figure 4a). The deposits exposed in the northwestern trench wall are grouped into five geological units (1–5), covered by a dark-coloured plough layer rich in organic matter (labelled PL in Figure 4b). The detailed geological stratigraphy is provided by Van Balen et al. (2024), with a summary presented below.

Unit 1 is solely exposed in a pit on the foot wall of the trench floor (Figure 4b). This lowermost unit consists of grey, poorly sorted, medium to coarse sand with gravel, deposited by the Meuse River, forming the Beegden Formation (Schokker et al., 2007). Overlying Unit 1, Units 2–4 primarily comprise finer-grained sandy deposits. These finer grained deposits originated from local fluvial and aeolian sedimentation processes and are part of the Boxtel Formation (Schokker et al., 2007).

Unit 2 is present in the trench wall on the foot wall and comprises a ~1-m-thick deposit, largely lacking stratification (Figure 4b). This deposit includes light-grey loamy fine sand, loamy sand, fine sand, sand with small gravels, and gravelly sand. Close to, and within, the fault, remnants of decayed roots are found on the foot wall. These root remnants, characterized by a black colour and a distinctive comet shape, confirm the

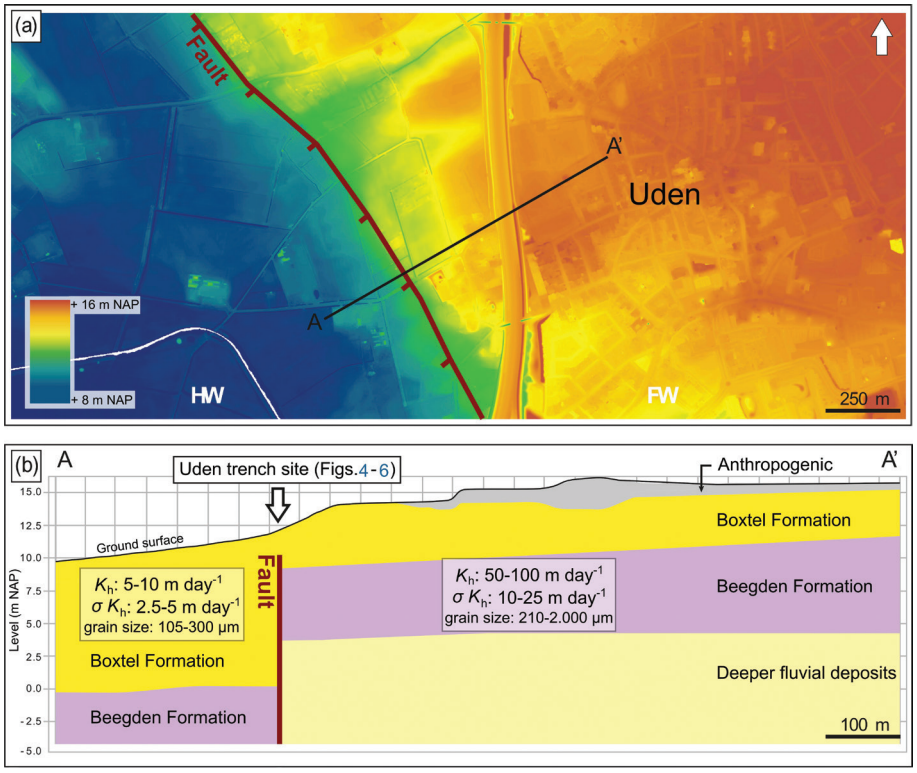

Figure 3. (a) Location of cross-section AA1 projected onto the digital elevation model (Actueel Hoogtebestand Nederland [AHN], 2022). The ground-surface levels range from ~10 m NAP on the hanging wall (HW) to ~15 m NAP on the foot wall (FW), with the steepest topographic offset occurring around the trench site and; (b) Hydrogeological cross section of the subsurface indicating the location of the Uden trench site and exhibiting juxtaposed layering. Additionally, these formations display contrasting horizontal conductivity values (K_h) with different associated uncertainty ranges (σK_h). This model-based, large-scale cross-section is compiled from the schematised national subsurface hydrogeological model (Hummelman et al., 2019a) and the geological model GeoTOP v1.6 (Stafleu et al., 2023), accessed via the national subsurface database DINOloket (2024).

https://doi.org/10.70712/NJG.v105.12686

migration of decayed particulate organic matter by groundwater flow in an oblique, upward direction towards the fault (Lapperre et al., 2025). On the hanging wall, Unit 2 was exposed in a pit on the trench floor, where it is composed of grey loamy fine sand (interpreted as cryoturbated) and dark-brown, humic gravelly sand.

Unit 3 comprises deposits fining upwards from gravelly coarse sand to fine sand and loamy fine sand. It is present on both the foot wall and the hanging wall in the exposed trench walls (Figure 4b). The finer upper part of Unit 3 can be interpreted as aeolian coversands, belonging to the Older Coversand II unit (e.g. Kasse et al., 2007; Vandenberghe et al., 2013). Remnants of decayed roots, similar to those in Unit 2 and including the comet shape, are also found in Unit 3.

Unit 4 is exposed exclusively on the hanging wall and comprises sand and loamy sand deposits (Figure 4b). These deposits lack gravel. Given their overall characteristics, this unit can be interpreted as aeolian coversands, corresponding to the Younger Coversand I and II series (e.g. Kasse et al., 2007; Vandenberghe et al., 2013).

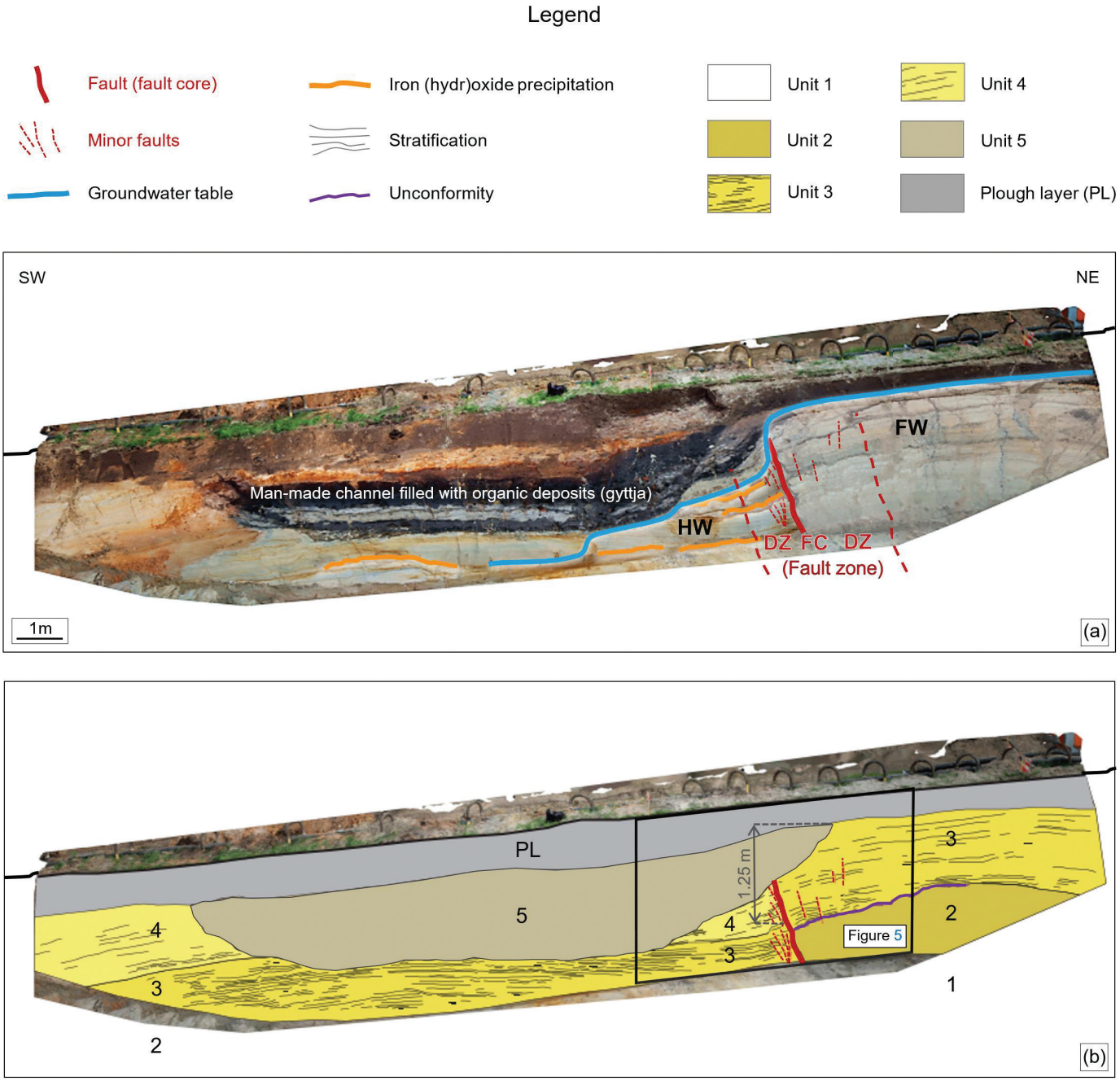

Figure 4. Position of the fault zone, fault core (FC) and damage zones (DZ) in the northwestern trench wall at the Uden site (after Van Balen et al., 2024). (a) A subvertical fault (fault core) separates the foot wall (FW) with a shallow groundwater table, from the hanging wall (HW), which features a deeper groundwater table sloping away from the fault, where FW and HW refer to larger-scale fault structures. This groundwater-level contrast is inferred from site-specific level measurements between 2018 and 2023 (Lapperre et al., 2025). Minor faults and iron (hydr)oxide precipitation occur near the fault, the latter occurring in the HW under oxic conditions due to the lowered groundwater table. A man-made channel in the HW is filled with organic deposits (gyttja); and (b) locations of Units 1–3 and the erosional unconformity in the FW, and Units 2–5 in the HW. The location of Figure 5 is also indicated.

https://doi.org/10.70712/NJG.v105.12686

Unit 5 primarily comprises organic deposits (gyttja) interspersed with a thin layer of fine sand. It is interpreted as the infill of a man-made channel with scooping traces at its base (Figure 4a). An archaeological inventory conducted by Hiddink (2019) disclosed artifacts such as pottery, a shoe sole, and iron slag within this unit. Radiocarbon dating results from Hiddink's study, along with pollen analyses by Van der Woude and Van Leeuwen (2020), suggest a (Late) Medieval origin. The channel likely served as either a moat or a water storage facility, possibly associated with a watermill.

Fault zone

The fault zone is ~3 m wide and comprises the fault (fault core) and the adjoining damage zones (Figures 4a and 5a). On the foot wall, the damage zone reaches a maximum width of ~2 m, while on the hanging wall, it is ~1 m wide. Both damage zones exhibit numerous minor faults each with a throw of a few centimetres. The fault itself (fault core) appears as a sharply delineated 3–15 cm wide subvertical fault core, and reveals a much larger displacement. According to Van Balen et al. (2024), the total fault throw at the top of Unit 3 is ~1.25 m (Figure 4b), and argues that it is the result from an abrupt displacement that represents a surface-rupturing earthquake with a magnitude of ~Mw 7. The numerous minor faults in the damage zones are attributed (Van Balen et al., 2024) to a Holocene trans-tensional event, characterized by smaller displacements and earthquake magnitudes, but still involving surface rupturing. Consequently, all fault displacements at the Uden trench site are attributed to seismic events.

According to Lapperre et al. (2025), thin-section microscope analysis shows that within the fault core and the flanking minor faults, elongated sand grains have rotated into a fault-parallel direction, largely perpendicular to the prevailing lateral groundwater flow. This rotation, initiated by fault displacement, is interpreted as the trigger for the subsequent precipitation of iron (hydr)oxides on the hanging wall and the along-fault accumulation of interporous fines (very fine sediments and organic matter) on the foot wall. These linked hydrogeological processes (Figure 5) have modified fault-zone permeability distribution (Lapperre et al., 2025).

Methods

Locating the fault

To determine the trench location, the fault position was identified using geological and geomorphological data, including DGM v2.2 and REGIS II v2.2 (DINOloket, 2018), elevation data (AHN, 2018), and satellite imagery (NSO, 2018) indicating soil moisture changes and crop marks. The fault position and trench boundaries were subsequently verified using manual auger drilling. Further details are provided by Van Balen et al. (2024) and Lapperre et al. (2025).

Sampling strategy

A total of 37 sediment samples (DL1–DL32, DL33A/B, and DL34–36) were collected from the northwestern and southeastern trench walls, as well as the trench floor, during phases of intermittent enlargement and deepening of the trench. The sample locations, orientations, and field codes are indicated in Figure 6. To analyse hydraulic conductivity, porosity, and grain-size distribution across the fault, samples were taken from specific trench locations reflecting observed differences in lithology, tectonic setting, and locations where fault-related hydrogeological processes with the potential to affect permeability were observed (Figure 5). Data clustering was then performed from the foot wall to the hanging wall (Figure 6), aligned with the groundwater flow direction. Consequently, five sampling sections (1–5) were designated, with specific details provided in Table 1. Unit 1, attributed to the Beegden Formation, is located below the trench floor and therefore falls outside the sampling interval and therefore is not sampled.

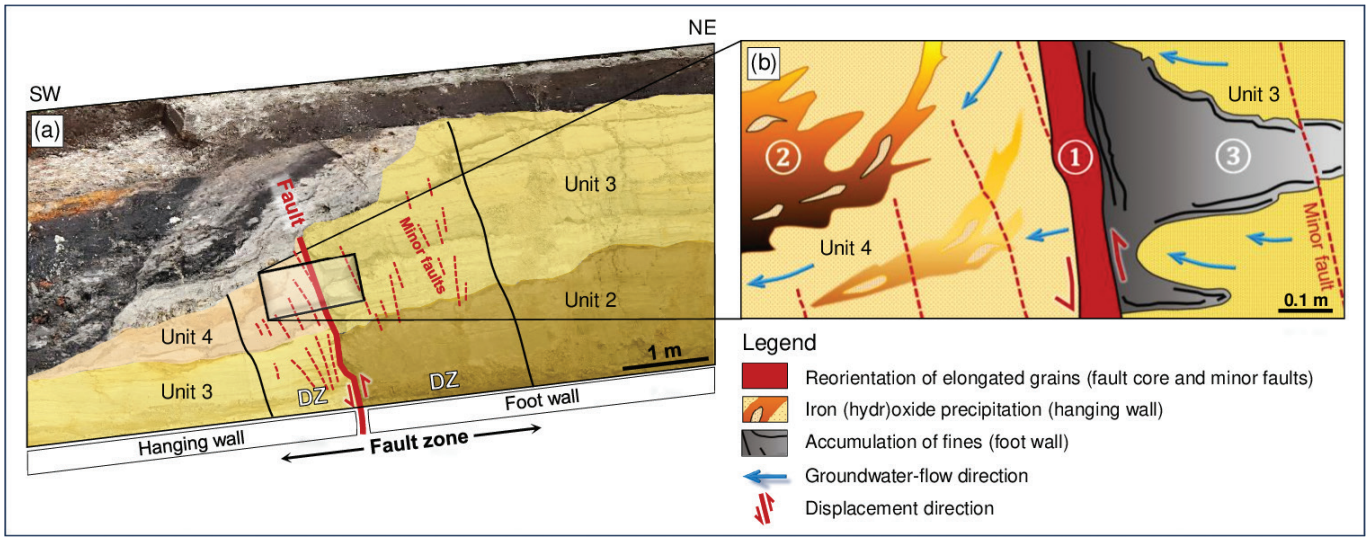

Figure 5. (a) Juxtaposed layering of unconsolidated sediments, grouped into Units 2–4, along the subvertical fault in the northwestern trench wall at the Uden site (after Van Balen et al., 2024). The ~3-m wide damage zone (DZ), ~2 m on the foot wall and ~1 m on the hanging wall, exhibits numerous minor faults; and (b) Schematised section of the fault and flanking parts of the damage zone, illustrating the order and location of the three (①–③) hydrogeological processes that have affected fault-zone permeability distribution in Units 3 and 4. The groundwater-flow direction (blue arrows) is inferred from site-specific level measurements (2018–2023) by Lapperre et al. (2025) and the red arrows indicate the displacement direction at the fault core.

https://doi.org/10.70712/NJG.v105.12686

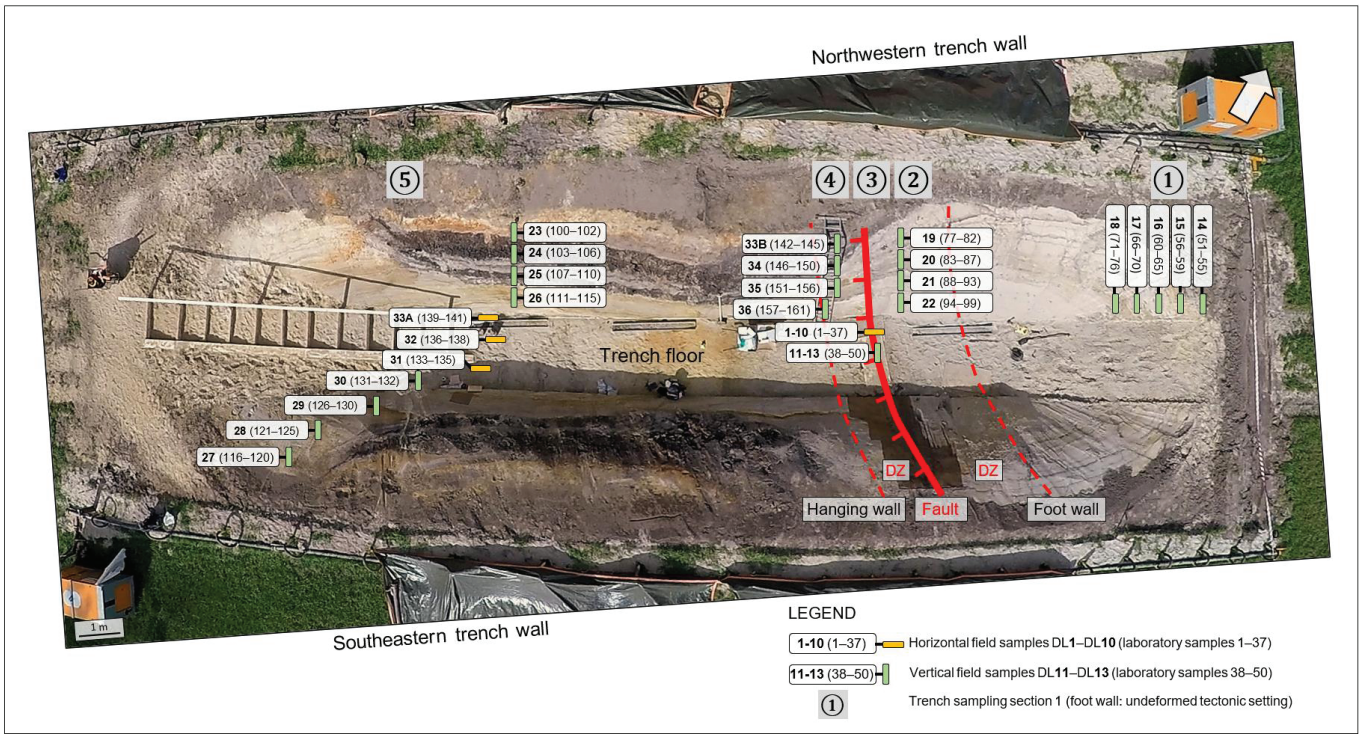

Figure 6. Aerial view from the Uden site showing the position of the fault and adjoining damage zones (DZ) on the foot wall and hanging wall. The location of the 37 sediment samples and resulting 161 laboratory samples is also indicated. Field sampling and data clustering occurred along the groundwater flow direction towards the fault: in the undeformed foot wall (Section 1), the deformed fault zone covering the fault and damage zones (Sections 2–4) and the undeformed hanging wall (Section 5). The fault (Section 3) is defined as the subvertical zone where multiple fault-related hydrogeological processes have affected permeability distribution (Lapperre et al., 2025).

Table 1. Details of trench sampling Sections 1–5 (Figure 6), including setting, sample coding, and conductivity distribution.

Sampling section	Tectonic position		Tectonic setting	Sedimentary setting[a]	Field samples	Laboratory samples[b]	Hydraulic conductivity samples (Table 2; Figure 8)	
(number)	(trench location)		(–)	(unit)	(code)	(code)	(# horizontal)	(# vertical)
1	Foot wall		Undeformed	2–3	DL14–DL18	51–76	13	13
2	Foot wall (DZ)[c]	Fault zone	Deformed	2–3	DL19–DL22	77–99	19	17
3	Fault[d]		Deformed	2–3	DL1–DL13	1–50	21	15
4	Hanging wall (DZ)		Deformed	3–5	DL33B–DL36	142–161	9	7
5	Hanging wall		Undeformed	3–4	DL23–DL33A	100–141	20	16
Total					37	161	82	68

[a]Sedimentary setting at trench level, following unit interpretation, is shown in Figure 4; [b]Attribution of each laboratory sample to the corresponding trench sampling section is shown in Appendix 1; [c]Damage Zone; [d]Defined as the subvertical zone where multiple fault-related hydrogeological processes have affected permeability distribution (Figure 5).

Most samples comprised a ~0.6-m-long PVC tube (Figure 7) with an internal diameter of 0.1 m, providing a sample volume of up to 4.71 L. All field samples were carefully and evenly driven into the exposed unconsolidated sediments, either horizontally (perpendicular to the fault) or vertically (parallel to the fault). Field samples DL2–DL4, DL13, and DL30–DL33A have reduced lengths due to the presence of coarse gravel, iron (hydr)oxide precipitation, or both, but still contain sufficient sediment volume for laboratory preparation.

Saturated hydraulic conductivity

A four-step approach was conducted to measure the saturated hydraulic conductivity, K_{sat} (m day^{-1}). In the first step, all field samples (Figure 7a) were opened lengthwise into a thicker (7 cm) and thinner (3 cm) part. The thinner part was used for describing and photographing the sediments and their structures (Figure 7b), while the thicker part was preserved for preparing the conductivity samples. In step 2, the number of samples, their positions, and sampling orientations (Figure 7c) were determined based on variations in lithologies and sedimentary structures. This resulted in the collection of 161 laboratory samples, taking into account specific hydrogeological characteristics potentially affecting permeability, such as the accumulation of fines, precipitation of iron (hydr)oxides, and the presence of coarser sediments. During step 3, the appropriate analysis method to measure K_{sat} was established. Samples with a volume of 100 mL (Figure 7d) and an expected conductivity of at least 0.01 m day^{-1} were measured twice

https://doi.org/10.70712/NJG.v105.12686

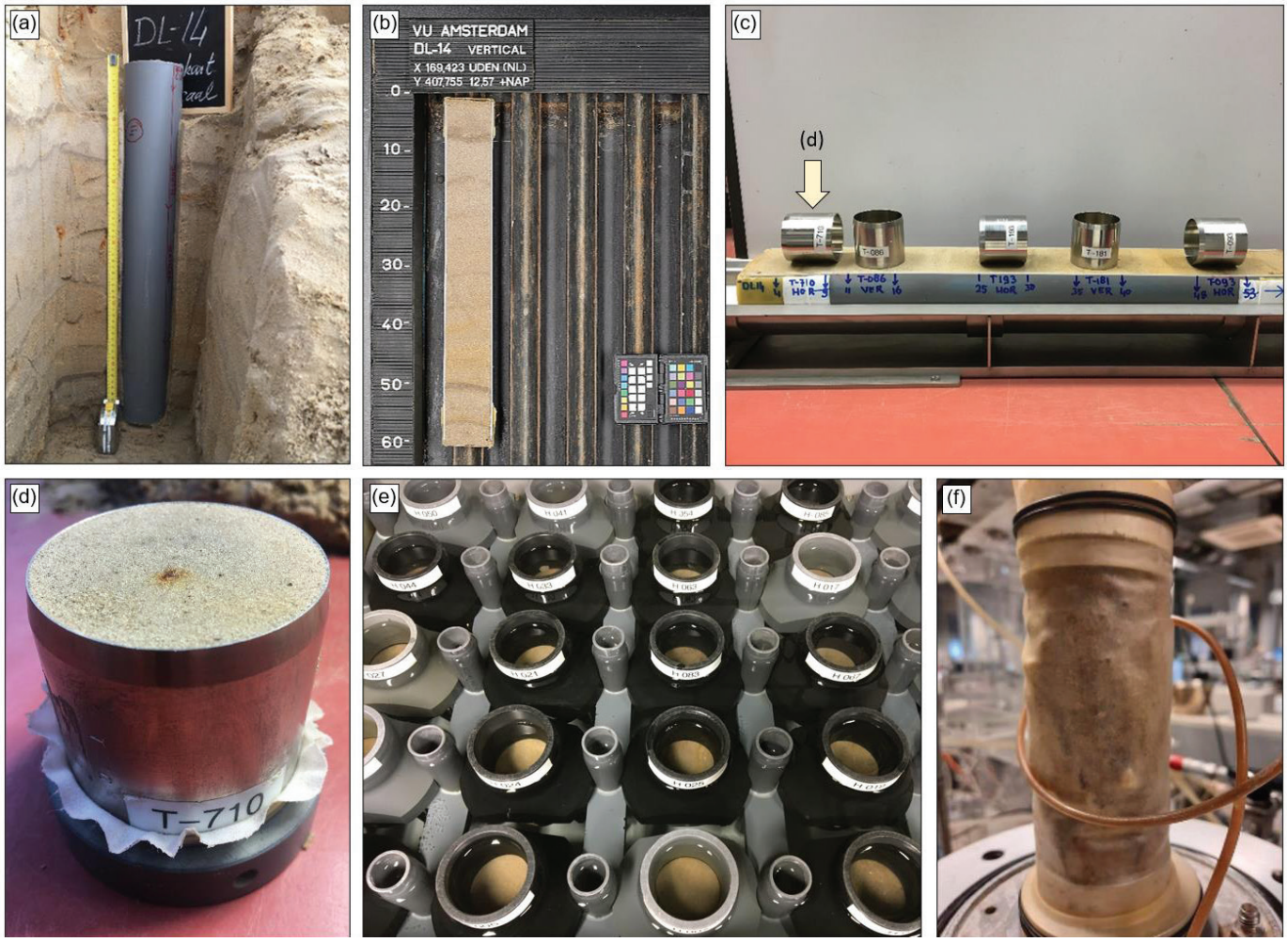

Figure 7. Overview of the workflow from field sample to saturated hydraulic conductivity value K_{sat} (m day^{-1}). (a) Vertical field sediment sample DL14 (4.71 L) in undeformed lithologies on the foot wall part of Section 1 (Figure 6 and Table 1); (b) Exposed lithologies after longitudinal opening of DL14; (c) Sampling strategy, including paired sampling, for saturated hydraulic conductivity measurements in the horizontal and vertical direction; (d) A fully prepared 100 mL laboratory sample, number 51 (labelled T-710), was collected parallel (lengthwise) to the vertical field sampling orientation, indicating a vertical saturated hydraulic conductivity value reflecting field conditions; (e) top view of the permeameter with 100 mL samples submerged in distilled water awaiting measurement using the falling-head method; and (f) Laboratory sample 10 with expected low permeability during triaxial testing. The position and sampling orientation of (d) are indicated in (c).

using a permeameter (Eijkelkamp, 2022), modified by TNO – Geological Survey of the Netherlands. The modification allows full saturation of the samples with degassed water to remove entrapped air, and employs highly accurate laser water-level measurements.

The final average saturated hydraulic conductivity was calculated when the results from the falling-head measurements (Figure 7e) for a single sample were consistent within a 10% range. A total of 153 samples were measured using this method at the TNO Permeability Laboratory (Buma & De Heer, 2024). The remaining eight samples, with an expected saturated conductivity below 0.01 m day^{-1}, were measured using triaxial testing (Figure 7f) for stratified lithologies (two samples) and modified oedometer testing for homogeneous lithologies (six samples). Both testing methods for low-permeability samples (NEN-EN-ISO 17892-11, 2019) were conducted at the geotechnical laboratory of Deltares (Delft, the Netherlands). Finally (step 4), all measurements were converted to standard K_{sat} values, expressed in m day^{-1} at 10°C, by correcting for water viscosity (Eijkelkamp, 2022). Due to one failed permeability measurement (sample 150) and 10 measurements originating from the man-made channel with organic deposits (samples 100–105 and 142–145), a total of 150 saturated hydraulic conductivity measurements are available for the analysis of horizontal and vertical permeability distribution across the fault (Table 1). These channel-derived samples were initially collected because they are located close to the fault. However, subsequent archaeological interpretation indicated that they represent a man-made feature. They were therefore excluded from further analysis. Details of each laboratory sample and its attribution to the corresponding trench section are presented in Appendix 1.

Total porosity

The permeability samples were also tested for total porosity by calculating the weight loss between a fully saturated sample and a sample oven-dried at 105°C for 24 hours, with the results expressed as a percentage (%). A total of 153 porosity measurements were conducted at the TNO Permeability Laboratory,

https://doi.org/10.70712/NJG.v105.12686

with the remaining eight samples tested at the geotechnical laboratory of Deltares. The total porosity for sample 150 could not be determined. Due to this single failure and the exclusion of the channel samples, 150 measurements remain available for the analysis of total porosity distribution.

Grain-size distribution, organic matter content, and carbonate content

The Sediment Laboratory at VU University Amsterdam conducted a total of 161 *GS* distribution measurements using a Sympatec HELOS KR Laser Diffraction Particle Sizer, with a measurement range of 0.12–2,000 µm. From each sample location, a representative volume of 2–5 g was collected and pretreated to remove organics and carbonates and to enhance dispersion of charged particles (Konert & Vandenberghe, 1997). Subsequently, these samples were sieved through a 1.6-mm mesh to prevent clogging of the particle sizer. In a limited number of samples, the presence of very few coarser grains (>1.6 mm), including gravel (>2 mm), was manually recorded, which did not affect the median *GS* or its classification (USDA, 1993). After excluding the channel-samples, 151 values remained available for analysis of *GS* distribution (Supplementary Material S1). From all sediment samples, a 2-gram pulverized subsample was collected to test for total organic matter content and total carbonate ($CaCO_3$) content, both expressed as a percentage of dry weight. Organic matter content was determined using Loss-On-Ignition (LOI) at 550°C (range 105–550°C), while carbonate content was determined by measuring weight loss at 1,000°C (range 800–1,000°C). These measurements were conducted using a LECO TGA-701 Thermo-Gravimetric Analyzer (TGA).

Statistical analyses

Descriptive statistics (minimum, maximum, quartiles, median, geometric mean, and standard deviation using n–1) were calculated for the conductivity, porosity, and *GS* datasets. The geometric mean was used for conductivity data due to its log-normal distribution, whereas the median was applied for porosity and *GS* data given their non-normal and partially skewed distributions. Data distributions and variability were visualised using boxplots. To evaluate statistical differences between sampling sections, a Kruskal–Wallis test ($p < 0.05$) was first applied to assess overall significance, followed by pairwise Mann–Whitney U tests to identify where significant differences occurred. Bonferroni adjustments were applied to p-values to account for multiple comparisons. To assess the influence of distribution shape and outliers, the standard deviation was compared with the interquartile range (IQR). These descriptive statistics and boxplots were generated in Microsoft Excel, while nonparametric statistical analyses (Kruskal–Wallis and Mann–Whitney U tests) were conducted in Python.

Results

Data structure and general results

The data structure, defined by the distribution of sampling positions (distance from the fault) and orientations (horizontal and vertical), supports the analysis of saturated hydraulic conductivity (K_{sat}), total porosity (P_{total}), and *GS* distribution across the fault, as well as the assessment of correlations between these parameters. The position and orientation of each field and laboratory sample, along with their association with the corresponding trench sampling section (Figure 6) and the measurement results, are presented in Appendix 1. Additionally, the findings are correlated with high-resolution photographs of each field sample, which are provided in Appendix 2. This appendix also presents the total organic matter and total carbonate content, the latter showing such low values that they are of no significance. Within this context, Unit 1 (Beegden Formation) was located below the trench floor and therefore not sampled. The dataset thus represents the overlying Units 2–5 (Figure 4b; Table 1).

The saturated hydraulic conductivities (Figure 8) vary by almost four orders of magnitude (Table 2). The lowest conductivity, 0.004 m day^{-1}, is attributed to the deformed sediments of the fault, while the highest conductivity, 32.1 m day^{-1}, is found in the undeformed sediments on the hanging wall. The geometric mean of the saturated hydraulic conductivity of the dataset is 2.3 m day^{-1}. The range in total porosities (Figure 10) varies from 27.4 to 39.4%, with a median value of 35.1%.The median *GS* (Figure 11) ranges from 146 to 479 µm, with a median value of 199 µm, indicating the presence of fine to medium sand. In addition, total organic matter contents (LOI at 550°C) are low in the dataset (Appendix 1), with values ranging from 0.16 to 0.97 wt% (weight percentage).

Building on this dataset structure, the statistical distributions of permeability, porosity, and *GS* were examined to further analyse their variability. Permeability shows considerable heterogeneity, with a geometric mean (2.3 m d^{-1}) that is substantially lower than the standard deviation (5.0 m d^{-1}), suggesting an uneven distribution of measured values. Porosity displays a relatively symmetric distribution with limited heterogeneity, as indicated by a median of 35.1% and a standard deviation of only 2.5%. The *GS* data show considerable heterogeneity, with a median of 199 µm and a standard deviation of 69 µm.

Saturated hydraulic conductivity distribution

From the foot wall through the fault zone to the hanging wall (Sections 1–5), the impact of faulting on the range and directional distribution of saturated hydraulic conductivities (K_{sat}) is evidenced through values spanning almost four orders of magnitude (0.004–32.1 m d^{-1}) (Figure 8). The deformed fault zone exhibits a distinct distribution pattern compared to the undeformed flanking sediments.

In Section 1 on the foot wall, undeformed sediments show a clear contrast between horizontal and vertical saturated hydraulic conductivities. The horizontal saturated hydraulic conductivities (K_h) vary by nearly one order of magnitude, while the vertical saturated hydraulic conductivities (K_v) span almost three orders of magnitude. The mean horizontal conductivity (geometric mean) of 5.9 m day^{-1} exceeds the mean vertical conductivity of 1.6 m day^{-1}. The corresponding K_h/K_v ratio yields an Anisotropy Ratio (AR) of 3.7 (Figure 8).

In Section 2 on the foot wall, the deformed sediments in the damage zone adjacent to the fault exhibit elevated horizontal and vertical conductivities. Horizontal conductivities (K_h) vary by slightly more than one order of magnitude, while vertical conductivities (K_v) span three orders of magnitude. The mean

https://doi.org/10.70712/NJG.v105.12686

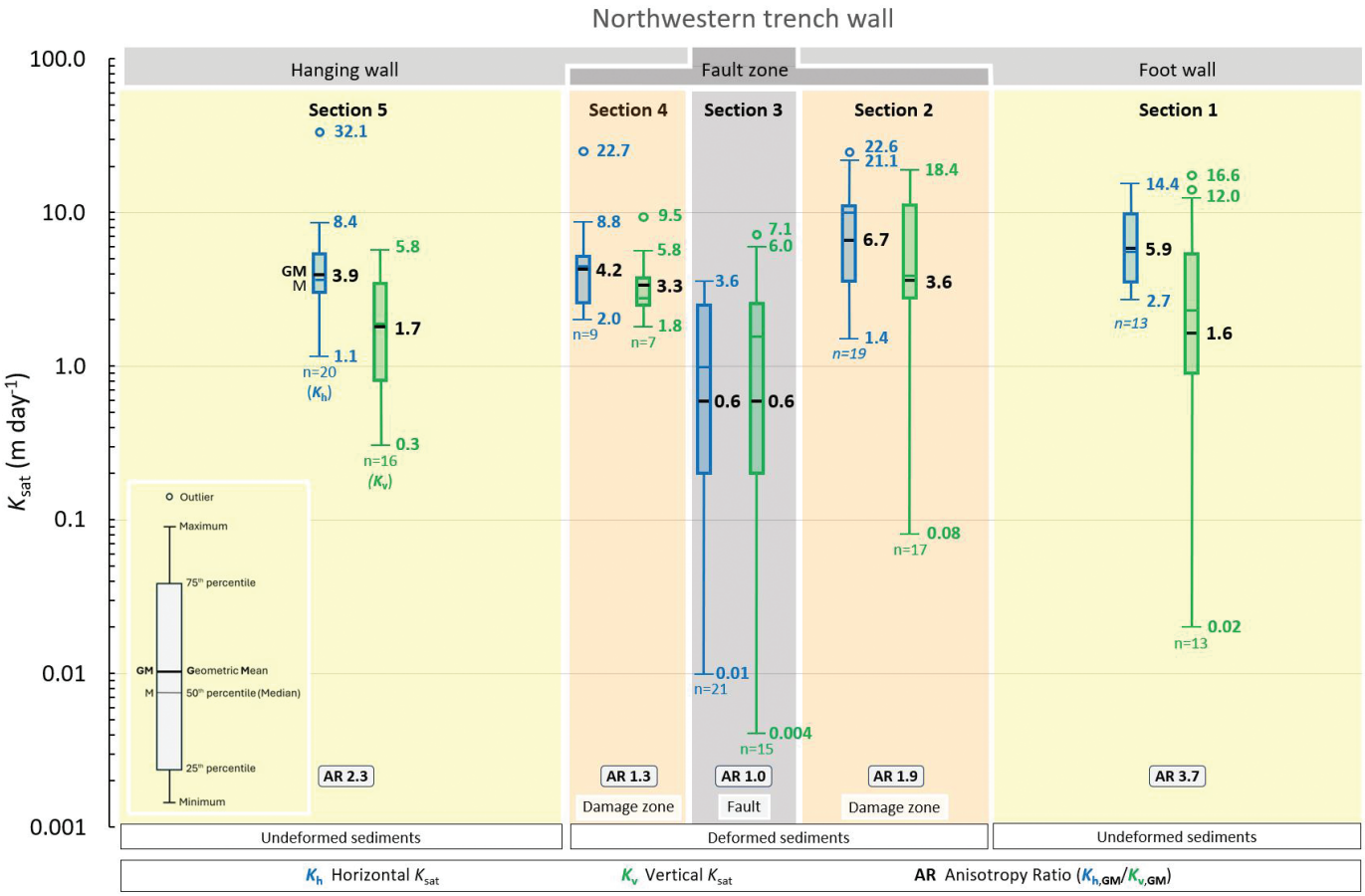

Figure 8. Distribution of saturated hydraulic conductivity (K_{sat}) along trench Sections 1–5, projected onto the schematised trench. The highest mean horizontal and vertical K_{sat} values occur in the foot-wall damage zone (Section 2). The fault (Section 3) exhibits the lowest mean horizontal hydraulic conductivity (0.6 m day^{-1}), which is significantly lower than in all other sections, and the lowest mean vertical value (0.6 m day^{-1}), significantly lower only relative to Section 2. Equal horizontal and vertical means result in an anisotropy ratio (AR) of 1.0, whereas higher AR values elsewhere indicate horizontal dominance. The inset explains the various boxplot elements.

Table 2. Overall results of the Uden trench site.

Parameter	Unit	Samples for analyses[a]	Statistic	Average	Lowest		Highest	
(–)	(–)	(*n*)	(–)	(value)	(value)	(code)[b]	(value)	(code)
Saturated hydraulic conductivity (K_{sat})[c,d]	m day^{-1}	150	Geometric mean	2.3	0.004	(50)	32.1	112
Total porosity (P_{total})	%	150	Median	35.1	27.4	(66)	39.4	106[e]
Median grain size (*GS*)[f]	µm	151	Median	199	146	(23)[g]	479	47

[a]Moat samples (100–105 and 142–145) excluded (Appendix 2); [b]Laboratory sample codes are in Table 1 and Appendix 1; [c]Total measurements in the horizontal and vertical direction; [d]Measurement results converted to international standard at 10°C; [e]Also measured in samples 109 and 153; [f]Based on a measurement range of 0.12–2,000 µm, classified according to USDA (1993); [g]Also measured in samples 89, 137, and 160.

horizontal conductivity is 6.7 m day^{-1} and surpasses the vertical conductivity, which is 3.6 m day^{-1}. This fault-flanking section exhibits the highest mean horizontal and vertical conductivities among all five sections and has an AR of 1.9 (Figure 8).

Trench sampling Section 3 encompasses the sub-vertical fault (Figure 8) and exhibits the lowest hydraulic conductivities of all six sampling sections. Within the fault, reorientation of elongated grains, iron (hydr)oxide precipitation, and accumulation of fine sediments and organic matter have affected the permeability distribution (Figure 5). Horizontal conductivities (K_h) vary over nearly two orders of magnitude (0.01–3.6 m day^{-1}), while vertical conductivities (K_v) span just over three orders of magnitude. The mean horizontal conductivity of 0.6 m day^{-1} equals the mean vertical conductivity, resulting in an AR of 1.0. Within the sub-vertical fault section, horizontal conductivities are not dominant.

The abrupt transition from higher horizontal conductivities in the damage zone on the foot wall (Section 2) to lower conductivities in the fault (Section 3) can be quantified by horizontal field samples DL7 (sediment samples 18, 20, and 21), DL9 (28–32), and DL10 (33, 34, and 36) collected from the trench floor (Figure 9a). The horizontal conductivity values (K_h) in these samples show a reduction from a range of 10.5–22.6 m day^{-1} in the damage zone on the foot wall to a range of 0.04–2.9

https://doi.org/10.70712/NJG.v105.12686

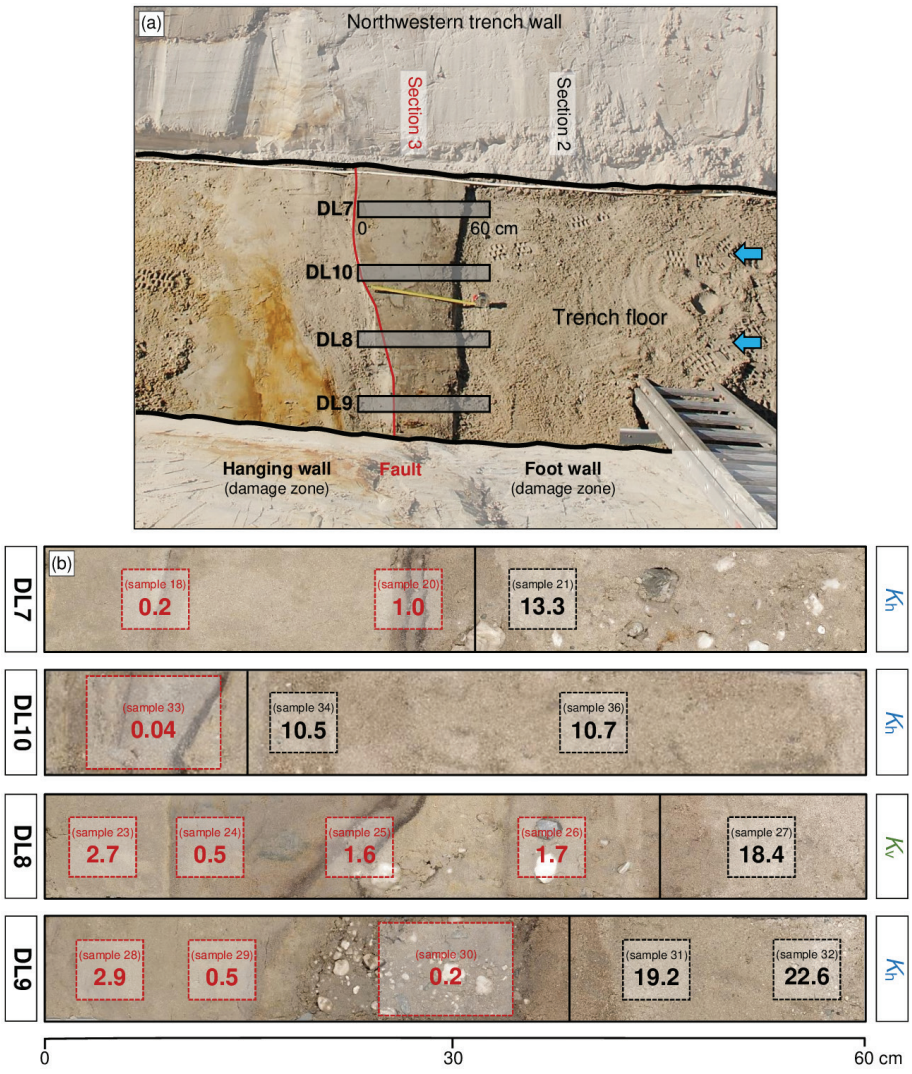

Figure 9. Fault-related permeability transition from the foot-wall damage zone (Section 2) towards the fault (Section 3), with the red line marking the fault core where fines have accumulated. (a) Top view showing the position of horizontal field samples DL7–DL10, projected onto the trench floor from their deeper sampling level. Blue arrows indicate groundwater flow towards the fault (obliquely upward); and (b) DL7, DL9, and DL10 show a reduction in horizontal conductivity (K_h) of up to two orders of magnitude, while vertical conductivity (K_v) in DL8 is reduced by one to two orders. The vertical black lines indicate the abrupt conductivity decrease at field-sample scale.

m day^{-1} in the fault over a horizontal distance of a few centimetres (up to ~10 cm; Figure 9b). The most substantial reduction in horizontal conductivity is observed in field sample DL10, where the damage zone sediment samples 34 and 36 have values ranging from 10.5 to 10.7 m day^{-1}, while the flanking fault-sediment sample 33, where fines have accumulated, shows a horizontal conductivity of only 0.04 m day^{-1}. These sediments demonstrate a fault-related permeability reduction by more than two orders of magnitude. The horizontal permeability reduction in field samples DL7 and DL9 is also abrupt and amounts to approximately one and two orders of magnitude, respectively. This abrupt permeability change corresponds consistently with the interface between the deformed sediments in the damage zone and the fault, where fine sediments and organic matter have accumulated, as evidenced by field sample DL10 (Figure 9b).

The abrupt transition from higher vertical conductivities in the damage zone on the foot wall (Section 2) to lower conductivities in the fault (Section 3) can be quantified by horizontal field samples DL8 (sediment samples: 23–27), likewise occurring over a horizontal distance of a few centimetres (up to ~10 cm; Figure 9b). In this sample, the deformed foot-wall sediments have a vertical conductivity of 18.4 m day^{-1} (sample 27). The flanking sediment samples (23–26) within the fault accumulation zone exhibit lower vertical conductivities, ranging from 0.5 to 2.7 m day^{-1}. This zone shows diffuse interporous accumulation of fine sediments and precipitation of particulate organic matter in multiple thin, brownish-to-black bands (Figure 9b; Appendix 2).

Trench sampling Section 4 covers the damage zone on the hanging wall (Figure 8) and exhibits increased conductivities, showing similarities to the foot-wall damage zone. The horizontal conductivities (K_h) of the deformed sediments in this section range from 2.0 to 22.7 m day^{-1}, while the vertical conductivities (K_v) range from 1.8 to 9.5 m day^{-1}, resulting in permeability variations by approximately one order of magnitude in both directions. The mean horizontal conductivity from the hanging-wall damage zone measures 4.2 m day^{-1}, exceeding the mean vertical conductivity of 3.3 m day^{-1}. This fault-flanking section has an AR of 1.3 and largely resembles the damage zone on the foot wall.

https://doi.org/10.70712/NJG.v105.12686

On the hanging wall, the undeformed sediments of trench sampling Section 5 (Figure 8) show lower conductivities compared to the adjacent damage zone. This section reveals a mean horizontal conductivity (K_h) of 3.9 m day^{-1} and a vertical mean (K_v) of 1.7 m day^{-1}. The corresponding AR of 2.3 indicates dominance of horizontal conductivity. Although the highest saturated hydraulic conductivity value (32.1 m day^{-1}) was measured in laboratory sample 112 attributed to Section 5 (Appendix 2), the median conductivities of the undeformed sediments on the hanging wall are lower than those of the deformed sediments in the flanking damage zone.

When comparing the directional hydraulic conductivity means from all sections, it appears that the mean K_h of the fault (0.6 m d^{-1}) is significantly lower than in all other sections. The mean K_v (also 0.6 m d^{-1}) is lower than the mean vertical hydraulic conductivity in all other sections, but significantly so only when compared to the foot-wall damage zone.

Total porosity distribution

Cross-fault total porosity in unconsolidated sediments ranges from 27.4 to 39.4% across all sections, representing the minimum and maximum values of the dataset (Figure 10).

The undeformed foot-wall sediments (Section 1) have a median total porosity of 34.2%. Closer to the fault, the deformed foot-wall damage zone (Section 2) shows the lowest median total porosity of 33.1%. The fault (Section 3) has a median total porosity of 34.1%, which falls within the range of all foot-wall sediments.

Compared to the foot wall (Sections 1–2) and fault sediments (Section 3), those on the hanging wall (Sections 4–5) exhibit higher median total porosities. The deformed sediments in the fault-flanking damage zone (Section 4) have a median value of 37.0%, while the undeformed sediments (Section 5) have a median of 36.4%. Although these differences are small, the increase in median total porosity in the hanging-wall sediments by approximately 2–4% is statistically significant (Kruskal–Wallis test; $p < 0.05$).

GS distribution

Variation in cross-fault median *GS* distribution, derived from samples representing each section, is shown in Figure 11. Median grain sizes range from 146 to 479 µm, indicating the presence of fine- to medium-grained sands, where the repeated value of 146 µm (Section 2–5) likely reflects a characteristic of the sampled sedimentary unit, with additional contribution from grouping into predefined grain size classes used in the analyses. Sample specifications and grain size parameters, including fine (clay and silt) and coarse (sand) fractions, are provided in Appendix 1, whereas grain size distribution curves for all samples are included in Supplementary Material S1. Since the dataset shows no evidence of

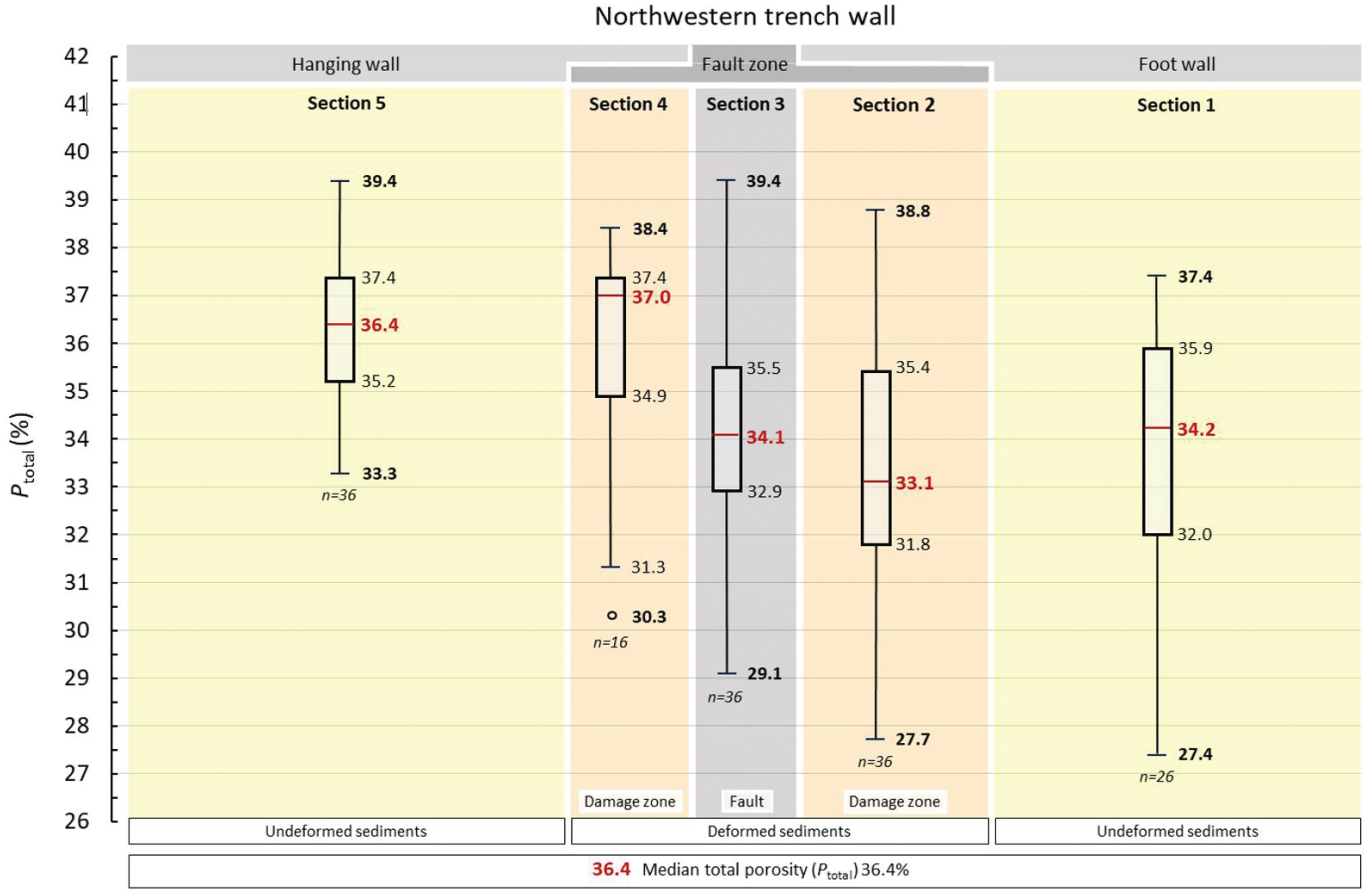

Figure 10. Distribution of total porosity (P_{total}) along trench Sections 1–5, projected onto the schematised trench. Median P_{total} values on the foot wall range from 34.2 (Section 1) to 33.1% (Section 2). The fault (Section 3) exhibits a median P_{total} of 34.1%, which falls within this foot-wall range. Away from the fault, on the hanging wall, median P_{total} values are significantly higher, with values of 37.0% (Section 4) and 36.4% (Section 5), compared to Sections 1–3. The boxplot layout is explained in Figure 8, and Appendix 2 provides total-porosity values for all 150 samples.

https://doi.org/10.70712/NJG.v105.12686

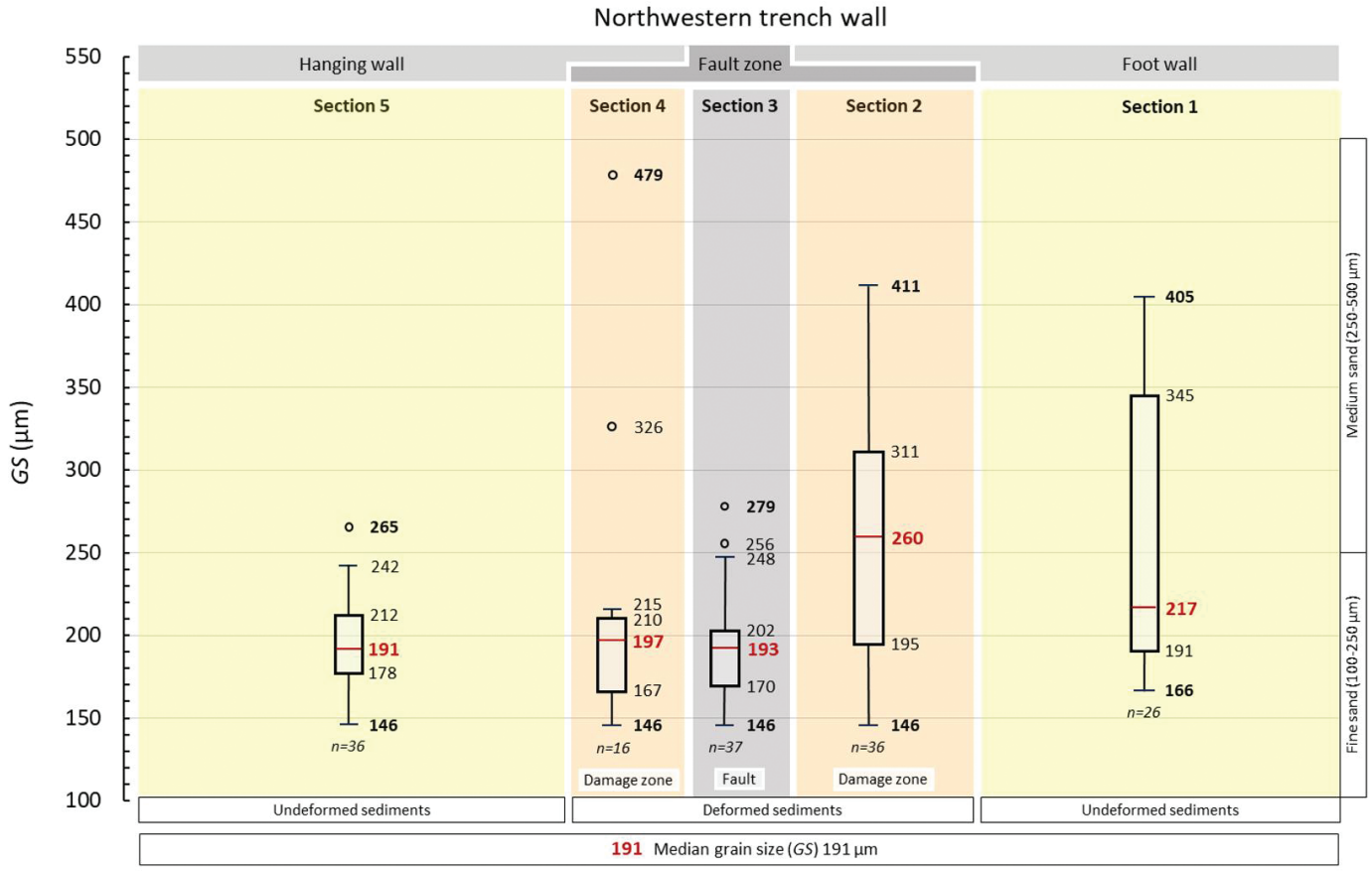

Figure 11. Distribution of median grain sizes (*GS*) along trench sampling Sections 1–5, projected onto the schematised trench. Median values on the foot wall range from 217 µm (Section 1) to 260 µm (Section 2). The fault (Section 3) contains finer sediments, with a median grain size of 193 µm. Away from the fault, onto the hanging wall, median grain sizes decrease from 197 µm (Section 4) to 191 µm (Section 5). Overall, foot-wall sediments (Sections 1 and 2) are significantly coarser than those in the fault (Section 3) and hanging wall (Section 5). The boxplot layout is explained in Figure 8, and Appendix 2 provides grain size distributions for all 151 samples.

bimodality, the median grain size is used as a representative measure of the overall distribution, consistent with the approach applied to hydraulic conductivity (geometric mean) and total porosity (median).

Away from the fault, the undeformed sediments on the foot wall (Section 1) have a median grain size of 217 µm. Also on the foot wall, but closer to the fault, the disturbed sediments in the damage zone (Section 2) display the coarsest median grain size, at 260 µm. The fault (Section 3), however, comprises finer sediments, with a median grain size of 193 µm, and shows an abrupt decrease in median grain size of 67 µm compared to Section 2. In the hanging-wall damage zone (Section 4), the widest range in median grain sizes (146–479 µm) is observed. The sediments in this zone have a median grain size of 197 µm, which is coarser than those in the fault but finer than those in the damage zone on the foot wall. The undeformed sediments on the hanging wall, located away from the fault (Section 5), have a median grain size of 191 µm and exhibit the smallest range (146–265 µm) of all sampled sections.

The grain size distribution of the unconsolidated sediments at the Uden trench site (Figure 11) reveals a pattern of coarser sediments on the foot wall and finer sediments within the fault and on the hanging wall. This pattern is supported by differences in median grain size, with the deformed sediments in the fault (Section 3), the hanging-wall damage zone (Section 4), and the sediments away from the fault on the hanging wall (Section 5) all showing lower median grain sizes than the foot-wall sediments (Sections 1 and 2), although only Sections 3 and 5 differ significantly (Kruskal–Wallis test; $p < 0.05$).

Saturated hydraulic conductivity and total porosity

Saturated hydraulic conductivity values were compared with their corresponding total porosities (Figure 12; Table 3). Across all sections, the dataset shows a generally negative correlation, where higher conductivities tend to correspond to lower total porosities. This relationship is overall very weak to negligible in most sections, but strong in the deformed hanging-wall sediments.

In the undeformed sediments flanking the fault zone (Figure 12a), the foot-wall conductivities correspond to lower total porosities (Section 1), whereas those from the hanging wall correspond to higher total porosities (Section 5). The calculated correlation factors indicate that the negative trend between conductivity and total porosity is very weak to negligible. This is reflected in the dataset, where a single total-porosity value (e.g. 35%) encompasses hydraulic conductivity values spanning just over three orders of magnitude (0.02–32.1 m day^{-1}). Conversely, a conductivity value (e.g. 6.0 m day^{-1}) corresponds to a wide range of total porosities (27.4–39.4%) (Figure 12a).

https://doi.org/10.70712/NJG.v105.12686

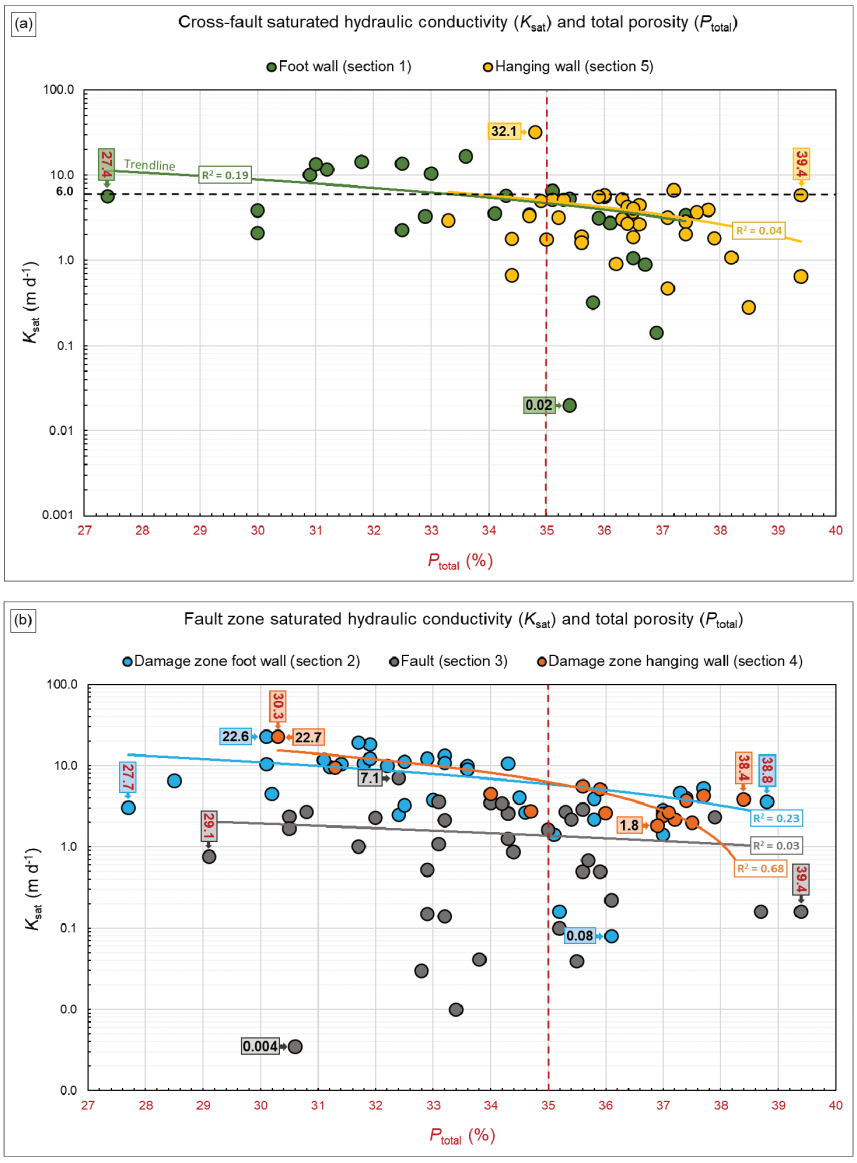

Figure 12. Saturated hydraulic conductivity (K_{sat}) and total porosity (P_{total}). (a) At a cross-fault scale, undeformed foot-wall sediments (Section 1) exhibit lower P_{total} values than undeformed hanging-wall sediments (Section 5), with both displaying a weak negative correlation with K_{sat}; and (b) Within the deformed fault zone, the fault (Section 3) shows the widest variability in both K_{sat} (0.004–7.1 m day^{-1}) and P_{total} (29.1–39.4%), whereas the hanging-wall damage zone (Section 4) spans only one order of magnitude in K_{sat} (1.8–22.7 m day^{-1}) despite a similarly broad P_{total} range (30.3–38.4%) and exhibits a moderate negative correlation (R^2 = 0.68). Logarithmic trendlines with their associated R^2 values are also shown.

Table 3. Correlations between saturated hydraulic conductivity (K_{sat}), total porosity (P_{total}), and grain size (*GS*) across trench sampling Sections 1–5, expressed as coefficient of determination (R^2).

Sampling section	Tectonic position	Tectonic setting	Correlation	R^2	Result
1	Foot wall	Undeformed	K_{sat}–P_{total}	0.19	Very weak to negligible negative correlation
			K_{sat}–*GS*	0.64	Moderate to strong positive correlation
2	Foot wall	Deformed	K_{sat}–P_{total}	0.23	Weak negative correlation
			K_{sat}–*GS*	0.69	Moderate to strong positive correlation
3	Fault	Deformed	K_{sat}–P_{total}	0.03	Negligible negative correlation
			K_{sat}–*GS*	0.00	No correlation
4	Hanging wall	Deformed	K_{sat}–P_{total}	0.68	Moderate to strong negative correlation
			K_{sat}–*GS*	0.85	Strong positive correlation
5	Hanging wall	Undeformed	K_{sat}–P_{total}	0.04	Very weak to negligible negative correlation
			K_{sat}–*GS*	0.23	Weak positive correlation

https://doi.org/10.70712/NJG.v105.12686

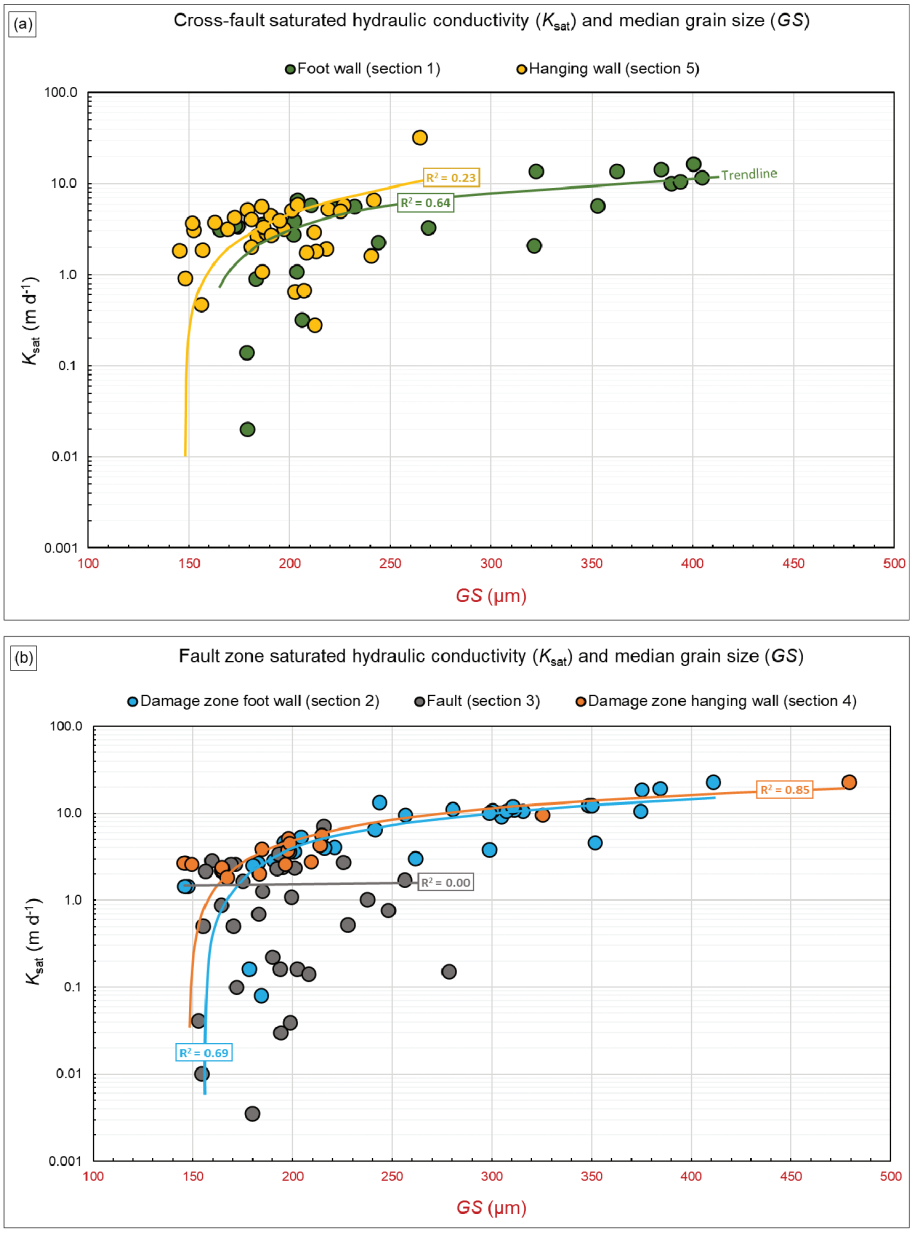

Figure 13. Saturated hydraulic conductivity (K_{sat}), median grain size (*GS*), and trends. (a) At a cross-fault scale, undeformed foot-wall sediments (Section 1) show a positive correlation between K_{sat} and *GS*; and (b) Within the deformed fault zone, the foot-wall (Section 2) and hanging-wall (Section 4) damage zones show a similar trend, whereas the fault (Section 3) exhibits no such correlation, and the hanging wall (Section 5) shows only a weak correlation. Logarithmic trendlines with their associated R^2 values are also shown.

The deformed sediments within the fault zone (Figure 12b) exhibit distinct behaviour in the relationship between conductivity and total porosity. The damage zone on the foot wall (Section 2) shows a weak, whereas the fault (Section 3) exhibits a negligible relationship and the greatest variability in both K_{sat} (0.004–7.1 m day^{-1}) and P_{total} (29.1–39.4%). The fault-flanking damage zone on the hanging wall (Section 4) shows a distinct correlation pattern, in which a wide range of total porosity values (30.3–38.4%) corresponds to a relatively limited conductivity variation (1.8–22.7 m day^{-1}). This section is the only one in which the regression analysis and corresponding trendline exhibit a moderate to strong negative correlation where higher total porosities correspond to lower conductivities (Figure 12b).

Saturated hydraulic conductivity and median grain size distribution

The relationship between saturated hydraulic conductivity and grain size varies across the fault, with larger K_{sat} values generally corresponding to coarser grain sizes, while the fault (Section 3) exhibits distinct behaviour (Figure 13; Table 3). The saturated hydraulic conductivity values of the five cross-fault sampling sections (Figure 6) are compared with the corresponding median grain sizes, starting with the undeformed Sections 1 and 5 away from the fault (Figure 13a) and followed by the deformed Sections 2–4 representing the fault zone (Figure 13b).

Within the undeformed sediments, variability in saturated hydraulic conductivity on the foot wall (Section 1) is largely

https://doi.org/10.70712/NJG.v105.12686

explained by grain size distribution, whereas on the hanging wall (Section 5) the correlation is much weaker, which may be related to the narrow grain size distribution with varying hydraulic conductivities, among other factors. Both correlations are illustrated in Figure 13a.

Within the deformed fault zone, the damage zones flanking the fault show a different hydraulic conductivity-to-grain size correlation compared to the fault itself. Both the damage zone on the foot wall (Section 2) and that on the hanging wall (Section 4) confirm that coarser median grain sizes correspond to higher saturated hydraulic conductivity values, as illustrated in Figure 13b. In contrast, conductivity values within the fault (Section 3) show no relationship with variations in median grain size, as shown by the corresponding trendline. This is further evidenced by the distinctly lower K_{sat} values in Section 3, which largely fall below the damage-zone trends, illustrating the hydraulic drop-out of the fault relative to grain size variation. Together, these findings indicate that the fault occupies a distinct position, as it alone lacks the hydraulic–grain size correlation observed, to varying extents, in all other sections.

Discussion

Hydraulic conductivity distribution across the fault

Directly measured directional hydraulic conductivity data in fault settings are scarce. A review of such data and cross-fault groundwater-level steps in the RVRS identified only six locations with quantitative, non-directional hydraulic conductivity data, all within unconsolidated sediment settings (Lapperre et al., 2019). These locations show a saturated hydraulic conductivity (K_{sat}) range spanning just over three orders of magnitude. A hydrogeological trench study along the Peel Boundary Fault in Bakel similarly reported a range of just over three orders of magnitude (Lapperre et al., 2022). The 150 directional hydraulic conductivity values presented in this study span almost four orders of magnitude. This wider overall range is likely related to the larger number of samples, which capture near-fault lithological variability in greater detail compared to previous studies. In addition to the locations identified by Lapperre et al. (2019, 2022), other case studies in the same rift system have documented cross-fault groundwater-level steps (Casillas-Trasvina et al., 2022; Deckers et al., 2018). However, these studies do not provide directly measured K_{sat} values (i.e. derived from field- or laboratory-based testing). In this setting, our study provides an extensive, directionally resolved dataset derived from direct measurements, contributing to improved insight into fault-related permeability distribution.

The fault zone (Sections 2–4) exhibits significant directional variation in hydraulic conductivities. The highest hydraulic conductivities, in both horizontal and vertical directions, occur in the foot-wall damage zone (Section 2), where they are statistically higher than those in the fault (Section 3). Section 2 exhibits the largest mean horizontal conductivity (K_h) of 6.7 m day^{-1} and the largest mean vertical conductivity (K_v) of 3.6 m day^{-1}. The hanging-wall damage zone (Section 4) also shows increased conductivities, although only the horizontal values reach statistical significance when compared to the fault.

Enhanced K_h may be attributed to prolonged fault-related groundwater flow towards the fault (Figure 2c) and associated internal erosion, during which interporous fines such as clay, silt, very fine sand, and fine sand (Lapperre et al., 2025) were gradually mobilised and transported from the foot-wall sediment matrix towards the fault (Section 3). Internal erosion is considered a plausible mechanism, supported by trench observations at the study site (Figures 5b and 9a) and by the presence of groundwater flow directed towards the fault zone under a strong hydraulic gradient associated with an average fault-related groundwater-level step of approximately 2 m (Lapperre et al., 2025), which suggests that such erosion is hydrologically feasible. Our dataset does not allow for additional analyses regarding potential coarsening in the damage zones. Enhanced K_v appears to be related to the presence of numerous minor faults (Figure 5) and the reorientation of elongated grains induced by fault movement along the fault plane, which likely serve as conduits for vertical groundwater flow (Lapperre et al., 2025). While the washing out of fines predominantly affects horizontal permeability, here the vertically aligned grain orientation and minor faults are interpreted to outweigh such effects and enhance permeability in the vertical direction. Both permeability-enhancing processes also appear to apply to the hydraulic conductivity distribution of the deformed sediments in the hanging-wall damage zone (Section 4). Similar to the foot wall, the hydraulic conductivities of the deformed sediments in the hanging-wall damage zone discussed in this section (Figure 8) tend to be higher than those measured in the undeformed sediments away from the fault (Section 5), although substantial overlap is present in the measurements.

The lowest hydraulic conductivities are measured within the fault (Figure 8), where horizontal values range from 0.01 to 3.6 m day^{-1} and vertical values span 0.004–7.1 m day^{-1}, both with a median of 0.6 m day^{-1}. These horizontal fault conductivities are significantly lower than those in all other sections, while vertical fault conductivities are significantly lower only when compared with the foot-wall damage zone (Section 2). These low values are attributed to the combined effects of interporous fines accumulation (clay, silt, very fine sand, and organic matter), iron (hydr)oxide precipitation (Figure 5), and the subvertical reorientation of elongated grains likely further reduces horizontal conductivity. Together, these processes reduce pore space and are interpreted as the primary cause of permeability reduction, with fault-induced grain rotation acting as an initial trigger (Lapperre et al., 2025). Fine fractions are present across all sections, and their distribution at sample level is documented in Appendix 1 (including total organic matter), while full grain size distribution curves for all samples are provided in Supplementary Material S1. LOI values indicate that organic contents are generally low (< ~1 wt%), suggesting that their contribution to fault permeability reduction is likely limited to local pore clogging in thin, dark-coloured layers (Figure 5b). Due to the combined effects of these hydrogeological processes, hydraulic conductivities within the fault are low in both directions, yielding equal mean values (Figure 8) and thereby an AR of 1.0. This makes the fault the only section where horizontal conductivity is not dominant.

Hydraulic conductivity for local-scale studies

To accurately model local-scale phenomena such as near-fault groundwater fluxes, fault-related groundwater temperature anomalies, the transport of groundwater contaminants, and the magnitude and variability of the cross-fault groundwater level step, detailed information on the hydraulic conductivity

https://doi.org/10.70712/NJG.v105.12686

distribution is essential (e.g. Sanchez-Villa et al., 2006; Zhu et al., 2016). Such a distribution can be obtained from directional field measurements, which better assess the conduit–barrier function of faults in unconsolidated sediments. Our findings indicate that the inferred hydrological impact of faults in unconsolidated sediments in the subsurface (Bense & Person, 2006; Bense et al., 2013; Cook et al., 2022) is also evident near the surface (Figure 8).

Larger-scale hydraulic conductivity data obtained from pumping tests, groundwater models, and national subsurface hydrogeological models (e.g. REGIS II v2.2.2; Hummelman et al., 2019b) are typically used in regional-scale studies (Broers et al., 2021; Díaz-Curiel et al., 2022; Zhou & Li, 2011). However, their applicability at the local scale is limited, as such data often do not consider conductivity anisotropy, are inferred rather than directly measured, and lack the resolution needed to assess both spatial distribution and correlation with local-scale lithology variations, as well as the fault-related hydrogeological processes discussed earlier. Recent catchment-scale modelling efforts (e.g. Casillas-Trasvina et al., 2022) reveal the need for locally constrained conductivity data, as calibrated saturated horizontal fault conductivities are often defined at relatively coarse resolutions, do not explicitly account for anisotropy, and are not designed to capture near-surface fault-zone dynamics.

This limitation is evidenced by the variability and anisotropy in hydraulic conductivity observed between the fault, damage zones, and undeformed sediments, as identified in this study. These spatial contrasts and directional behaviour are not resolved in regional-scale models such as REGIS and demonstrate that relying solely on such schematisations may overlook key aspects of the fault-related hydraulic conductivity distribution and its impact on groundwater flow.

Near-surface fault-zone groundwater flow

The results from the Uden trench site have three implications for fault-zone hydrogeology.

First, when assessing near-surface groundwater flow in a fault setting, both horizontal and vertical permeability contrasts between the fault, damage zones, and adjacent undeformed sediments must be taken into account. A groundwater-level step develops when lateral groundwater flow encounters a fault that presents a larger hydraulic resistance (lower saturated hydraulic conductivity) than adjacent sediments, necessitating a higher hydraulic gradient within the fault. Conversely, upward seepage in the foot-wall damage zone and downward flow in the hanging-wall damage zone, flanking the fault, can redistribute groundwater and has the potential to reduce the lateral flux into the fault, thereby diminishing the magnitude of the step. The presented data provide robust insight into the spatial distribution of directional saturated hydraulic conductivity in a fault setting. Such data are essential for improving the modelling of near-surface fault zones. The observed permeability contrasts and associated flow mechanisms are representative of the study area. However, their expression may vary with local lithological composition. This emphasises the need to incorporate site-specific conductivity data in local groundwater models.

Next, the ecological functioning of seepage-related areas on the foot-wall side of faults, locally known as 'wijstgronden', depends on sustained upward groundwater flow. In many locations, historical agricultural practices such as (deep) ploughing across faults have mechanically disturbed both the low-permeability fault and the fault-flanking vertically conductive damage zones. This has likely affected fault-related groundwater dynamics. Current restoration efforts, for example those initiated by regional waterboards, largely aim to re-establish the horizontal barrier effect of the fault.

However, our results suggest that at the study site, the damage zone on the foot-wall side (Section 2) plays an important role in facilitating vertical upward flow of iron-rich groundwater towards the surface, although this may not apply everywhere. This implies that future restoration efforts should not only focus on reinforcing horizontal permeability contrasts within the fault but also on restoring or maintaining vertical conductivity pathways in the damage zones. In areas where vertical permeability has been diminished, promoting deep-rooting vegetation may offer a means of reactivating vertical flow pathways. Additionally, renewed upward flow could in turn enhance iron (hydr)oxide precipitation within the hanging-wall damage zone (Section 4), which is expected to further contribute to the restoration of fault-zone hydraulic structure where it has been lost.

Finally, the results from this study help explain several field phenomena that illustrate near-surface conduit–barrier interactions and their influence on groundwater behaviour. This explanation is supported by the observed vertical conductivity contrasts and upward flow potential within the foot-wall damage zone identified in this study. One such phenomenon is the occurrence of temperature anomalies in phreatic groundwater systems at fault locations, where groundwater temperatures may be up to 8°C higher than near-surface values (Bense et al., 2008), supporting the interpretation that warmer, deeper groundwater ascends on the foot-wall side. Such upward flow may be driven by cross-fault hydraulic gradients and is facilitated by enhanced vertical conductivity within the foot-wall damage zone, although it is probably not the only factor controlling it. This upward movement of groundwater likely explains the occurrence of small sand volcanoes in cross-fault watercourses, which expel groundwater, gas bubbles, and sand. These vents are frequently observed in the field, often marking the position of the foot-wall damage zone. Additional indicators, such as soil moisture patterns reflecting sharp transitions between wetter and drier areas, can likewise be interpreted in the context of fault-induced groundwater flow. As such, these field phenomena can serve as reliable diagnostic indicators for identifying the fault's location in near-surface settings.

Total porosities, saturated hydraulic conductivities, and median grain sizes in a fault setting

Generally, finer sediments such as clay and loam have higher total porosities (P_{total}) and lower saturated hydraulic conductivities (K_{sat}), whereas coarser sediments such as sand and gravel exhibit lower P_{total} and higher K_{sat} (Freeze & Cherry, 1979) . In the cross-fault dataset, this expected relationship is absent and instead tends to be weakly reversed (Figures 12a and 12b). At the Uden trench site, porosities below ~35% coincide with higher and more variable K_{sat}, whereas porosities above ~35% are associated with lower K_{sat} and a narrower range. This negative pattern is subtle overall in Sections 1–3 and 5, but is more clearly expressed in the hanging-wall damage zone (Section 4),

https://doi.org/10.70712/NJG.v105.12686

where the regression analysis indicates a moderate to strong negative correlation (R^2 = 0.68; Figure 12b). This deviation from the common correlation may be attributed to generally low clay contents and to processes that locally modify pore structure and connectivity. The mobilisation, migration, and accumulation of these fines have the potential to alter hydraulic conductivity without necessarily affecting total porosity. This interpretation is supported by the grain size distributions (Supplementary Material S1), which show predominantly unimodal curves with subtle fine-end shoulders, indicating the presence of a minor fine fraction. Although distinct bimodal peaks are absent, these curves suggest that even relatively small amounts of fines may influence hydraulic conductivity. This may occur when the accumulation of fines partially blocks pore funnels, thereby impacting hydraulic conductivity while leaving total porosity relatively unchanged. In the damage zone, the rotation of elongated grains affects vertical conductivities without significantly changing total porosity. Permeability variations, including those occurring in a fault setting, are therefore likely governed by changes in pore size and pore connectivity. Such changes can result from grain reorientation, iron (hydr)oxide precipitation, and interporous migration and accumulation of fines (Lapperre et al., 2025), and are not adequately captured by measuring total porosity alone. Future studies that incorporate pore size and pore connectivity, for example through effective porosity measurements derived from tracer-based techniques (e.g. Stephens et al., 1998), may therefore better explain observed permeability variations.

In contrast to the conductivity–porosity relationship, the distribution of saturated hydraulic conductivities (K_{sat}) generally shows a positive correlation with median grain size (*GS*) (Figures 13a and 13b). With coefficients of determination (R^2) ranging from 0.64 to 0.85, this correlation is strong in the undeformed and deformed foot-wall sediments (Sections 1 and 2) and very strong in the deformed hanging-wall sediments (Section 4). The correlation in the undeformed sediments on the hanging wall (Section 5) is weak (R^2 = 0.23) and appears to result from a narrow grain size range combined with a wider conductivity distribution. However, the fault-conductivity distribution (Section 3) shows no correlation with median grain size (Figure 13b). This exception to the overall positive correlation can be explained by the fact that within the fault, the initial grain size distribution has been altered by the accumulation of interporous fines, as schematically illustrated in Figure 5b and observed in the Uden trench (Lapperre et al., 2025). This effect is also evident in the fault-related data points in Figure 13b, which deviate from the unaffected population.

The porosity and conductivity distributions are related to grain size, with coarser sediments displaying higher conductivities and finer sediments lower. In a fault setting, this distribution is also influenced by multiple fault-related effects, including the reorientation of elongated grains, iron (hydr) oxide precipitation, and the interporous migration and accumulation of fines. These fault-related processes are expected to be the dominant control on the observed conductivity patterns, as all sediments flanking the fault are unconsolidated, predominantly sandy, and exhibit only a range in median grain size of only 69 µm between the highest (260 µm in Section 2) and lowest (191 µm in Section 5) value (Figure 11).

Evolution of conductivity distribution

Building on the observations from the Uden trench site, we propose a conceptual model illustrating how the conductivity distribution could evolve (Figure 14). This evolution reflects the influence of time-dependent processes, including the reorientation of elongated grains, precipitation of iron (hydr)oxides and the internal erosion and accumulation of fines. On the foot wall, the fault-parallel accumulation layer thickens from a few

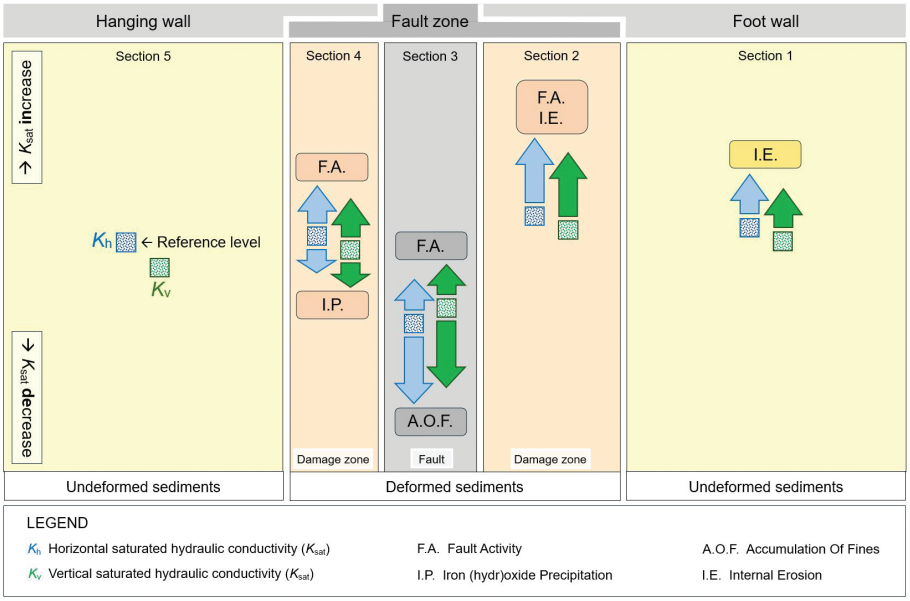

Figure 14. Expected future evolution of cross-fault hydraulic conductivity distribution and its potential triggers. Driven by ongoing internal erosion, conductivities on the foot-wall (Section 1) are expected to increase, particularly in the damage zone (Section 2), where occasional fault activity further enhances K_v. Within the fault (Section 3), conductivities may decrease as ongoing fine accumulation outweighs the effects of fault activity. In the hanging-wall damage zone (Section 4), iron (hydr)oxide precipitation reduces conductivities, while fault activity increases them, resulting in an expected net rise. Conductivities of the undeformed hanging-wall sediments (Section 5) are most likely to remain stable and serve as the best available reference level in the schematisation.

https://doi.org/10.70712/NJG.v105.12686

centimetres to a maximum of around 0.3–0.4 m directly against the fault near the trench floor (Figure 9a). It is characterised by a grey colour with alternating layers of silt, very fine sand, and brownish-to-black laminae of particulate organic matter (Figure 9b). The observed increase in thickness with depth (Lapperre et al., 2025) suggests that deeper parts of the fault have experienced more extensive accumulation. Additionally, the accumulation with increasing depth towards the trench floor shows multiple alternations of silt and fine sand, separated by thin laminae enriched with organic matter. Lapperre et al. (2025) suggest that the silt accumulations at the fault formed during past cold climatic conditions when mixing and mobilisation of sediments occurred due to repeated freezing and thawing (Bockheim & Tarnocai, 1998; Wang et al., 2023), with the fault serving as the trapping location for mobilised fines. Evidence for such cold-climate conditions at the trench location was observed by Van Balen et al. (2024). The organic laminae likely reflect the migration and accumulation of organic matter from decayed root remnants, related to soil development during warmer climatic conditions comparable to those today. On the hanging wall, several orange-coloured iron (hydr)oxide precipitation bands have developed over time in response to a rising groundwater table during sedimentation (Figure 4a). In addition, the reorientation of elongated grains is linked to occasional fault activity rather than continuous processes. Consequently, all these inferred processes together evidence that the permeability of the fault has changed over time and is likely to continue evolving. This anticipated future change, along with its triggers, is schematised in Figure 14.

On the foot wall, fine sediment grains and particulate organic matter migrate towards the fault, leading to internal erosion of the unconsolidated sediment matrix as particles are mobilised and pores develop. The resulting porosity increase is expected to cause higher hydraulic conductivities in both horizontal and vertical directions, as internal erosion is likely still active. This is supported by: (1) a persistent hydraulic gradient driving groundwater flow, confirmed by multi-year measurements; (2) the continued availability of unconsolidated very fine to fine sediments as a migration source (Lapperre et al., 2025); and (3) trench observations of multilayered accumulations expanding away from the fault into the foot wall, which suggest an ongoing process. The process of internal erosion is expected to be strongest in the foot-wall flanking damage zone and to diminish away from the fault towards the undeformed sediments (Figure 14). A temporary boost in vertical hydraulic conductivity within this damage zone may result from occasional fault activity, which creates porous, subvertical minor faults. In the main fault, where the accumulation of fines predominates, future hydraulic conductivities are likely to decrease in both horizontal and vertical directions. However, earthquakes may temporarily enhance local fault zone conductivities by injecting liquefied sands into newly formed subvertical minor faults, thereby keeping them open and porous (Wang, 2022). Such fluidised sediments are observed in the main fault at the Bakel trench site (Van Balen et al., 2019) and near the fault at the Uden trench site (Van Balen et al., 2024). In the long term, the cumulative impact of sporadic fault activity and ongoing accumulation of fine sediment is anticipated to reduce pore space again, diminishing future conductivities within the fault (Figure 14). In the hanging-wall damage zone, two opposing processes affect near-fault conductivities. Similar to the foot-wall damage zone, recurrent fault activity has the potential to enhance both horizontal and vertical hydraulic conductivities. However, the precipitation of iron (hydr) oxides (Figures 4a and 5b) reduces conductivities (Lapperre et al., 2025). The combined effect of these processes could result in a slow and steady increase in conductivity in both horizontal and vertical directions. This anticipated net increase is supported by the observation that the deformed sediments in the hanging-wall damage zone (Section 4) exhibit higher hydraulic conductivity values than the undeformed sediments away from the fault zone (Section 5) (Figure 8). This suggests that recurrent seismic activity may repeatedly promote sediment unpacking and the development of minor faults, which enhance permeability over time and ultimately outweigh the gradual conductivity reduction caused by iron (hydr)oxide precipitation. Away from the fault on the hanging wall (Section 5), undeformed sediments appear unaffected by the fault-related hydrogeological processes discussed. Therefore, their conductivity distribution is expected to remain largely constant (Figure 14).

Conclusions

Extensive laboratory measurements of saturated horizontal and vertical hydraulic conductivity (K_{sat}) were conducted on unconsolidated samples from the PBFZ in the Netherlands, part of the RVRS. The results demonstrated a fault-related conductivity range spanning almost four orders of magnitude, with values ranging from 0.004 to 32.1 m day^{-1}, and quantified the near-surface conduit–barrier architecture of the fault. The lowest hydraulic conductivities were found within the fault, with horizontal fault conductivity ranging from 0.01 to 3.6 m day^{-1} (mean 0.6 m day^{-1}), while vertical values varied from 0.004 to 7.1 m day^{-1} (mean also 0.6 m day^{-1}). The mean horizontal fault conductivity is significantly lower than the mean values of all other sampling sections, whereas the mean vertical fault conductivity is only significantly reduced compared to the fault-flanking damage zone on the foot wall. These fault conductivities, indicating reduced permeability, largely result from the accumulation of fines, contributing to the fault's barrier function causing a permanent cross-fault groundwater-level step.

The deformed sediments of the foot-wall damage zone exhibited the highest mean horizontal conductivity of 6.7 m day^{-1} and a mean vertical conductivity of 3.6 m day^{-1}, both significantly higher than those in the flanking fault. The vertical conductivity of the hanging-wall damage zone also exhibited a higher mean of 3.3 m day^{-1}, although this difference is not statistically significant among the sampling sections. These higher conductivities in the fault-flanking damage zones, particularly in the vertical direction, account for the conduit character of the fault zone.

The hydraulic conductivity distribution shows varying degrees of correlation with the cross-fault median grain size distribution, except for the fault. In the undeformed sediments away from the fault, the correlation is strong on the foot wall and weak on the hanging wall. In the fault-flanking damage zones, the grain size distribution also shows a clear correlation with enhanced conductivities. However, the fault holds a distinct position and shows no such relationship, most likely because it represents the zone where multiple fault-related hydrogeological processes have altered both conductivity and grain size

https://doi.org/10.70712/NJG.v105.12686

distribution. In contrast, total porosity shows little to no overall correlation with hydraulic conductivity within the cross-fault sampling sections, apart from a localised moderate negative correlation observed in the hanging-wall damage zone.

Due to the inferred prolonged and ongoing hydrogeological processes (such as internal erosion, migration and accumulation of interporous fines, and iron (hydr)oxide precipitation), along with occasional faulting (including subvertical reorientation of elongated grains, the development of minor faults, and fluidisations), the permeability distribution related to faults in unconsolidated sediments is expected to evolve over time, with fault conductivities decreasing and damage-zone conductivities increasing. These conductivity-affecting processes operate in specific parts of the fault zone and flanking lithologies, and on different time scales. Therefore, the current permeability distribution at the Uden trench site not only exhibits spatial (cross-fault) and directional (horizontal and vertical) variability, but is also expected to evolve over geological timescales. The near-surface conduit–barrier architecture of the fault has changed in the past and will continue to do so.

Data availability statement

The position and sampling direction of the 37 field samples, as well as the results from the 161 laboratory samples and their classification for interpretation, are presented in a table in Appendix 1. These findings are also linked to a high-resolution photo of each field sample, shown in Appendix 2. The full grain size distributions are provided in Supplementary Material S1. All data supporting this study are available via the Dutch 4TU Research Data Repository under DOI: [insert DOI].

Acknowledgements

We are deeply grateful to Hans and Christa de Bruin for their generous permission to excavate the trench on their property. Our thanks also go to the Water Authority Aa en Maas (Chris van Rens and Emmy Zwier), the Province of Noord-Brabant (Thea Huijsmans, Erik Heskes, and Martin Meffert), the drinking water company Brabant Water (Jeroen Castelijns), TNO – Geological Survey of the Netherlands in Utrecht (Eppie de Heer, Wim Booltink, and Pieter van der Klugt), Jon and Tom Mensink, and Mark Kerkhoff for their preparatory work and support during fieldwork. We extend our gratitude to the VU University Sediment Laboratory (Martine Hagen and Oeki Verhage) for their professional contributions to this study. Special thanks to Esmee Sanders for her meticulous fine-tuning of multiple figures. Without their assistance, conducting the Uden trench study and presenting the results in this manuscript would not have been possible. We also gratefully acknowledge the constructive comments of three anonymous reviewers, whose suggestions on statistical presentation, clarity of interpretation, and overall readability have significantly strengthened this manuscript.

Competing interests

The Province of Noord-Brabant, Water Authority Aa en Maas, and drinking water company Brabant Water financially supported this research into fault-zone hydrogeology in The Roer Valley Rift System. The corresponding author, on behalf of all the authors, states that these funders did not exert any influence on any aspect of the research.

References

Actueel Hoogtebestand Nederland, 2018. AHN3: Actueel Hoogtebestand Nederland – Versie 3 [Current Dutch Elevation –Version 3]. Dataset accessed June 2018. https://Rijkswaterstaat.ahn.nl.

Actueel Hoogtebestand Nederland, 2022. AHN4: Actueel Hoogtebestand Nederland – Versie 4 [Current Dutch Elevation – Version 4]. Dataset accessed February 2024. https://Rijkswaterstaat.ahn.nl.

Anderson, E.I. & Bakker, M., 2008. Groundwater flow through anisotropic fault zones in multiaquifer systems. Water Resources Research **44**(W11433): 1–11. DOI: 10.1029/2008WR006925

Antonellini, M. & Aydin, A., 1994. Effect of faulting on fluid flow in porous sandstones: petrophysical properties. Bulletin of the American Association of Petroleum Geologists **78**(3): 355–377. DOI: 10.1306/BDFF90AA-1718-11D7-8645000102C1865D

Aubert, I., Lamarche, J. & Léonide, P., 2021. Ternary fault permeability diagram: an innovative way to estimate fault zones hydraulics. Journal of Structural Geology **147**(104349): 1–9. DOI: 10.1016/j.jsg.2021.104349

Babiker, M. & Gudmundsson, A., 2004. The effects of dykes and faults on groundwater flow in an arid land: the Red Sea Hills, Sudan. Journal of Hydrology **297**(1): 256–273. DOI: 10.1016/j.jhydrol.2004.04.018

Bakker, M., 2006. Analytic element modeling of embedded multiaquifer domains. Ground Water **44**(1): 81–85. DOI: 10.1111/j.1745-6584.2005.00080.x

Bense, V.F., 2004. The hydraulic properties of faults in unconsolidated sediments and their impact on groundwater flow: a study in the Roer Valley Rift System and adjacent areas in the Lower Rhine Embayment. PhD thesis. VU University Amsterdam, 143 pp. https://research.vu.nl/ws/portalfiles/portal/42171286/complete+dissertation.pdf

Bense, V.F., Gleeson, T., Loveless, S.E., Bour, O. & Scibek, J., 2013. Fault zone hydrogeology. Earth-Science Reviews **127**: 171–192. DOI: 10.1016/j.earscirev.2013.09.008

Bense, V.F. & Kooi, H., 2004. Temporal and spatial variations of shallow subsurface temperature as a record of lateral variations in groundwater flow. Journal of Geophysical Research **109**(B04103): 1–13. DOI: 10.1029/2003JB002782

Bense, V.F. & Person, M.A., 2006. Faults as conduit–barrier system to fluid flow in siliciclastic sedimentary aquifers. Water Resources Research **42**(W05421): 1–18. DOI: 10.1029/2005WR004480

Bense, V.F., Person, M.A., Chaudhary, K., You, Y., Cremer, N. & Simon, S., 2008. Thermal anomalies indicate preferential flow along faults in unconsolidated sedimentary aquifers. Geophysical Research Letters **35**(L24406): 1–6. DOI: 10.1029/2008GL036017

Bense, V.F. & Van Balen, R., 2004. The effect of fault relay and clay smearing on groundwater flow patterns in the Lower Rhine Embayment. Basin Research **16**(3): 397–411. DOI: 10.1111/j.1365-2117.2004.00238.x

Bense, V.F., Van Balen, R.T. & De Vries, J.J., 2003a. The impact of faults on the hydrogeological conditions in the Roer Valley Rift System: an overview. Netherlands Journal of Geosciences **82**(1): 41–54. DOI: 10.1017/S0016774600022782

Bense, V.F., Van den Berg, E.H. & Van Balen, R.T., 2003b. Deformation mechanisms and hydraulic properties of fault zones in unconsolidated sediments; the Roer Valley Rift System, the Netherlands. Hydrogeology Journal **11**: 319–332. DOI: 10.1007/s10040-003-0262-8

Bockheim, J.G. & Tarnocai, C., 1998. Recognition of cryoturbation for classifying permafrost-affected soils. Geoderma **81**(3–4): 281–293. DOI: 10.1016/S0016-7061(97)00115-8

Broers, H.P., Sültenfuß, J., Aeschbach, W., Kersting, A., Menkovich, A., De Weert, J. & Castelijns, J., 2021. Paleoclimate signals and groundwater age distributions from 39 public water works in the Netherlands; insights from noble gases and carbon, hydrogen and oxygen isotope tracers. Water Resources Research **57**: 1–26. DOI: 10.1029/2020WR029058

Buma, J. & De Heer, E., 2024. Praktijkrichtlijn bepaling verzadigde doorlatendheid en porositeit van niet-cohesieve grondmonsters: Praktijkrichtlijn TNO-GDN [Practical guideline determination of saturated conductivity and porosity of non-cohesive soil samples]. Internal report TNO, Utrecht 2024 R11257: 1–27.

Caine, J.S., Evans, J.P. & Forster, C.B., 1996. Fault zone architecture and permeability structure. Geology **24**(11): 1025–1028. DOI: 10.1130/0091-7613(1996)024%3C1025:FZAAPS%3E2.3.CO;2

Casillas-Trasvina, A., Rogiers, B., Beerten, K., Wouters, L. & Walraevens, K., 2022. Exploring the hydrological effects of normal faults at the boundary of the Roer Valley Graben in Belgium using a catchment-scale groundwater flow model. Hydrogeology Journal **30**(2): 627–645. DOI: 10.1007/s10040-021-02423-y

Cook, P.G., Banks, E.W., Marshall, S.K., Harrington, G.A., Batlle-Aguilar, J., Dogramaci, S. & Turnadge, C., 2022. Inferring fault hydrology using groundwater age tracers. Journal of Hydrology **610**: 1–16. DOI: 10.1016/j.jhydrol.2022.127905

Deckers, J., Van Noten, K., Schiltz, M., Lecocq, T. & Vanneste, K., 2018. Integrated study on the topographic and shallow subsurface expression of the Grote Brogel Fault at the boundary of the Roer Valley Graben, Belgium. Tectonophysics **722**: 486–506. DOI: 10.1016/j.tecto.2017.11.019

Díaz-Curiel, J., Biosca, B., Arévalo-Lomas, L., Miguel, M.J. & Caparrini, N., 2022. Advances in the hydraulic interpretation of water wells using flowmeter logs. Hydrology and Earth System Sciences **26**(10): 2617–2636. DOI: 10.5194/hess-26-2617-2022

DINOloket, 2018. Data en Informatie van de Nederlandse Ondergrond TNO-GDN [Data and Information on the Dutch Subsurface TNO-GDN]. Dataset accessed June 2018. https://dinoloket.nl.

DINOloket, 2024. Data en Informatie van de Nederlandse Ondergrond TNO-GDN [Data and Information on the Dutch Subsurface TNO-GDN]. Dataset accessed February 2024. https://dinoloket.nl.

Eijkelkamp, 2022. Laboratory permeameters: user manual (version 2022-06). Eijkelkamp Soil and Water, Giesbeek, the Netherlands. https://royaleijkelkamp.com/media/bhghn3me/m-0902e-permeameter.pdf

Freeze, R.A. & Cherry, J.A., 1979. Groundwater. Freeze and Cherry Groundwater Book. Englewood Cliffs, NJ: Prentice-Hall, 604 pp.

Gumm, L.P., Bense, V.F., Dennis, P.F., Hiscock, K.M., Cremer, N. & Simon, S., 2016. Dissolved noble gases and stable isotopes as tracers of preferential fluid flow along faults in the Lower Rhine Embayment, Germany. Hydrogeology Journal **24**: 99–108. DOI: 10.1007/s10040-015-1321-7

Haneberg, W.C., 1995. Steady state groundwater flow across idealized faults. Water Resources Research **31**(7): 1815–1820. DOI: 10.1029/95WR01178

Hiddink, H.A., 2019. Uden-Peelrandbreuk: Archeologisch onderzoek van een laat-middeleeuwse gracht in een proefsleuf aan de Lageburchtweg [Uden-Peel Boundary Fault: Archaeological Inventory of a Late Medieval Moat in a Trench at Lageburchtweg]. Report 631. VU University Amsterdam.

Houtgast, R.F. & Van Balen, R.T., 2000. Neotectonics of the Roer Valley Rift System, the Netherlands. Global and Planetary Change, Amsterdam **27**(1–4): 131–146. DOI: 10.1016/S0921-8181(01)00063-7

Hummelman, J., Maljers, D., Menkovic, A., Reindersma, R., Stafleu, J. & Vernes, R., 2019a. Totstandkomingsrapport Digitaal Geologisch Model (DGM) [Development report Digital Geological Model DGM]. TNO-report 2019 R11653. Utrecht: TNO. https://broloket.nl/sites/default/files/Totstandkomingsrapport-DGM.pdf

Hummelman, J., Maljers, D., Menkovic, A., Reindersma., R., Vernes, R. & Stafleu, J., 2019b. Totstandkomingsrapport Hydrogeologisch Model (REGIS II) [Development report hydrogeological model REGIS II]. TNO-report 2019 R11654. Utrecht: TNO. https://dinoloket.nl/sites/default/files/Totstandkomingsrapport-REGIS-II.pdf

Kasse, C., Vandenberghe, D., De Corte, F. & Van Den Haute P., 2007. Late Weichselian fluvio-aeolian sands and coversands of the type locality Grubbenvorst (southern Netherlands): sedimentary environments, climate record and age. Journal of Quaternary Science **22**: 695–708. DOI: 10.1002/jqs.1087

Kettermann, M., Thronberens, S., Juarez, O., Urai J.L., Ziegler, M., Asmus, S. & Krüger U., 2016. Mechanisms of clay smear formation in unconsolidated sediments – insights from 3-D observations of excavated normal faults. Solid Earth **7**(3): 789–815. DOI: 10.5194/se-7-789-2016

KNMI, 2024. Dataset Aardbevingscatalogus [Earthquake Catalog Dataset]. Dataset accessed January 2024. https://knmi.nl/kennis-en-datacentrum/dataset/aardbevingscatalogus

Konert, M. & Vandenberghe, J., 1997. Comparison of laser grain size analysis with pipette and sieve analysis: a solution for the underestimation of the clay fraction. Sedimentology **44**: 523–535. DOI: 10.1,046/j.1365-3091.1997.d01-38.x

Lapperre, R.E., Bense, V.F., Kasse, C. & Van Balen R.T., 2022. Temporal and spatial variability of cross-fault groundwater-level differences: the impact of fault-induced permeability reduction, precipitation and evapotranspiration. Hydrogeology Journal **30**: 1233–1257. DOI: 10.1007/s10040-022-02465-w

Lapperre, R.E., Kasse, C., Bense, V.F. & Van Balen R.T., 2025. Fault sealing in unconsolidated sediments through interporous accumulation of fines. Hydrogeology Journal **33**: 1721–1743. DOI: 10.1007/s10040-025-02958-4

Lapperre, R.E., Kasse, C., Bense, V.F., Woolderink, H.A.G. & Van Balen, R.T., 2019. An overview of fault zone permeabilities and groundwater level steps in the Roer Valley Rift System. Netherlands Journal of Geosciences **98**: 1–12. DOI: 10.1017/njg.2019.4

Michon, L. & Van Balen, R.T., 2005. Characterization and quantification of active faulting in the Roer valley rift system based on high precision digital elevation models. Quaternary Science Reviews **24**(3–4): 455–472. DOI: 10.1016/j.quascirev.2003.11.009

Michon, L., Van Balen, R.T., Merle, O. & Pagnier, H., 2003. The Cenozoic evolution of the Roer Valley Rift System integrated at a European scale. Tectonophysics **367**(1–2): 101–126. DOI: 10.1016/S0040-1951(03)00132-X

NEN-EN-ISO 17892-11, 2019. Geotechnical investigation and testing: laboratory testing of soil, part 11: permeability tests. ISO 17892-11:2019. Delft: International Organization for Standardization (ISO).

NSO, 2018. Netherlands Space Office. Accessed early 2018. https://www.satellietdataportaal.nl

NSO, 2023. Netherlands Space Office. Accessed February 2024. https://www.satellietdataportaal.nl

Sanchez-Vila, X., Guadagnini, A. & Carrera, J., 2006. Representative hydraulic conductivities in saturated groundwater flow. Reviews of Geophysics **44**(3): 1–46. DOI: 10.1029/2005RG000169

Schokker, J., Cleveringa, P., Murray, A.S., Wallinga, J. & Westerhoff, W.E., 2005. An OSL dated Middle and Late Quaternary sedimentary record in the Roer Valley Graben (southeastern Netherlands). Quatenary Science Reviews **24**(20–21): 2243–2264. DOI: 10.1016/j.quascirev.2005.01.010

Schokker, J., Weerts, H.J.T., Westerhoff, W.E., Berendsen, H.J.A. & Den Otter, C., 2007. Introduction of the Boxtel formation and implications for Quaternary lithostratigraphy of the Netherlands. Netherlands Journal of Geosciences **86**(3): 197–210. DOI: 10.1017/S0016774600077805

Scibek, J., 2020. Multidisciplinary database of permeability of fault zones and surrounding protolith rocks at world-wide sites. Scientific Data **7**(95): 1–14. DOI: 10.1038/s41597-020-0435-5

Scibek, J., Gleeson, T. & McKenzie, J.M., 2016. The biases and trends in fault zone hydrogeology conceptual models: global compilation and categorical data analysis. Geofluids **16**(4): 782–798. DOI: 10.1111/gfl.12188

Sheldon, H.A., Crombez, V., Poulet, T., Kelka, U., Kunzmann, M. & Kerrison, E., 2023. Realistic permeability distributions in faults and sediments: the key to predicting fluid flow in sedimentary basins. Basin Research **35**: 2118–2139. DOI: 10.1111/bre.12792

Stafleu, J., Reindersma, R., De Bruijn, R., Kars, R., Schokker, J., Menkovic, A., Van de Ven, T., Heerema, C. & Koster, K., 2023. Totstandkomingsrapport GeoTOP – aanvullingen bij versie v1.6 [Development report GeoTOP – additions to version v1.6]. TNO-report 2023 R11636. Utrecht: TNO. https://publications.tno.nl/publication/34641369/HBwQy0/TNO-2023-R11636.pdf

Stephens, D.B., Hsu, K.C., Prieksat, M.A., Ankeny, M.D., Blandford, N., Roth, T.L., Kelsey, J.A. & Whitworth J.R., 1998. A comparison of estimated and calculated effective porosity. Hydrogeology Journal **6**: 156–165. DOI: 10.1007/s100400050141

USDA, 1993. Soil Survey Manual. Soil Survey Staff, Soil Conservation Service. U.S. Department of Agriculture Handbook 18. Washington, DC: U.S. Department of Agriculture, 437 pp.

Van Balen, R.T., Bakker, M.A.J., Kasse, C., Wallinga, J. & Woolderink H.A.G., 2019. A Late Glacial surface rupturing earthquake at the Peel Boundary fault zone, Roer Valley Rift System, the Netherlands. Quaternary Science Reviews **218**: 254–266. DOI: 10.1016/j.quascirev.2019.06.033

Van Balen, R.T., Houtgast, R.F. & Cloetingh, S.A.P.L., 2005. Neotectonics of the Netherlands: a review. Quaternary Science Reviews **24**(3–4): 439–454. DOI: 10.1016/j.quascirev.2004.01.011

Van Balen, R.T., Kasse, C., Wallinga, J. & Woolderink H.A.G., 2021. Middle to Late Pleistocene faulting history of the Heerlerheide fault, Roer Valley Rift System, influenced by glacio-isostacy and mining-induced displacement. Quaternary Science Reviews **268**: 1–18. DOI: 10.1016/j.quascirev.2021.107111

Van Balen, R.T., Lapperre, R.E., Woolderink, H.A.G., Wallinga, J. & Kasse, C., 2024. Magnitudes and surface rupture lengths of paleo-earthquakes at the NW-part of the Peel Boundary fault zone, Roer Valley Rift System. Tectonophysics **879**: 1–15. DOI: 10.1016/j.tecto.2024.230322

Van der Woude, J. & Van Leeuwen, J., 2020. Een gegraven watergang bij de Peelrand als spiegel van de middeleeuwse vegetatie [A dug watercourse at the Peel Boundary Fault as mirror of the medieval vegetation]. Grondboor & Hamer **74**(5–6): 208–213. https://natuurtijdschriften.nl/pub/1021596/9.-G-H2020nr5-6_art-644vander-Woude.pdf

Vandenberghe, D.A.G., Derese, C., Kasse, C. & Van den haute, P., 2013. Late Weichselian (fluvio-)aeolian sediments and Holocene drift-sands of the classic type locality in Twente (E Netherlands): a high-resolution dating study using optically stimulated luminescence. Quaternary Science Reviews **68**: 96–113. DOI: 10.1016/j.quascirev.2013.02.009

Wang, C.-Y., 2022. A new mechanism for earthquake-enhanced permeability. Water Resources Research **58**(5): 1–9. DOI: 10.1029/2021WR031503

Wang, T., Li, J., Hou, J., Ma, Y., Li, P., Tong, Y., Li, J. & Li, Z., 2023. Hydrological and sediment connectivity under freeze-thaw meltwater compound erosion conditions on a loessal slope. International Soil and Water Conservation Research **11**(2): 402–411. DOI: 10.1016/j.iswcr.2022.11.002

Westerhoff, W.E., Kemna, H.A. & Boenigk, W., 2008. The confluence area of Rhine, Meuse, and Belgian rivers: Late Pliocene and Early Pleistocene fluvial history of the northern Lower Rhine Embayment. Netherlands Journal of Geosciences **87**(1): 107–125. DOI: 10.1017/S0016774600024070

Zhou, Y. & Li, W., 2011. A review of regional groundwater flow modeling. Geoscience Frontiers **2**(2): 205–214. DOI: 10.1016/j.gsf.2011.03.003

Zhu, L., Gong, H., Chen, Y., Li, X., Chang, X. & Cui, Y., 2016. Improved estimation of hydraulic conductivity by combining stochastically simulated hydrofacies with geophysical data. Scientific Reports **6**: 22224. DOI: 10.1038/srep22224

https://doi.org/10.70712/NJG.v105.12686

Appendix 1

Sample (number)	Field sample (field code)	Laboratory sample position in field sample (Appendix 2) (cm)	Coordinate field sample[a] (X & Y)	Field sample depth and sample direction (m NAP)[b]	Tectonic position (Fig. 6)	Tectonic setting (–)	Trench sampling section analyses (Fig. 6)	Median grain size (GZ)[c] (µm)	Clay (< 8 µm) (vol%)	Silt (8–63 µm) (vol%)	Sand (63–2,000 µm) (vol%)	Total organic matter (LOI 550°C)[d] (wt%)	Total carbonate ($CaCO_3$) (wt%)	Total porosity (P_{total})[e] (%)	Saturated hydraulic conductivity (K_{sat})[f] (m d^{-1} at 10°C)	Hydraulic conductivity direction (–)	Measuring method (–)
1	DL1	12–17	169,417.264 407,750.578	10.234 (horizontal sample)	Fault	Deformed	Section 3	171	1.14	3.54	95.31	0.75	0.42	34.3	2.6	Horizontal (K_h)	Permeameter[g]
2	DL1	24–29	169,417.264 407,750.578	10.234 (horizontal sample)	Fault	Deformed	Section 3	169	1.31	5.38	93.31	0.32	0.25	34.3	2.6	Horizontal (K_h)	Permeameter
3	DL1	44–49	169,417.264 407,750.578	10.234 (horizontal sample)	Damage zone foot wall	Deformed	Section 2	304	0.60	0.70	98.70	0.19	0.05	33.6	10.0	Horizontal (K_h)	Permeameter
4	DL2	5–10	169,416.522 407,751.300	10.231 (horizontal sample)	Fault	Deformed	Section 3	164	1.35	5.19	93.46	0.73	0.37	34.4	0.9	Horizontal (K_h)	Permeameter
5	DL2	13–18	169,416.522 407,751.300	10.231 (horizontal sample)	Fault	Deformed	Section 3	195	1.06	2.62	96.31	0.52	0.32	30.5	2.4	Horizontal (K_h)	Permeameter
6	DL3	4–6	169,416.422 407,751.427	10.248 (horizontal sample)	Fault	Deformed	Section 3	172	1.37	5.83	92.80	0.64	0.41	35.2	0.1	Vertical (K_v)	Modified oedometer[h]
7	DL4	0–5	169,416.536 407,751.417	10.333 (horizontal sample)	Fault	Deformed	Section 3	153	1.62	5.82	92.56	0.85	0.46	33.8	0.04	Horizontal (K_h)	Permeameter
8	DL5	4 –9	169,417.332 407,750.021	10.267 (horizontal sample)	Fault	Deformed	Section 3	195	0.89	3.25	95.85	0.26	0.23	34.0	3.5	Vertical (K_v)	Permeameter
9	DL5	12–17	169,417.332 407,750.021	10.267 (horizontal sample)	Fault	Deformed	Section 3	185	1.10	3.63	95.27	0.33	0.24	34.3	1.3	Horizontal (K_h)	Permeameter
10	DL5	26–36	169,417.332 407,750.021	10.267 (horizontal sample)	Fault	Deformed	Section 3	228	1.12	2.79	96.09	0.59	0.16	32.9	0.5	Horizontal (K_h)	Triaxial[h]
11	DL5	43–48	169,417.332 407,750.021	10.267 (horizontal sample)	Damage zone foot wall	Deformed	Section 2	242	0.81	1.96	97.23	0.30	0.18	28.5	6.5	Horizontal (K_h)	Permeameter
12	DL5	50–55	169,417.332 407,750.021	10.267 (horizontal sample)	Damage zone foot wall	Deformed	Section 2	257	0.66	0.98	98.36	0.19	0.14	31.2	9.6	Vertical (K_v)	Permeameter
13	DL6	7–17	169,416.738 407,750.991	10.212 (horizontal sample)	Fault	Deformed	Section 3	202	1.01	2.40	96.59	0.58	0.22	38.7	0.2	Horizontal (K_h)	Triaxial
14	DL6	22–27	169,416.738 407,750.991	10.212 (horizontal sample)	Fault	Deformed	Section 3	193	1.07	3.16	95.77	0.28	0.20	34.2	3.4	Vertical (K_v)	Permeameter
15	DL6	32–37	169,416.738 407,750.991	10.212 (horizontal sample)	Fault	Deformed	Section 3	199	0.94	2.95	96.11	0.25	0.17	33.1	3.6	Horizontal (K_h)	Permeameter
16	DL6	43–48	169,416.738 407,750.991	10.212 (horizontal sample)	Fault	Deformed	Section 3	216	0.90	1.38	97.73	0.43	0.17	32.4	7.1	Vertical (K_v)	Permeameter
17	DL6	55–60	169,416.738 407,750.991	10.212 (horizontal sample)	Damage zone foot wall	Deformed	Section 2	262	0.62	0.77	98.61	0.21	0.12	27.7	3.0	Horizontal (K_h)	Permeameter

https://doi.org/10.7012/NJG.v105.12686

Sample (number)	Field sample (field code)	Laboratory sample position in field sample (Appendix 2) (cm)	Coordinate field sample[a] (X & Y)	Field sample depth and sample direction (m NAP)[b]	Tectonic position (Fig. 6)	Tectonic setting (–)	Trench sampling section analyses (Fig. 6)	Median grain size (GZ)[c] (µm)	Clay (< 8 µm) (vol%)	Silt (8–63 µm) (vol%)	Sand (63–2,000 µm) (vol%)	Total organic matter (LOI 550°C)[d] (wt%)	Total carbonate ($CaCO_3$) (wt%)	Total porosity (P_{total})[e] (%)	Saturated hydraulic conductivity (K_{sat})[f] (m d^{-1} at 10°C)	Hydraulic conductivity direction (–)	Measuring method (–)
18	DL7	7–12	169,416.255 407,751.128	9.869 (horizontal sample)	Fault	Deformed	Section 3	190	0.96	1.92	97.12	0.42	0.26	36.1	0.2	Horizontal (K_h)	Permeameter
19	DL7	16–21	169,416.255 407,751.128	9.869 (horizontal sample)	Fault	Deformed	Section 3	208	0.86	1.19	97.94	0.33	0.21	33.2	0.1	Vertical (K_v)	Permeameter
20	DL7	25–30	169,416.255 407,751.128	9.869 (horizontal sample)	Fault	Deformed	Section 3	238	1.04	2.28	96.68	0.63	0.28	31.7	1.0	Horizontal (K_h)	Permeameter
21	DL7	35–40	169,416.255 407,751.128	9.869 (horizontal sample)	Damage zone foot wall	Deformed	Section 2	244	0.95	1.79	97.26	0.26	0.17	33.2	13.3	Horizontal (K_h)	Permeameter
22	DL7	49–54	169,416.255 407,751.128	9.869 (horizontal sample)	Damage zone foot wall	Deformed	Section 2	280	1.01	1.09	97.91	0.20	0.14	32.5	11.2	Vertical (K_v)	Permeameter
23	DL8	3–8	169,416.798 407,750.394	9.832 (horizontal sample)	Fault	Deformed	Section 3	146	1.35	5.20	93.45	0.37	0.31	35.3	2.7	Vertical (K_v)	Permeameter
24	DL8	11–16	169,416.798 407,750.394	9.832 (horizontal sample)	Fault	Deformed	Section 3	155	1.58	9.49	88.94	0.59	0.44	35.6	0.5	Vertical (K_v)	Permeameter
25	DL8	21–26	169,416.798 407,750.394	9.832 (horizontal sample)	Fault	Deformed	Section 3	175	1.10	2.01	96.89	0.74	0.35	35.0	1.6	Vertical (K_v)	Permeameter
26	DL8	35–40	169,416.798 407,750.394	9.832 (horizontal sample)	Fault	Deformed	Section 3	256	0.69	1.57	97.73	0.40	0.18	30.5	1.7	Vertical (K_v)	Permeameter
27	DL8	49–54	169,416.798 407,750.394	9.832 (horizontal sample)	Damage zone foot wall	Deformed	Section 2	375	0.75	0.89	98.35	0.24	0.15	31.9	18.4	Vertical (K_v)	Permeameter
28	DL9	4–9	169,417.110 407,749.991	9.791 (horizontal sample)	Fault	Deformed	Section 3	159	1.18	2.76	96.06	0.32	0.24	35.6	2.9	Horizontal (K_h)	Permeameter
29	DL9	12–17	169,417.110 407,749.991	9.791 (horizontal sample)	Fault	Deformed	Section 3	170	1.23	3.43	95.34	0.41	0.26	35.9	0.5	Horizontal (K_h)	Permeameter
30	DL9	25–35	169,417.110 407,749.991	9.791 (horizontal sample)	Fault	Deformed	Section 3	279	0.92	2.27	96.81	0.60	0.33	32.9	0.2	Horizontal (K_h)	Triaxial
31	DL9	43–48	169,417.110 407,749.991	9.791 (horizontal sample)	Damage zone foot wall	Deformed	Section 2	384	0.83	0.92	98.25	0.24	0.13	31.7	19.2	Horizontal (K_h)	Permeameter
32	DL9	53–58	169,417.110 407,749.991	9.791 (horizontal sample)	Damage zone foot wall	Deformed	Section 2	411	0.71	0.51	98.78	0.20	0.13	30.1	22.6	Horizontal (K_h)	Permeameter
33	DL10	5–15	169,416.563 407,750.840	9.791 (horizontal sample)	Fault	Deformed	Section 3	199	1.06	1.38	97.56	0.76	0.27	35.5	0.04	Horizontal (K_h)	Triaxial
34	DL10	18–23	169,416.563 407,750.840	9.791 (horizontal sample)	Damage zone foot wall	Deformed	Section 2	315	0.71	1.01	98.29	0.31	0.15	31.4	10.5	Horizontal (K_h)	Permeameter

https://doi.org/10.70712/NJG.v105.12686

Sample (number)	Field sample (field code)	Laboratory sample position in field sample (Appendix 2) (cm)	Coordinate field sample[a] (X & Y)	Field sample depth and sample direction (m NAP)[b]	Tectonic position (Fig. 6)	Tectonic setting (–)	Trench sampling section analyses (Fig. 6)	Median grain size (GZ)[c] (µm)	Clay (< 8 µm) (vol%)	Silt (8–63 µm) (vol%)	Sand (63–2,000 µm) (vol%)	Total organic matter (LOI 550°C)[d] (wt%)	Total carbonate ($CaCO_3$) (wt%)	Total porosity (P_{total})[e] (%)	Saturated hydraulic conductivity (K_{sat})[f] (m d^{-1} at 10°C)	Hydraulic conductivity direction (–)	Measuring method (–)
35	DL10	29–34	169,416.563 407,750.840	9.791 (horizontal sample)	Damage zone foot wall	Deformed	Section 2	305	0.88	1.46	97.66	0.24	0.14	33.6	9.0	Vertical (K_v)	Permeameter
36	DL10	39–44	169,416.563 407,750.840	9.791 (horizontal sample)	Damage zone foot wall	Deformed	Section 2	300	0.95	1.66	97.39	0.25	0.14	34.3	10.7	Horizontal (K_h)	Permeameter
37	DL10	49–54	169,416.563 407,750.840	9.791 (horizontal sample)	Damage zone foot wall	Deformed	Section 2	311	0.83	1.16	98.01	0.24	0.14	33.2	10.9	Vertical (K_v)	Permeameter
38	DL11	5–10	169,416.112 407,750.808	9.712 (vertical sample)	Fault	Deformed	Section 3	183	1.03	2.93	96.04	0.30	0.20	35.7	0.7	Vertical (K_v)	Permeameter
39	DL11	13–18	169,416.112 407,750.808	9.712 (vertical sample)	Fault	Deformed	Section 3	199	0.97	1.67	97.36	0.33	0.27	33.1	1.1	Horizontal (K_h)	Permeameter
40	DL11	25–30	169,416.112 407,750.808	9.712 (vertical sample)	Fault	Deformed	Section 3	194	1.03	2.23	96.74	0.46	0.31	32.8	0.03	Vertical (K_v)	Permeameter
41	DL11	35–40	169,416.112 407,750.808	9.712 (vertical sample)	Fault	Deformed	Section 3	226	0.84	1.76	97.41	0.32	0.22	30.8	2.7	Horizontal (K_h)	Permeameter
42	DL11	45–50	169,416.112 407,750.808	9.712 (vertical sample)	Fault	Deformed	Section 3	248	1.33	5.75	92.92	0.56	0.39	29.1	0.8	Horizontal (K_h)	Permeameter
43	DL12	6–11	169,416.483 407,750.304	9.662 (vertical sample)	Fault	Deformed	Section 3	154	1.36	2.65	95.99	0.63	0.29	33.4	0.01	Horizontal (K_h)	Permeameter
44	DL12	14–19	169,416.483 407,750.304	9.662 (vertical sample)	Fault	Deformed	Section 3	165	1.37	5.08	93.56	0.37	0.25	33.2	2.2	Horizontal (K_h)	Permeameter
45	DL12	25–30	169,416.483 407,750.304	9.662 (vertical sample)	Fault	Deformed	Section 3	192	1.25	4.52	94.22	0.33	0.23	32.0	2.3	Vertical (K_v)	Permeameter
46	DL12	46–51	169,416.483 407,750.304	9.662 (vertical sample)	Damage zone hanging wall	Deformed	Section 4	326	0.75	0.73	98.53	0.29	0.18	31.3	9.5	Vertical (K_v)	Permeameter
47	DL12	52–57	169,416.483 407,750.304	9.662 (vertical sample)	Damage zone hanging wall	Deformed	Section 4	479	0.69	0.63	98.69	0.24	0.16	30.3	22.7	Horizontal (K_h)	Permeameter
48	DL13	3–8	169,416.790 407,749.827	9.667 (vertical sample)	Damage zone hanging wall	Deformed	Section 4	198	0.91	1.66	97.43	0.25	0.20	35.9	5.1	Horizontal (K_h)	Permeameter
49	DL13	10–15	169,416.790 407,749.827	9.667 (vertical sample)	Fault	Deformed	Section 3	156	1.35	4.23	94.43	0.35	0.27	35.4	2.2	Vertical (K_v)	Permeameter
50	DL13	20–30	169,416.790 407,749.827	9.667 (vertical sample)	Fault	Deformed	Section 3	180	1.51	5.68	92.81	0.59	0.28	30.6	0.004	Vertical (K_v)	Triaxial

https://doi.org/10.7012/NJG.v105.12686

Sample (number)	Field sample (field code)	Laboratory sample position in field sample (Appendix 2) (cm)	Coordinate field sample[a] (X & Y)	Field sample depth and sample direction (m NAP)[b]	Tectonic position (Fig. 6)	Tectonic setting (–)	Trench sampling section analyses (Fig. 6)	Median grain size (GZ)[c] (µm)	Clay (< 8 µm) (vol%)	Silt (8–63 µm) (vol%)	Sand (63–2,000 µm) (vol%)	Total organic matter (LOI 550°C)[d] (wt%)	Total carbonate ($CaCO_3$) (wt%)	Total porosity (P_{total})[e] (%)	Saturated hydraulic conductivity (K_{sat})[f] (m d^{-1} at 10°C)	Hydraulic conductivity direction (–)	Measuring method (–)
51	DL14	4–9	169,423.325 407,754.898	12.567 (vertical sample)	Foot wall	Undeformed	Section 1	206	1.02	3.59	95.39	0.32	0.17	35.8	0.3	Vertical (K_v)	Permeameter
52	DL14	11–16	169,423.325 407,754.898	12.567 (vertical sample)	Foot wall	Undeformed	Section 1	202	0.82	2.21	96.96	0.26	0.19	36.1	2.7	Horizontal (K_h)	Permeameter
53	DL14	25–30	169,423.325 407,754.898	12.567 (vertical sample)	Foot wall	Undeformed	Section 1	174	0.85	1.48	97.67	0.25	0.17	37.4	3.4	Vertical (K_v)	Permeameter
54	DL14	35–40	169,423.325 407,754.898	12.567 (vertical sample)	Foot wall	Undeformed	Section 1	232	0.66	0.99	98.36	0.26	0.18	36.0	5.6	Horizontal (K_h)	Permeameter
55	DL14	48–53	169,423.325 407,754.898	12.567 (vertical sample)	Foot wall	Undeformed	Section 1	204	0.86	2.74	96.41	0.34	0.20	36.5	1.1	Vertical (K_v)	Permeameter
56	DL15	8–13	169,422.762 407,754.504	12.014 (vertical sample)	Foot wall	Undeformed	Section 1	179	1.09	3.33	95.58	0.57	0.23	35.4	0.02	Vertical (K_v)	Permeameter
57	DL15	20–25	169,422.762 407,754.504	12.014 (vertical sample)	Foot wall	Undeformed	Section 1	204	0.70	1.13	98.17	0.21	0.17	35.1	6.6	Horizontal (K_h)	Permeameter
58	DL15	38–43	169,422.762 407,754.504	12.014 (vertical sample)	Foot wall	Undeformed	Section 1	223	0.70	1.52	97.78	0.23	0.17	35.4	5.4	Vertical (K_v)	Permeameter
59	DL15	53–58	169,422.762 407,754.504	12.014 (vertical sample)	Foot wall	Undeformed	Section 1	203	0.87	3.13	96.00	0.23	0.19	30.0	3.9	Horizontal (K_h)	Permeameter
60	DL16	6–11	169,422.171 407,754.094	11.457 (vertical sample)	Foot wall	Undeformed	Section 1	173	1.04	3.35	95.61	0.27	0.23	34.7	3.4	Horizontal (K_h)	Permeameter
61	DL16	14–19	169,422.171 407,754.094	11.457 (vertical sample)	Foot wall	Undeformed	Section 1	166	1.15	3.90	94.94	0.31	0.23	35.9	3.1	Vertical (K_v)	Permeameter
62	DL16	26–31	169,422.171 407,754.094	11.457 (vertical sample)	Foot wall	Undeformed	Section 1	179	1.10	4.26	94.64	0.37	0.26	36.9	0.1	Vertical (K_v)	Permeameter
63	DL16	34–39	169,422.171 407,754.094	11.457 (vertical sample)	Foot wall	Undeformed	Section 1	211	0.89	2.35	96.76	0.24	0.17	34.3	5.7	Horizontal (K_h)	Permeameter
64	DL16	43–48	169,422.171 407,754.094	11.457 (vertical sample)	Foot wall	Undeformed	Section 1	183	1.12	3.47	95.41	0.35	0.22	36.7	0.9	Vertical (K_v)	Permeameter
65	DL16	52–57	169,422.171 407,754.094	11.457 (vertical sample)	Foot wall	Undeformed	Section 1	187	1.20	4.59	94.20	0.37	0.26	34.1	3.5	Horizontal (K_h)	Permeameter
66	DL17	5–10	169,421.662 407,753.707	10.906 (vertical sample)	Foot wall	Undeformed	Section 1	353	0.75	0.90	98.35	0.22	0.14	27.4	5.7	Horizontal (K_h)	Permeameter
67	DL17	21–26	169,421.662 407,753.707	10.906 (vertical sample)	Foot wall	Undeformed	Section 1	405	0.84	0.97	98.19	0.22	0.16	31.2	11.6	Vertical (K_v)	Permeameter
68	DL17	30–35	169,421.662 407,753.707	10.906 (vertical sample)	Foot wall	Undeformed	Section 1	384	0.84	0.79	98.37	0.21	0.14	31.8	14.4	Horizontal (K_h)	Permeameter
69	DL17	43–48	169,421.662 407,753.707	10.906 (vertical sample)	Foot wall	Undeformed	Section 1	244	2.32	5.25	92.43	0.57	0.25	32.5	2.3	Vertical (K_v)	Permeameter
70	DL17	52–57	169,421.662 407,753.707	10.906 (vertical sample)	Foot wall	Undeformed	Section 1	389	1.12	1.40	97.47	0.33	0.05	30.9	10.0	Horizontal (K_h)	Permeameter

https://doi.org/10.70712/NJG.v105.12686

Sample (number)	Field sample (field code)	Laboratory sample position in field sample (Appendix 2) (cm)	Coordinate field sample[a] (X & Y)	Field sample depth and sample direction (m NAP)[b]	Tectonic position (Fig. 6)	Tectonic setting (–)	Trench sampling section analyses (Fig. 6)	Median grain size (GZ)[c] (µm)	Clay (< 8 µm) (vol%)	Silt (8–63 µm) (vol%)	Sand (63–2,000 µm) (vol%)	Total organic matter (LOI 550°C)[d] (wt%)	Total carbonate ($CaCO_3$) (wt%)	Total porosity (P_{total})[e] (%)	Saturated hydraulic conductivity (K_{sat})[f] (m d^{-1} at 10°C)	Hydraulic conductivity direction (–)	Measuring method (–)
71	DL18	5–10	169,421.215 407,753.417	10.290 (vertical sample)	Foot wall	Undeformed	Section 1	322	0.83	0.95	98.23	0.23	0.18	32.5	13.7	Horizontal (K_v)	Permeameter
72	DL18	13–18	169,421.215 407,753.417	10.290 (vertical sample)	Foot wall	Undeformed	Section 1	394	0.67	0.44	98.88	0.20	0.15	33.0	10.4	Horizontal (K_h)	Permeameter
73	DL18	21– 26	169,421.215 407,753.417	10.290 (vertical sample)	Foot wall	Undeformed	Section 1	400	0.73	0.50	98.76	0.21	0.15	33.6	16.6	Vertical (K_v)	Permeameter
74	DL18	28–33	169,421.215 407,753.417	10.290 (vertical sample)	Foot wall	Undeformed	Section 1	362	0.89	0.98	98.12	0.26	0.17	31.0	13.6	Horizontal (K_h)	Permeameter
75	DL18	37–42	169,421.215 407,753.417	10.290 (vertical sample)	Foot wall	Undeformed	Section 1	321	2.82	5.25	91.93	0.97	0.45	30.0	2.1	Vertical (K_v)	Permeameter
76	DL18	45–50	169,421.215 407,753.417	10.290 (vertical sample)	Foot wall	Undeformed	Section 1	269	1.16	3.11	95.73	0.26	0.16	32.9	3.3	Horizontal (K_h)	Permeameter
77	DL19	6–11	169,415.887 407,753.399	12.115 (vertical sample)	Damage zone foot wall	Deformed	Section 2	191	0.74	1.12	98.14	0.37	0.20	37.0	2.9	Vertical (K_v)	Permeameter
78	DL19	14–19	169,415.887 407,753.399	12.115 (vertical sample)	Damage zone foot wall	Deformed	Section 2	184	1.04	3.57	95.39	0.79	0.36	36.1	0.1	Vertical (K_v)	Permeameter
79	DL19	25–30	169,415.887 407,753.399	12.115 (vertical sample)	Damage zone foot wall	Deformed	Section 2	221	0.71	1.68	97.60	0.30	0.23	34.5	4.0	Horizontal (K_h)	Permeameter
80	DL19	33–38	169,415.887 407,753.399	12.115 (vertical sample)	Damage zone foot wall	Deformed	Section 2	216	0.75	1.48	97.77	0.52	0.24	37.4	4.0	Vertical (K_v)	Permeameter
81	DL19	43–48	169,415.887 407,753.399	12.115 (vertical sample)	Damage zone foot wall	Deformed	Section 2	183	0.95	2.82	96.23	0.40	0.23	34.6	2.7	Horizontal (K_h)	Permeameter
82	DL19	51–56	169,415.887 407,753.399	12.115 (vertical sample)	Damage zone foot wall	Deformed	Section 2	196	0.79	0.91	98.31	0.32	0.23	37.3	4.6	Horizontal (K_h)	Permeameter
83	DL20	14–19	169,416.215 407,752.993	11.448 (vertical sample)	Damage zone foot wall	Deformed	Section 2	201	0.80	2.30	96.90	0.43	0.24	38.8	3.6	Vertical (K_v)	Permeameter
84	DL20	23–28	169,416.215 407,752.993	11.448 (vertical sample)	Damage zone foot wall	Deformed	Section 2	204	0.70	1.12	98.18	0.24	0.19	37.7	5.3	Horizontal (K_h)	Permeameter
85	DL20	32–37	169,416.215 407,752.993	11.448 (vertical sample)	Damage zone foot wall	Deformed	Section 2	195	0.73	2.12	97.15	0.26	0.17	35.8	4.0	Vertical (K_v)	Permeameter
86	DL20	42–47	169,416.215 407,752.993	11.448 (vertical sample)	Damage zone foot wall	Deformed	Section 2	180	0.85	2.87	96.28	0.27	0.19	32.4	2.5	Vertical (K_v)	Permeameter

https://doi.org/10.7012/NJG.v105.12686

Sample (number)	Field sample (field code)	Laboratory sample position in field sample (Appendix 2) (cm)	Coordinate field sample[a] (X & Y)	Field sample depth and sample direction (m NAP)[b]	Tectonic position (Fig. 6)	Tectonic setting (–)	Trench sampling section analyses (Fig. 6)	Median grain size (GZ)[c] (µm)	Clay (< 8 µm) (vol%)	Silt (8–63 µm) (vol%)	Sand (63–2,000 µm) (vol%)	Total organic matter (LOI 550°C)[d] (wt%)	Total carbonate ($CaCO_3$) (wt%)	Total porosity (P_{total})[e] (%)	Saturated hydraulic conductivity (K_{sat})[f] (m d^{-1} at 10°C)	Hydraulic conductivity direction (–)	Measuring method (–)
87	DL20	51–56	169,416.215 407,752.993	11.448 (vertical sample)	Damage zone foot wall	Deformed	Section 2	194	0.89	3.63	95.48	0.29	0.17	32.5	3.3	Horizontal (K_h)	Permeameter
88	DL21	4–9	169,416.541 407,752.630	10.738 (vertical sample)	Damage zone foot wall	Deformed	Section 2	147	1.32	5.43	93.24	0.47	0.21	37.0	1.4	Vertical (K_v)	Permeameter
89	DL21	12–17	169,416.541 407,752.630	10.738 (vertical sample)	Damage zone foot wall	Deformed	Section 2	146	1.43	6.58	91.99	0.46	0.20	35.1	1.4	Horizontal (K_h)	Permeameter
90	DL21	20–25	169,416.541 407,752.630	10.738 (vertical sample)	Damage zone foot wall	Deformed	Section 2	178	1.09	3.63	95.27	0.48	0.20	35.2	0.2	Vertical (K_v)	Permeameter
91	DL21	30–35	169,416.541 407,752.630	10.738 (vertical sample)	Damage zone foot wall	Deformed	Section 2	164	1.31	5.45	93.24	0.40	0.18	35.8	2.2	Horizontal (K_h)	Permeameter
92	DL21	43–48	169,416.541 407,752.630	10.738 (vertical sample)	Damage zone foot wall	Deformed	Section 2	307	0.68	0.86	98.45	0.22	0.10	31.8	10.6	Horizontal (K_h)	Permeameter
93	DL21	52–57	169,416.541 407,752.630	10.738 (vertical sample)	Damage zone foot wall	Deformed	Section 2	311	0.75	1.15	98.09	0.21	0.08	31.1	11.9	Vertical (K_v)	Permeameter
94	DL22	4–9	169,416.878 407,752.196	10.150 (vertical sample)	Damage zone foot wall	Deformed	Section 2	299	0.82	1.40	97.78	0.26	0.11	32.2	10.0	Horizontal (K_h)	Permeameter
95	DL22	13–18	169,416.878 407,752.196	10.150 (vertical sample)	Damage zone foot wall	Deformed	Section 2	299	0.89	1.27	97.84	0.33	0.12	33.0	3.8	Vertical (K_v)	Permeameter
96	DL22	25–30	169,416.878 407,752.196	10.150 (vertical sample)	Damage zone foot wall	Deformed	Section 2	348	0.84	1.17	97.99	0.25	0.12	32.9	12.3	Vertical (K_v)	Permeameter
97	DL22	34–39	169,416.878 407,752.196	10.150 (vertical sample)	Damage zone foot wall	Deformed	Section 2	374	1.15	2.14	96.72	0.25	0.17	30.1	10.4	Horizontal (K_h)	Permeameter
98	DL22	44–49	169,416.878 407,752.196	10.150 (vertical sample)	Damage zone foot wall	Deformed	Section 2	350	0.98	1.26	97.76	0.20	0.14	31.9	12.3	Horizontal (K_h)	Permeameter
99	DL22	52–57	169,416.878 407,752.196	10.150 (vertical sample)	Damage zone foot wall	Deformed	Section 2	352	1.54	2.85	95.61	0.52	0.21	30.2	4.5	Vertical (K_v)	Permeameter
100	DL23	12–17	169,408.592 407,749.475	11.803 (vertical sample)	Hanging wall	Man-made channel	excluded from analyses	204	2.60	3.37	94.03	1.13	0.24	39.1	1.8	Vertical (K_v)	Permeameter

https://doi.org/10.70712/NJG.v105.12686

Sample (number)	Field sample (field code)	Laboratory sample position in field sample (Appendix 2) (cm)	Coordinate field sample[a] (X & Y)	Field sample depth and sample direction (m NAP)[b]	Tectonic position (Fig. 6)	Tectonic setting (–)	Trench sampling section analyses (Fig. 6)	Median grain size (GZ)[c] (µm)	Clay (< 8 µm) (vol%)	Silt (8–63 µm) (vol%)	Sand (63–2,000 µm) (vol%)	Total organic matter (LOI 550°C)[d] (wt%)	Total carbonate ($CaCO_3$) (wt%)	Total porosity (P_{total})[e] (%)	Saturated hydraulic conductivity (K_{sat})[f] (m d^{-1} at 10°C)	Hydraulic conductivity direction (–)	Measuring method (–)
101	DL23	24–29	169,408.592 407,749.475	11.803 (vertical sample)	Hanging wall	Man-made channel	excluded from analyses	201	1.79	3.66	94.55	1.97	0.26	43.1	0.3	Vertical (K_v)	Permeameter
102	DL23	53–55	169,408.592 407,749.475	11.803 (vertical sample)	Hanging wall	Man-made channel	excluded from analyses	34	16.17	50.48	33.35	43.19	10.70	79.5	0.1	Vertical (K_v)	Modified oedometer
103	DL24	3–8	169,409.084 407,748.533	11.121 (vertical sample)	Hanging wall	Man-made channel	excluded from analyses	228	0.95	0.89	98.16	0.72	0.37	39.5	2.5	Vertical (K_v)	Permeameter
104	DL24	28–33	169,409.084 407,748.533	11.121 (vertical sample)	Hanging wall	Man-made channel	excluded from analyses	205	1.22	2.76	96.02	1.11	0.50	36.7	0.01	Horizontal (K_h)	Permeameter
105	DL24	39–44	169,409.084 407,748.533	11.121 (vertical sample)	Hanging wall	Man-made channel	excluded from analyses	210	0.81	2.53	96.66	0.29	0.18	36.2	1.2	Horizontal (K_h)	Permeameter
106	DL24	50–55	169,409.084 407,748.533	11.121 (vertical sample)	Hanging wall	Undeformed	Section 5	203	0.78	1.58	97.64	0.38	0.18	39.4	0.7	Vertical (K_v)	Permeameter
107	DL25	6–11	169,409.328 407,748.170	10.528 (vertical sample)	Hanging wall	Undeformed	Section 5	186	0.80	2.18	97.02	0.34	0.19	38.2	1.1	Horizontal (K_h)	Permeameter
108	DL25	17–22	169,409.328 407,748.170	10.528 (vertical sample)	Hanging wall	Undeformed	Section 5	213	0.78	2.34	96.88	0.33	0.15	38.5	0.3	Vertical (K_v)	Permeameter
109	DL25	34–39	169,409.328 407,748.170	10.528 (vertical sample)	Hanging wall	Undeformed	Section 5	227	0.63	0.90	98.46	0.19	0.16	39.4	5.8	Vertical (K_v)	Permeameter
110	DL25	48–53	169,409.328 407,748.170	10.528 (vertical sample)	Hanging wall	Undeformed	Section 5	169,.38	0.85	2.68	96.47	0.21	0.18	37.1	3.2	Horizontal (K_h)	Permeameter
111	DL26	10–15	169,409.682 407,747.649	9.860 (vertical sample)	Hanging wall	Undeformed	Section 5	148	1.28	7.28	91.44	0.32	0.23	36.2	0.9	Vertical (K_v)	Permeameter
112	DL26	20–25	169,409.682 407,747.649	9.860 (vertical sample)	Hanging wall	Undeformed	Section 5	265	0.52	0.64	98.84	0.22	0.24	34.8	32.1	Horizontal (K_h)	Permeameter
113	DL26	30–35	169,409.682 407,747.649	9.860 (vertical sample)	Hanging wall	Undeformed	Section 5	184	0.76	1.80	97.44	0.24	0.24	36.6	2.7	Vertical (K_v)	Permeameter
114	DL26	45–50	169,409.682 407,747.649	9.860 (vertical sample)	Hanging wall	Undeformed	Section 5	152	1.30	7.65	91.05	0.25	0.25	36.3	3.1	Horizontal (K_h)	Permeameter
115	DL26	53–58	169,409.682 407,747.649	9.860 (vertical sample)	Hanging wall	Undeformed	Section 5	197	0.74	1.90	97.36	0.24	0.23	35.2	3.2	Horizontal (K_h)	Permeameter
116	DL27	7–12	169,406.240 407,741.484	11.119 (vertical sample)	Hanging wall	Undeformed	Section 5	191	1.24	1.90	96.86	0.27	0.17	36.6	4.5	Horizontal (K_h)	Permeameter
117	DL27	18–23	169,406.240 407,741.484	11.119 (vertical sample)	Hanging wall	Undeformed	Section 5	242	0.68	0.80	98.52	0.26	0.15	37.2	6.6	Horizontal (K_h)	Permeameter
118	DL27	29–34	169,406.240 407,741.484	11.119 (vertical sample)	Hanging wall	Undeformed	Section 5	218	0.93	2.82	96.25	0.34	0.19	35.6	1.9	Vertical (K_v)	Permeameter

https://doi.org/10.7072/NJG.v105.12686

Sample (number)	Field sample (field code)	Laboratory sample position in field sample (Appendix 2) (cm)	Coordinate field sample[a] (X & Y)	Field sample depth and sample direction (m NAP)[b]	Tectonic position (Fig. 6)	Tectonic setting (–)	Trench sampling section analyses (Fig. 6)	Median grain size (GZ)[c] (µm)	Clay (< 8 µm) (vol%)	Silt (8–63 µm) (vol%)	Sand (63–2,000 µm) (vol%)	Total organic matter (LOI 550°C)[d] (wt%)	Total carbonate ($CaCO_3$) (wt%)	Total porosity (P_{total})[e] (%)	Saturated hydraulic conductivity (K_{sat})[f] ($m\ d^{-1}$ at 10°C)	Hydraulic conductivity direction (–)	Measuring method (–)
119	DL27	39–44	169,406.240 407,741.484	11.119 (vertical sample)	Hanging wall	Undeformed	Section 5	241	0.81	2.32	96.87	0.33	0.18	35.6	1.6	Vertical (K_v)	Permeameter
120	DL27	52–57	169,406.240 407,741.484	11.119 (vertical sample)	Hanging wall	Undeformed	Section 5	219	0.72	0.88	98.40	0.25	0.15	36.3	5.2	Horizontal (K_h)	Permeameter
121	DL28	4–9	169,406.563 407,742.760	10.484 (vertical sample)	Hanging wall	Undeformed	Section 5	189	0.86	1.27	97.86	0.30	0.18	37.4	2.9	Vertical (K_v)	Permeameter
122	DL28	19–24	169,406.563 407,742.760	10.484 (vertical sample)	Hanging wall	Undeformed	Section 5	213	0.76	1.72	97.52	0.25	0.21	34.4	1.8	Vertical (K_v)	Permeameter
123	DL28	28–33	169,406.563 407,742.760	10.484 (vertical sample)	Hanging wall	Undeformed	Section 5	212	0.78	1.49	97.73	0.24	0.22	33.3	2.9	Horizontal (K_h)	Permeameter
124	DL28	40–45	169,406.563 407,742.760	10.484 (vertical sample)	Hanging wall	Undeformed	Section 5	207	0.78	1.99	97.24	0.24	0.18	34.4	0.7	Vertical (K_v)	Permeameter
125	DL28	50–55	169,406.563 407,742.760	10.484 (vertical sample)	Hanging wall	Undeformed	Section 5	195	0.74	1.71	97.55	0.19	0.13	37.8	3.9	Horizontal (K_h)	Permeameter
126	DL29	3–8	169,406.599 407,743.586	9.769 (vertical sample)	Hanging wall	Undeformed	Section 5	208	0.70	1.78	97.52	0.18	0.14	35.0	1.8	Vertical (K_v)	Permeameter
127	DL29	12–17	169,406.599 407,743.586	9.769 (vertical sample)	Hanging wall	Undeformed	Section 5	181	0.82	2.41	96.77	0.20	0.13	37.4	2.0	Horizontal (K_h)	Permeameter
128	DL29	25–30	169,406.599 407,743.586	9.769 (vertical sample)	Hanging wall	Undeformed	Section 5	187	0.88	2.99	96.13	0.26	0.17	34.7	3.3	Horizontal (K_h)	Permeameter
129	DL29	34–39	169,406.599 407,743.586	9.769 (vertical sample)	Hanging wall	Undeformed	Section 5	201	0.79	2.57	96.64	0.19	0.12	35.1	5.1	Vertical (K_v)	Permeameter
130	DL29	44–49	169,406.599 407,743.586	9.769 (vertical sample)	Hanging wall	Undeformed	Section 5	204	0.75	2.50	96.75	0.21	0.10	36.0	5.8	Horizontal (K_h)	Permeameter
131	DL30	4–9	169,408.351 407,743.995	9.397 (vertical sample)	Hanging wall	Undeformed	Section 5	157	1.02	5.16	93.82	0.29	0.16	36.5	1.9	Vertical (K_v)	Permeameter
132	DL30	27–32	169,408.351 407,743.995	9.397 (vertical sample)	Hanging wall	Undeformed	Section 5	225	0.69	1.16	98.15	0.19	0.14	34.9	5.0	Horizontal (K_h)	Permeameter
133	DL31	3–8	169,409.702 407,745.356	9.335 (horizontal sample)	Hanging wall	Undeformed	Section 5	186	0.83	3.15	96.02	0.23	0.15	35.9	5.6	Horizontal (K_h)	Permeameter
134	DL31	12–17	169,409.702 407,745.356	9.335 (horizontal sample)	Hanging wall	Undeformed	Section 5	179	0.89	3.55	95.57	0.24	0.13	35.3	5.2	Horizontal (K_h)	Permeameter
135	DL31	21–26	169,409.702 407,745.356	9.335 (horizontal sample)	Hanging wall	Undeformed	Section 5	163	0.99	5.89	93.12	0.26	0.20	36.5	3.7	Horizontal (K_h)	Permeameter
136	DL32	3–8	169,412.530 407,746.903	9.599 (horizontal sample)	Hanging wall	Undeformed	Section 5	152	1.00	5.22	93.78	0.26	0.19	37.6	3.7	Horizontal (K_h)	Permeameter
137	DL32	13–18	169,412.530 407,746.903	9.599 (horizontal sample)	Hanging wall	Undeformed	Section 5	146	1.14	6.59	92.27	0.35	0.22	37.9	1.8	Horizontal (K_h)	Permeameter
138	DL32	22–27	169,412.530 407,746.903	9.599 (horizontal sample)	Hanging wall	Undeformed	Section 5	156	1.01	5.11	93.88	0.31	0.22	37.1	0.5	Vertical (K_v)	Permeameter
139	DL33A	4–9	169,409.565 407,745.633	9.245 (horizontal sample)	Hanging wall	Undeformed	Section 5	173	0.93	3.17	95.90	0.24	0.20	36.4	4.2	Vertical (K_v)	Permeameter

Sample (number)	Field sample (field code)	Laboratory sample position in field sample (Appendix 2) (cm)	Coordinate field sample[a] (X & Y)	Field sample depth and sample direction (m NAP)[b]	Tectonic position (Fig. 6)	Tectonic setting (–)	Trench sampling section analyses (Fig. 6)	Median grain size (GZ)[c] (µm)	Clay (< 8 µm) (vol%)	Silt (8–63 µm) (vol%)	Sand (63–2,000 µm) (vol%)	Total organic matter (LOI 550°C)[d] (wt%)	Total carbonate ($CaCO_3$) (wt%)	Total porosity (P_{total})[e] (%)	Saturated hydraulic conductivity (K_{sat})[f] ($m\ d^{-1}$ at 10°C)	Hydraulic conductivity direction (–)	Measuring method (–)
140	DL33A	15–20	169,409.565 407,745.633	9.245 (horizontal sample)	Hanging wall	Undeformed	Section 5	181	0.84	2.59	96.57	0.22	0.16	36.5	4.1	Vertical (K_v)	Permeameter
141	DL33A	25–30	169,409.565 407,745.633	9.245 (horizontal sample)	Hanging wall	Undeformed	Section 5	191	0.82	1.95	97.24	0.27	0.17	36.4	2.7	Horizontal (K_h)	Permeameter
142	DL33B	2–7	169,414.490 407,752.734	11.983 (vertical sample)	Damage zone hanging wall	Man-made channel	excluded from analyses	199	1.26	2.70	96.04	2.86	0.38	48.1	1.6	Vertical (K_v)	Permeameter
143	DL33B	13–18	169,414.490 407,752.734	11.983 (vertical sample)	Damage zone hanging wall	Man-made channel	excluded from analyses	196	1.96	4.31	93.73	4.53	0.53	55.9	0.2	Vertical (K_v)	Permeameter
144	DL33B	29–34	169,414.490 407,752.734	11.983 (vertical sample)	Damage zone hanging wall	Man-made channel	excluded from analyses	218	0.81	1.31	97.89	1.68	0.29	43.9	2.4	Vertical (K_v)	Permeameter
145	DL33B	45–50	169,414.490 407,752.734	11.983 (vertical sample)	Damage zone hanging wall	Man-made channel	excluded from analyses	179	0.93	2.45	96.62	0.37	0.27	39.8	3.8	Horizontal (K_h)	Permeameter
146	DL34	3–8	169,414.860 407,752.314	11.429 (vertical sample)	Damage zone hanging wall	Deformed	Section 4	215	0.79	1.76	97.45	0.23	0.16	35.6	5.6	Horizontal (K_h)	Permeameter
147	DL34	11–16	169,414.860 407,752.314	11.429 (vertical sample)	Damage zone hanging wall	Deformed	Section 4	185	0.81	1.06	98.13	0.27	0.17	38.4	3.8	Vertical (K_v)	Permeameter
148	DL34	20–25	169,414.860 407,752.314	11.429 (vertical sample)	Damage zone hanging wall	Deformed	Section 4	196	0.92	3.46	95.62	0.33	0.20	37.0	2.6	Horizontal (K_h)	Permeameter
149	DL34	28–32	169,414.860 407,752.314	11.429 (vertical sample)	Damage zone hanging wall	Deformed	Section 4	209	0.96	3.05	96.00	0.26	0.17	34.7	2.8	Vertical (K_v)	Permeameter
150	DL34	44–54	169,414.860 407,752.314	11.429 (vertical sample)	Fault	Deformed	Section 3	205	1.44	3.77	94.80	0.67	0.19	failed	failed	Vertical (K_v)	Triaxial
151	DL35	4–9	169,415.052 407,752.049	10.833 (vertical sample)	Damage zone hanging wall	Deformed	Section 4	183	0.94	2.58	96.48	0.22	0.15	37.5	2.0	Horizontal (K_h)	Permeameter

https://doi.org/10.70712/NJG.v105.12686

https://doi.org/10.70712/NJG.v105.12686

Sample (number)	Field sample (field code)	Laboratory sample position in field sample (Appendix 2) (cm)	Coordinate field sample[a] (X & Y)	Field sample depth and sample direction (m NAP)[b]	Tectonic position (Fig. 6)	Tectonic setting (–)	Trench sampling section analyses (Fig. 6)	Median grain size (GZ)[c] (µm)	Clay (< 8 µm) (vol%)	Silt (8–63 µm) (vol%)	Sand (63–2,000 µm) (vol%)	Total organic matter (LOI 550°C)[d] (wt%)	Total carbonate ($CaCO_3$) (wt%)	Total porosity (P_{total})[e] (%)	Saturated hydraulic conductivity (K_{sat})[f] (m d^{-1} at 10°C)	Hydraulic conductivity direction (–)	Measuring method (–)
152	DL35	14–19	169,415.052 407,752.049	10.833 (vertical sample)	Fault	Deformed	Section 3	201	0.83	1.72	97.45	0.31	0.16	37.9	2.3	Horizontal (K_h)	Permeameter
153	DL35	24–29	169,415.052 407,752.049	10.833 (vertical sample)	Fault	Deformed	Section 3	194	0.94	2.59	96.47	0.37	0.14	39.4	0.2	Vertical (K_v)	Permeameter
154	DL35	34–39	169,415.052 407,752.049	10.833 (vertical sample)	Damage zone hanging wall	Deformed	Section 4	214	0.73	1.05	98.22	0.16	0.17	37.7	4.3	Horizontal (K_h)	Permeameter
155	DL35	42–47	169,415.052 407,752.049	10.833 (vertical sample)	Damage zone hanging wall	Deformed	Section 4	198	0.79	1.71	97.50	0.19	0.17	37.4	3.7	Vertical (K_v)	Permeameter
156	DL35	52–57	169,415.052 407,752.049	10.833 (vertical sample)	Damage zone hanging wall	Deformed	Section 4	165	0.93	3.31	95.76	0.23	0.22	37.2	2.2	Vertical (K_v)	Permeameter
157	DL36	3–8	169,414.965 407,751.537	10.226 (vertical sample)	Damage zone hanging wall	Deformed	Section 4	165	0.92	3.66	95.42	0.25	0.21	37.0	2.4	Horizontal (K_h)	Permeameter
158	DL36	10–15	169,414.965 407,751.537	10.226 (vertical sample)	Damage zone hanging wall	Deformed	Section 4	167	0.94	4.42	94.64	0.25	0.21	36.9	1.8	Vertical (K_v)	Permeameter
159	DL36	20–25	169,414.965 407,751.537	10.226 (vertical sample)	Damage zone hanging wall	Deformed	Section 4	199	0.86	3.52	95.62	0.25	0.22	34.0	4.5	Horizontal (K_h)	Permeameter
160	DL36	42–47	169,414.965 407,751.537	10.226 (vertical sample)	Damage zone hanging wall	Deformed	Section 4	146	1.36	6.13	92.51	0.35	0.24	37.1	2.7	Horizontal (K_h)	Permeameter
161	DL36	51–56	169,414.965 407,751.537	10.226 (vertical sample)	Damage zone hanging wall	Deformed	Section 4	149	1.36	4.76	93.88	0.34	0.22	36.0	2.6	Vertical (K_v)	Permeameter

[a]Dutch 87 National Grid (RD)

[b]Level with respect to the Dutch Ordnance Datum

[c]Sympatec HELOS KR Laser Diffraction Particle Sizer

[d]Loss-On-Ignition at 550°C

[e]Weight loss: fully saturated versus oven-dried (105°C for 24 hours) sample

[f]Arithmetic average

[g]Measured at the TNO Permeability Laboratory

[h]Measured by the Deltares Institute for Applied Research

Appendix 2

Appendix 2

Location and orientation of field samples 1–36, grouped into trench sampling sections 1–5, and corresponding laboratory samples

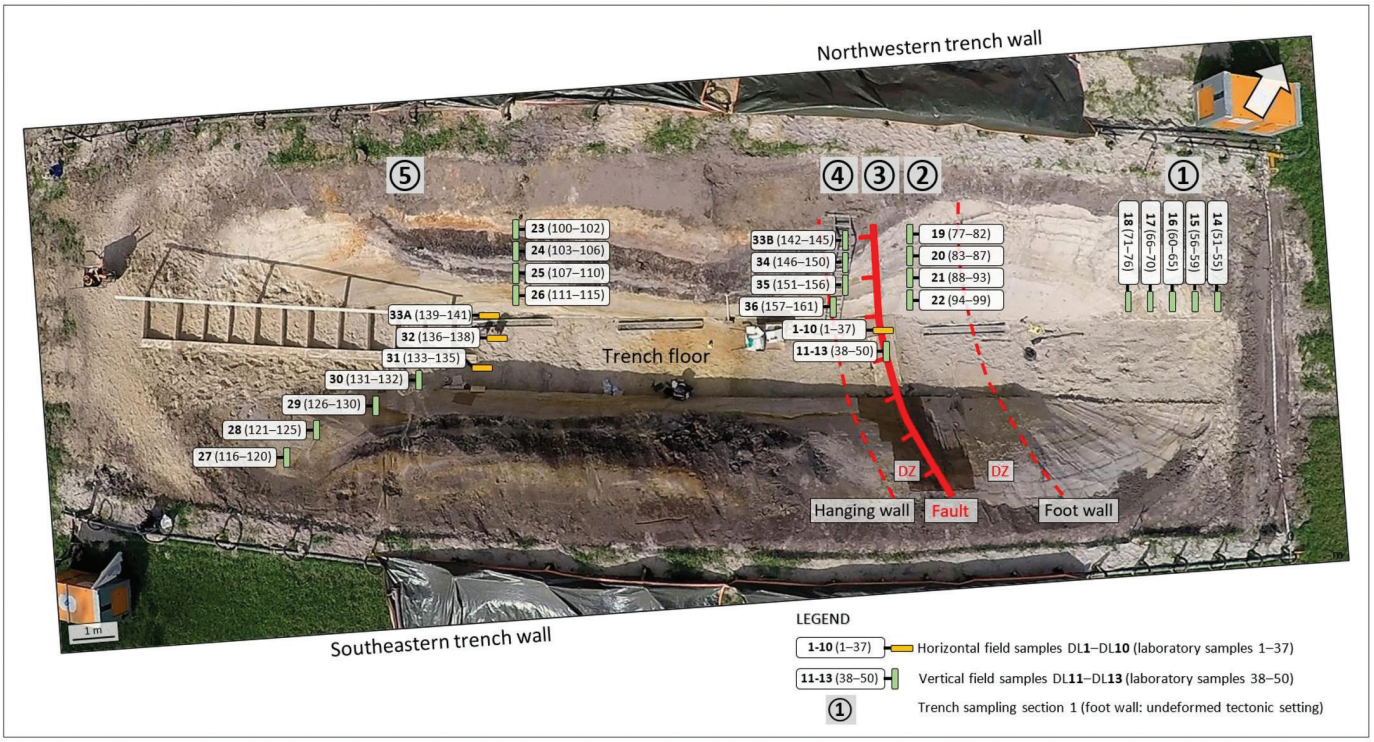

Field sample **DL1**

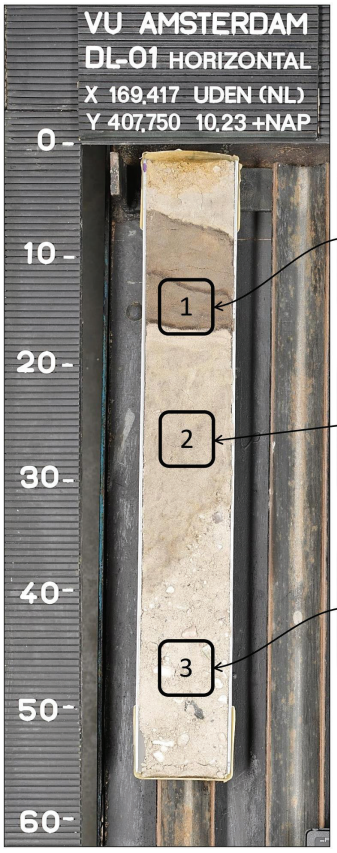

Laboratory sample **1** (12–17 cm - Appendix 1)
Attributed to trench sampling **section 3**

1.	General lithology (USDA):	fine sand
2.	Median grain size:	171 µm
3.	Total organic matter:	0.75%
4.	Total carbonate ($CaCO_3$):	0.42%
5.	Total porosity:	34.3%
6.	**Hydraulic conductivity (*K*):**	**2.6 m d^{-1} (K_h)** with permeameter
7.	Remark(s):	multiple accumulation bands organic matter

Laboratory sample **2** (24–29 cm - Appendix 1)
Attributed to trench sampling **section 3**

1.	General lithology (USDA):	fine sand
2.	Median grain size:	169 µm
3.	Total organic matter:	0.32%
4.	Total carbonate ($CaCO_3$):	0.25%
5.	Total porosity:	34.3%
6.	**Hydraulic conductivity (*K*):**	**2.6 m d^{-1} (K_h)** with permeameter
7.	Remark(s):	diffuse accumulation of fine sediments and organic matter

Laboratory sample **3** (44–49 cm - Appendix 1)
Attributed to trench sampling **section 2**

1.	General lithology (USDA):	medium sand
2.	Median grain size:	304 µm
3.	Total organic matter:	0.19%
4.	Total carbonate ($CaCO_3$):	0.05%
5.	Total porosity:	33.6%
6.	**Hydraulic conductivity (*K*):**	**10.0 m d^{-1} (K_h)** with permeameter
7.	Remark(s):	coarser sand and gravel

Field sample **DL2**

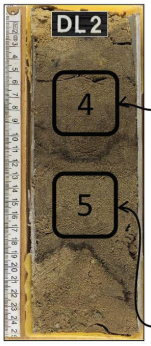

Laboratory sample **4** (5–10 cm - Appendix 1)
Attributed to trench sampling **section 3**

1.	General lithology (USDA):	fine sand
2.	Median grain size:	164 µm
3.	Total organic matter:	0.73%
4.	Total carbonate ($CaCO_3$):	0.37%
5.	Total porosity:	34.4%
6.	**Hydraulic conductivity (*K*):**	**0.9 m d^{-1} (K_h)** with permeameter
7.	Remark(s):	diffuse accumulation of fine sediments and organic matter

Laboratory sample **5** (13–18 cm - Appendix 1)
Attributed to trench sampling **section 3**

1.	General lithology (USDA):	fine sand
2.	Median grain size:	172 µm
3.	Total organic matter:	0.52%
4.	Total carbonate ($CaCO_3$):	0.31%
5.	Total porosity:	30.5%
6.	**Hydraulic conductivity (*K*):**	**2.4 m d^{-1} (K_h)** with permeameter
7.	Remark(s):	diffuse accumulation of fine sediments and organic matter

Field sample **DL3**

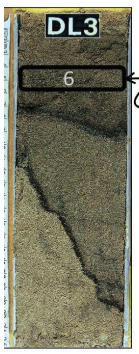

Laboratory sample **6** (4–6 cm - Appendix 1)
Attributed to trench sampling **section 3**

1.	General lithology (USDA):	fine sand
2.	Median grain size:	164 µm
3.	Total organic matter:	0.64%
4.	Total carbonate ($CaCO_3$):	0.41%
5.	Total porosity:	35.2%
6.	**Hydraulic conductivity (*K*):**	**0.1 m d^{-1} (K_v)** with mod. oedometer
7.	Remark(s):	diffuse accumulation of fine sediments and organic matter

https://doi.org/10.70712/NJG.v105.12686

Field sample **DL4**

Sample **7** (0–5 cm - Appendix 1)
Attributed to trench sampling **section 3**

1.	General lithology (USDA):	fine sand
2.	Median grain size:	153 µm
3.	Total organic matter:	0.85%
4.	Total carbonate ($CaCO_3$):	0.46%
5.	Total porosity:	33.8%
6.	**Hydraulic conductivity (*K*):**	**0.04 m d^{-1} (K_h)** with permeameter
7.	Remark(s):	diffuse accumulation of fine sediments and organic matter

Field sample **DL5**

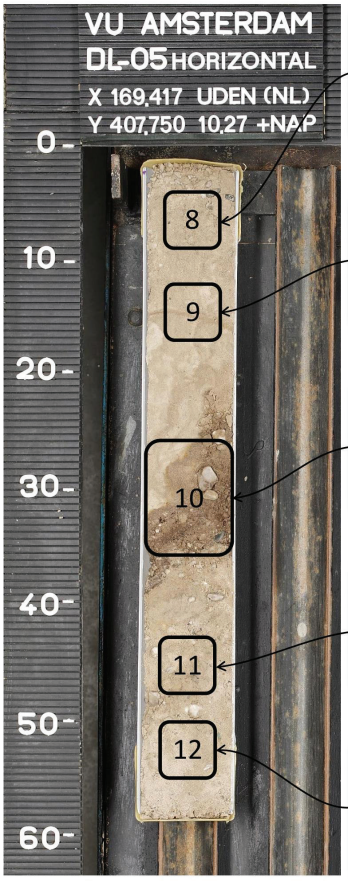

Laboratory sample **8** (4–9 cm - Appendix 1)
Attributed to trench sampling **section 3**

1.	General lithology (USDA):	fine sand
2.	Median grain size:	195 µm
3.	Total organic matter:	0.26%
4.	Total carbonate ($CaCO_3$):	0.23%
5.	Total porosity:	34.0%
6.	**Hydraulic conductivity (*K*):**	**3.5 m d^{-1} (K_v)** with permeameter
7.	Remark(s):	accumulation of fine sediments and little gravel

Laboratory sample **9** (12–17 cm - Appendix 1)
Attributed to trench sampling **section 3**

1.	General lithology (USDA):	fine sand
2.	Median grain size:	185 µm
3.	Total organic matter:	0.33%
4.	Total carbonate ($CaCO_3$):	0.24%
5.	Total porosity:	34.3%
6.	**Hydraulic conductivity (*K*):**	**1.3 m d^{-1} (K_h)** with permeameter
7.	Remark(s):	accumulation of fine sediments and little gravel

Laboratory sample **10** (26–36 cm - Appendix 1)
Attributed to trench sampling **section 3**

1.	General lithology (USDA):	fine sand
2.	Median grain size:	228 µm
3.	Total organic matter:	0.59%
4.	Total carbonate ($CaCO_3$):	0.16%
5.	Total porosity:	32.9%
6.	**Hydraulic conductivity (*K*):**	**0.5 m d^{-1} (K_h)** with triaxial
7.	Remark(s):	accumulation of fines in coarse(r) sediments with gravel

Laboratory sample **11** (43–48 cm - Appendix 1)
Attributed to trench sampling **section 2**

1.	General lithology (USDA):	fine sand
2.	Median grain size:	242 µm
3.	Total organic matter:	0.30%
4.	Total carbonate ($CaCO_3$):	0.18%
5.	Total porosity:	28.5%
6.	**Hydraulic conductivity (*K*):**	**6.5 m d^{-1} (K_h)** with permeameter
7.	Remark(s):	gravel pockets

Laboratory sample **12** (50–55 cm - Appendix 1)
Attributed to trench sampling **section 2**

1.	General lithology (USDA):	medium sand
2.	Median grain size:	257 µm
3.	Total organic matter:	0.19%
4.	Total carbonate ($CaCO_3$):	0.14%
5.	Total porosity:	31.2%
6.	**Hydraulic conductivity (*K*):**	**9.6 m d^{-1} (K_v)** with permeameter
7.	Remark(s):	gravel pockets

Field sample **DL6**

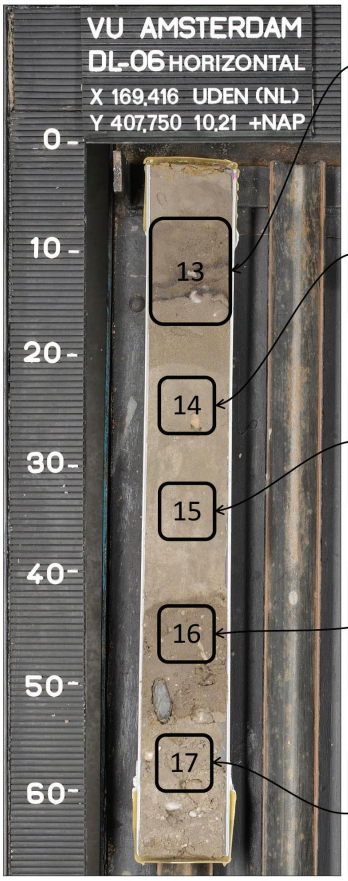

Laboratory sample **13** (7–17 cm - Appendix 1)
Attributed to trench sampling **section 3**

1.	General lithology (USDA):	fine sand
2.	Median grain size:	202 µm
3.	Total organic matter:	0.58%
4.	Total carbonate ($CaCO_3$):	0.22%
5.	Total porosity:	38.7%
6.	**Hydraulic conductivity (*K*):**	**0.2 m d^{-1} (K_h)** with triaxial
7.	Remark(s):	multiple accumulation bands organic matter

Laboratory sample **14** (22–27 cm - Appendix 1)
Attributed to trench sampling **section 3**

1.	General lithology (USDA):	fine sand
2.	Median grain size:	193 µm
3.	Total organic matter:	0.28%
4.	Total carbonate ($CaCO_3$):	0.20%
5.	Total porosity:	34.2%
6.	**Hydraulic conductivity (*K*):**	**3.4 m d^{-1} (K_v)** with permeameter
7.	Remark(s):	gravel present and accumulation of fines

Laboratory sample **15** (32–37 cm - Appendix 1)
Attributed to trench sampling **section 3**

1.	General lithology (USDA):	fine sand
2.	Median grain size:	199 µm
3.	Total organic matter:	0.25%
4.	Total carbonate ($CaCO_3$):	0.17%
5.	Total porosity:	33.1%
6.	**Hydraulic conductivity (*K*):**	**3.6 m d^{-1} (K_h)** with permeameter
7.	Remark(s):	gravel present and accumulation of fines

Laboratory sample **16** (43–48 cm - Appendix 1)
Attributed to trench sampling **section 3**

1.	General lithology (USDA):	fine sand
2.	Median grain size:	216 µm
3.	Total organic matter:	0.43%
4.	Total carbonate ($CaCO_3$):	0.17%
5.	Total porosity:	32.4%
6.	**Hydraulic conductivity (*K*):**	**7.1 m d^{-1} (K_v)** with permeameter
7.	Remark(s):	gravel present and accumulation of fines

Laboratory sample **17** (55–60 cm - Appendix 1)
Attributed to trench sampling **section 2**

1.	General lithology (USDA):	medium sand
2.	Median grain size:	262 µm
3.	Total organic matter:	0.21%
4.	Total carbonate ($CaCO_3$):	0.12%
5.	Total porosity:	27.7%
6.	**Hydraulic conductivity (*K*):**	**3.0 m d^{-1} (K_h)** with permeameter
7.	Remark(s):	coarser sediments with gravel

https://doi.org/10.70712/NJG.v105.12686

Field sample **DL7**

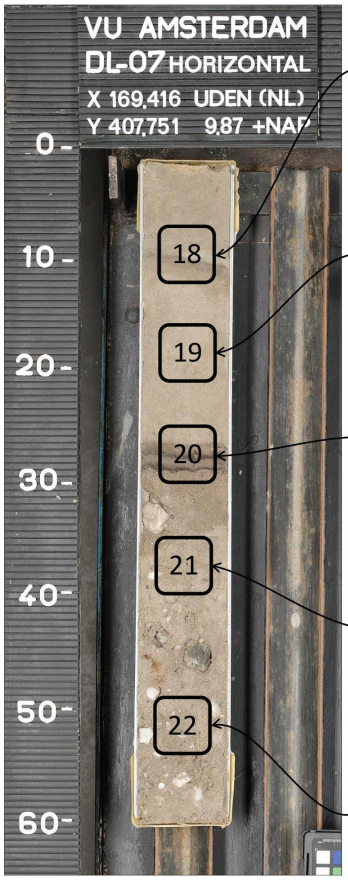

Laboratory sample **18** (7–12 cm - Appendix 1)
Attributed to trench sampling **section 3**

1.	General lithology (USDA):	fine sand
2.	Median grain size:	190 µm
3.	Total organic matter:	0.42%
4.	Total carbonate ($CaCO_3$):	0.26%
5.	Total porosity:	36.1%
6.	**Hydraulic conductivity (*K*):**	**0.2 m d^{-1} (K_h)** with permeameter
7.	Remark(s):	accumulation band organic matter

Laboratory sample **19** (16–21 cm - Appendix 1)
Attributed to trench sampling **section 3**

1.	General lithology (USDA):	fine sand
2.	Median grain size:	208 µm
3.	Total organic matter:	0.33%
4.	Total carbonate ($CaCO_3$):	0.21%
5.	Total porosity:	33.2%
6.	**Hydraulic conductivity (*K*):**	**0.1 m d^{-1} (K_v)** with permeameter
7.	Remark(s):	micro layering sediments

Laboratory sample **20** (25–30 cm - Appendix 1)
Attributed to trench sampling **section 3**

1.	General lithology (USDA):	fine sand
2.	Median grain size:	238 µm
3.	Total organic matter:	0.63%
4.	Total carbonate ($CaCO_3$):	0.28%
5.	Total porosity:	31.7%
6.	**Hydraulic conductivity (*K*):**	**1.0 m d^{-1} (K_h)** with permeameter
7.	Remark(s):	multiple accumulation bands organic matter

Laboratory sample **21** (35–40 cm - Appendix 1)
Attributed to trench sampling **section 2**

1.	General lithology (USDA):	fine sand
2.	Median grain size:	244 µm
3.	Total organic matter:	0.26%
4.	Total carbonate ($CaCO_3$):	0.17%
5.	Total porosity:	33.2%
6.	**Hydraulic conductivity (*K*):**	**13.3 m d^{-1} (K_h)** with permeameter
7.	Remark(s):	coarse sediments with gravel

Laboratory sample **22** (49–54 cm Appendix 1)
Attributed to trench sampling **section 2**

1.	General lithology (USDA):	medium sand
2.	Median grain size:	280 µm
3.	Total organic matter:	0.20%
4.	Total carbonate ($CaCO_3$):	0.14%
5.	Total porosity:	32.5%
6.	**Hydraulic conductivity (*K*):**	**11.2 m d^{-1} (K_v)** with permeameter
7.	Remark(s):	coarse sediments with gravel

Field sample **DL8**

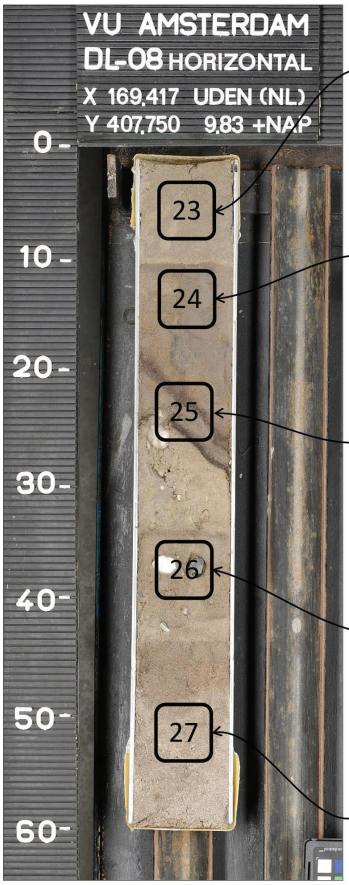

Laboratory sample **23** (3–8 cm - Appendix 1)
Attributed to trench sampling **section 3**

1.	General lithology (USDA):	fine sand
2.	Median grain size:	146 µm
3.	Total organic matter:	0.37%
4.	Total carbonate ($CaCO_3$):	0.31%
5.	Total porosity:	35.3%
6.	**Hydraulic conductivity (*K*):**	**2.7 m d^{-1} (K_v)** with permeameter
7.	Remark(s):	-

Laboratory sample **24** (11–16 cm - Appendix 1)
Attributed to trench sampling **section 3**

1.	General lithology (USDA):	fine sand
2.	Median grain size:	155 µm
3.	Total organic matter:	0.59%
4.	Total carbonate ($CaCO_3$):	0.44%
5.	Total porosity:	35.6%
6.	**Hydraulic conductivity (*K*):**	**0.5 m d^{-1} (K_v)** with permeameter
7.	Remark(s):	accumulation of fines

Laboratory sample **25** (21–26 cm - Appendix 1)
Attributed to trench sampling **section 3**

1.	General lithology (USDA):	fine sand
2.	Median grain size:	175 µm
3.	Total organic matter:	0.74%
4.	Total carbonate ($CaCO_3$):	0.35%
5.	Total porosity:	35.0%
6.	**Hydraulic conductivity (*K*):**	**1.6 m d^{-1} (K_h)** with permeameter
7.	Remark(s):	multiple accumulation bands organic matter

Laboratory sample **26** (35–40 cm - Appendix 1)
Attributed to trench sampling **section 3**

1.	General lithology (USDA):	medium sand
2.	Median grain size:	256 µm
3.	Total organic matter:	0.40%
4.	Total carbonate ($CaCO_3$):	0.18%
5.	Total porosity:	30.5%
6.	**Hydraulic conductivity (*K*):**	**1.7 m d^{-1} (K_v)** with permeameter
7.	Remark(s):	accumulation of fines in coarser sediment with gravel

Laboratory sample **27** (49–54 cm - Appendix 1)
Attributed to trench sampling **section 2**

1.	General lithology (USDA):	medium sand
2.	Median grain size:	375 µm
3.	Total organic matter:	0.24%
4.	Total carbonate ($CaCO_3$):	0.15%
5.	Total porosity:	31.9%
6.	**Hydraulic conductivity (*K*):**	**18.4 m d^{-1} (K_v)** with permeameter
7.	Remark(s):	coarse sediments with gravel

https://doi.org/10.70712/NJG.v105.12686

Field sample **DL9**

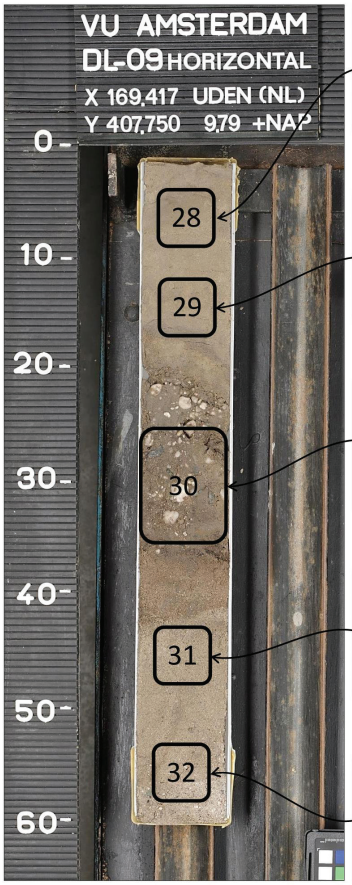

Laboratory sample **28** (4–9 cm - Appendix 1)
Attributed to trench sampling **section 3**

1. General lithology (USDA): fine sand
2. Median grain size: 159 µm
3. Total organic matter: 0.32%
4. Total carbonate ($CaCO_3$): 0.24%
5. Total porosity: 35.6%
6. **Hydraulic conductivity (*K*):** **2.9 m d^{-1} (K_h)** with permeameter
7. Remark(s): accumulation of fines

Laboratory sample **29** (12–17 cm - Appendix 1)
Attributed to trench sampling **section 3**

1. General lithology (USDA): fine sand
2. Median grain size: 170 µm
3. Total organic matter: 0.41%
4. Total carbonate ($CaCO_3$): 0.26%
5. Total porosity: 35.9%
6. **Hydraulic conductivity (*K*):** **0.5 m d^{-1} (K_h)** with permeameter
7. Remark(s): accumulation of fines

Laboratory sample **30** (25–35 cm - Appendix 1)
Attributed to trench sampling **section 3**

1. General lithology (USDA): medium sand
2. Median grain size: 279 µm
3. Total organic matter: 0.60%
4. Total carbonate ($CaCO_3$): 0.33%
5. Total porosity: 32.9%
6. **Hydraulic conductivity (*K*):** **0.2 m d^{-1} (K_h)** with triaxial
7. Remark(s): compact sand-silt-gravel layer

Laboratory sample **31** (43–48 cm - Appendix 1)
Attributed to trench sampling **section 2**

1. General lithology (USDA): medium sand
2. Median grain size: 384 µm
3. Total organic matter: 0.24%
4. Total carbonate ($CaCO_3$): 0.13%
5. Total porosity: 31.7%
6. **Hydraulic conductivity (*K*):** **19.2 m d^{-1} (K_h)** with permeameter
7. Remark(s): coarser sediments with gravel

Laboratory sample **32** (53–58 cm - Appendix 1)
Attributed to trench sampling **section 2**

1. General lithology (USDA): medium sand
2. Median grain size: 411 µm
3. Total organic matter: 0.20%
4. Total carbonate ($CaCO_3$): 0.13%
5. Total porosity: 30.1%
6. **Hydraulic conductivity (*K*):** **22.6 m d^{-1} (K_h)** with permeameter
7. Remark(s): coarser sediments with gravel

Field sample **DL10**

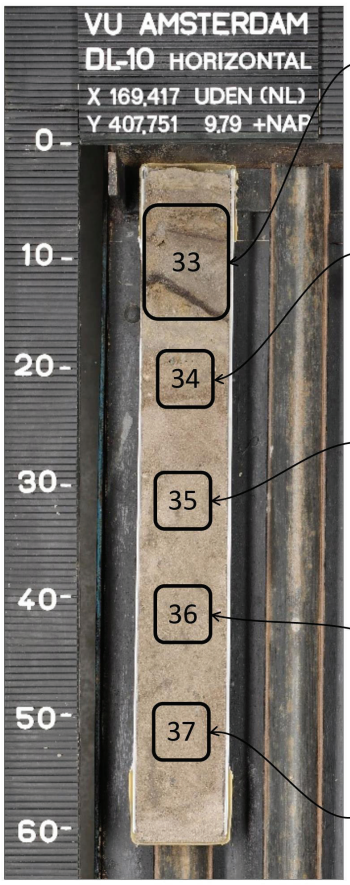

Laboratory sample **33** (5–15 cm - Appendix 1)
Attributed to trench sampling **section 3**

1. General lithology (USDA): fine sand
2. Median grain size: 199 µm
3. Total organic matter: 0.76%
4. Total carbonate ($CaCO_3$): 0.27%
5. Total porosity: 35.5%
6. **Hydraulic conductivity (*K*):** **0.04 m d^{-1} (K_h)** with triaxial
7. Remark(s): multiple accumulation bands organic matter in sample

Laboratory sample **34** (18–23 cm - Appendix 1)
Attributed to trench sampling **section 2**

1. General lithology (USDA): medium sand
2. Median grain size: 315 µm
3. Total organic matter: 0.31%
4. Total carbonate ($CaCO_3$): 0.15%
5. Total porosity: 31.4%
6. **Hydraulic conductivity (*K*):** **10.5 m d^{-1} (K_h)** with permeameter
7. Remark(s): coarser sediments with gravel

Laboratory sample **35** (29–34 cm - Appendix 1)
Attributed to trench sampling **section 2**

1. General lithology (USDA): medium sand
2. Median grain size: 305 µm
3. Total organic matter: 0.24%
4. Total carbonate ($CaCO_3$): 0.14%
5. Total porosity: 33.6%
6. **Hydraulic conductivity (*K*):** **9.0 m d^{-1} (K_v)** with permeameter
7. Remark(s): coarser sediments with gravel

Laboratory sample **36** (39–44 cm - Appendix 1)
Attributed to trench sampling **section 2**

1. General lithology (USDA): medium sand
2. Median grain size: 300 µm
3. Total organic matter: 0.25%
4. Total carbonate ($CaCO_3$): 0.14%
5. Total porosity: 34.3%
6. **Hydraulic conductivity (*K*):** **10.7 m d^{-1} (K_h)** with permeameter
7. Remark(s): coarser sediments with gravel

Laboratory sample **37** (49–54 cm - Appendix 1)
Attributed to trench sampling **section 2**

1. General lithology (USDA): medium sand
2. Median grain size: 311 µm
3. Total organic matter: 0.24%
4. Total carbonate ($CaCO_3$): 0.14%
5. Total porosity: 33.2%
6. **Hydraulic conductivity (*K*):** **10.9 m d^{-1} (K_v)** with permeameter
7. Remark(s): coarser sediments with gravel

https://doi.org/10.70712/NJG.v105.12686

Field sample **DL11**

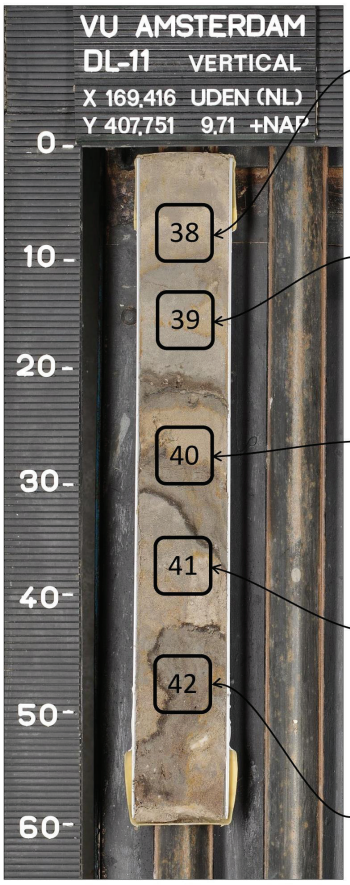

Laboratory sample **38** (5–10 cm - Appendix 1)
Attributed to trench sampling **section 3**

9.	General lithology (USDA):	fine sand
10.	Median grain size:	183 µm
11.	Total organic matter:	0.30%
12.	Total carbonate ($CaCO_3$):	0.20%
13.	Total porosity:	35.7%
14.	**Hydraulic conductivity (*K*):**	**0.7 m d^{-1} (K_v)** with permeameter
15.	Remark(s):	accumulation of fines and iron precipitation

Laboratory sample **39** (13–18 cm - Appendix 1)
Attributed to trench sampling **section 3**

1.	General lithology (USDA):	fine sand
2.	Median grain size:	199 µm
3.	Total organic matter:	0.33%
4.	Total carbonate ($CaCO_3$):	0.27%
5.	Total porosity:	33.1%
6.	**Hydraulic conductivity (*K*):**	**1.1 m d^{-1} (K_h)** with permeameter
7.	Remark(s):	accumulation of fines and iron discolorations

Laboratory sample **40** (25–30 cm - Appendix 1)
Attributed to trench sampling **section 3**

1.	General lithology (USDA):	fine sand
2.	Median grain size:	194 µm
3.	Total organic matter:	0.46%
4.	Total carbonate ($CaCO_3$):	0.31%
5.	Total porosity:	32.8%
6.	**Hydraulic conductivity (*K*):**	**0.03 m d^{-1} (K_v)** with permeameter
7.	Remark(s):	accumulation of fines and iron discolorations

Laboratory sample **41** (35–40 cm - Appendix 1)
Attributed to trench sampling **section 3**

1.	General lithology (USDA):	fine sand
2.	Median grain size:	226 µm
3.	Total organic matter:	0.32%
4.	Total carbonate ($CaCO_3$):	0.22%
5.	Total porosity:	30.8%
6.	**Hydraulic conductivity (*K*):**	**2.7 m d^{-1} (K_h)** with permeameter
7.	Remark(s):	accumulation of fines and iron discolorations

Laboratory sample **42** (45–50 cm - Appendix 1)
Attributed to trench sampling **section 3**

1.	General lithology (USDA):	fine sand
2.	Median grain size:	248 µm
3.	Total organic matter:	0.56%
4.	Total carbonate ($CaCO_3$):	0.39%
5.	Total porosity:	29.1%
6.	**Hydraulic conductivity (*K*):**	**0.8 m d^{-1} (K_h)** with permeameter
7.	Remark(s):	accumulation of fines and iron precipitation

Field sample **DL12**

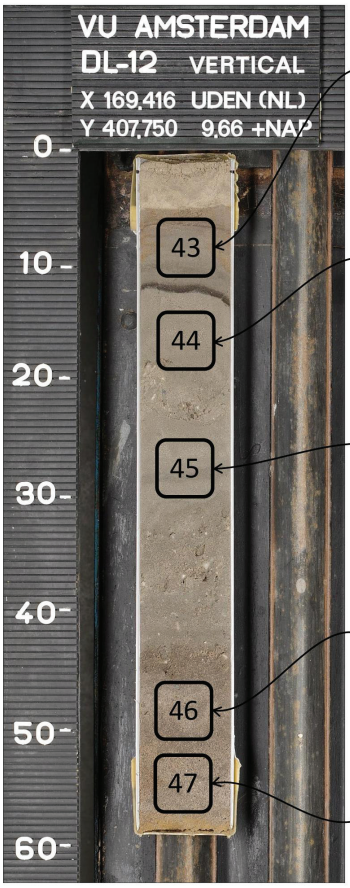

Laboratory sample **43** (6–11 cm - Appendix 1)
Attributed to trench sampling **section 3**

1.	General lithology (USDA):	fine sand
2.	Median grain size:	154 µm
3.	Total organic matter:	0.63%
4.	Total carbonate ($CaCO_3$):	0.29%
5.	Total porosity:	33.4%
6.	**Hydraulic conductivity (*K*):**	**0.01 m d^{-1} (K_h)** with permeameter
7.	Remark(s):	accumulation of fines and iron discolorations

Laboratory sample **44** (14–19 cm - Appendix 1)
Attributed to trench sampling **section 3**

1.	General lithology (USDA):	fine sand
2.	Median grain size:	165 µm
3.	Total organic matter:	0.37%
4.	Total carbonate ($CaCO_3$):	0.25%
5.	Total porosity:	33.2%
6.	**Hydraulic conductivity (*K*):**	**2.2 m d^{-1} (K_h)** with permeameter
7.	Remark(s):	accumulation of fines

Laboratory sample **45** (25–30 cm - Appendix 1)
Attributed to trench sampling **section 3**

1.	General lithology (USDA):	fine sand
2.	Median grain size:	192 µm
3.	Total organic matter:	0.33%
4.	Total carbonate ($CaCO_3$):	0.23%
5.	Total porosity:	32.0%
6.	**Hydraulic conductivity (*K*):**	**2.3 m d^{-1} (K_v)** with permeameter
7.	Remark(s):	accumulation of fines

Laboratory sample **46** (46–51 cm - Appendix 1)
Attributed to trench sampling **section 4**

1	General lithology (USDA):	medium sand
2.	Median grain size:	326 µm
3.	Total organic matter:	0.29%
4.	Total carbonate ($CaCO_3$):	0.18%
5.	Total porosity:	31.3%
6.	**Hydraulic conductivity (*K*):**	**9.5 m d^{-1} (K_v)** with permeameter
7.	Remark(s):	coarser sediments with gravel

Laboratory sample **47** (52–57 cm - Appendix 1)
Attributed to trench sampling **section 4**

1.	General lithology (USDA):	medium sand
2.	Median grain size:	479 µm
3.	Total organic matter:	0.24%
4.	Total carbonate ($CaCO_3$):	0.16%
5.	Total porosity:	30.3%
6.	**Hydraulic conductivity (*K*):**	**22.7 m d^{-1} (K_h)** with permeameter
7.	Remark(s):	coarser sediments with gravel

https://doi.org/10.70712/NJG.v105.12686

Field sample **DL13**

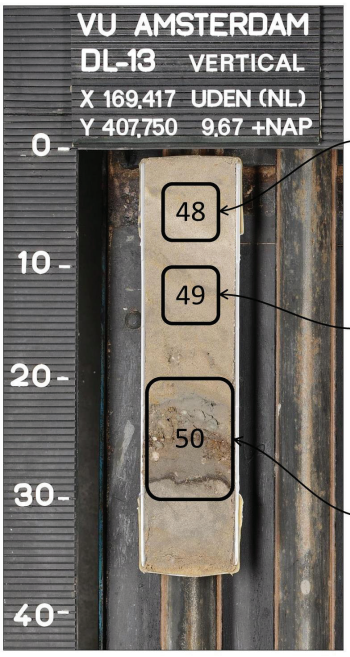

Laboratory sample **48** (3–8 cm - Appendix 1)
Attributed to trench sampling **section 4**

1. General lithology (USDA): fine sand
2. Median grain size: 198 µm
3. Total organic matter: 0.25%
4. Total carbonate ($CaCO_3$): 0.20%
5. Total porosity: 35.9%
6. **Hydraulic conductivity (*K*):** **5.1 m d^{-1} (K_h)** with permeameter
7. Remark(s): -

Laboratory sample **49** (10–15 cm - Appendix 1)
Attributed to trench sampling **section 3**

1. General lithology (USDA): fine sand
2. Median grain size: 156 µm
3. Total organic matter: 0.35%
4. Total carbonate ($CaCO_3$): 0.27%
5. Total porosity: 35.4%
6. **Hydraulic conductivity (*K*):** **2.2 m d^{-1} (K_v)** with permeameter
7. Remark(s): accumulation of organic matter

Laboratory sample **50** (20–30 cm - Appendix 1)
Attributed to trench sampling **section 3**

1. General lithology (USDA): fine sand
2. Median grain size: 180 µm
3. Total organic matter: 0.59%
4. Total carbonate ($CaCO_3$): 0.28%
5. Total porosity: 30.6%
6. **Hydraulic conductivity (*K*):** **0.004 m d^{-1} (K_v)** with triaxial
7. Remark(s): accumulation of fines (compact layering) in coarser sediments

Field sample **DL14**

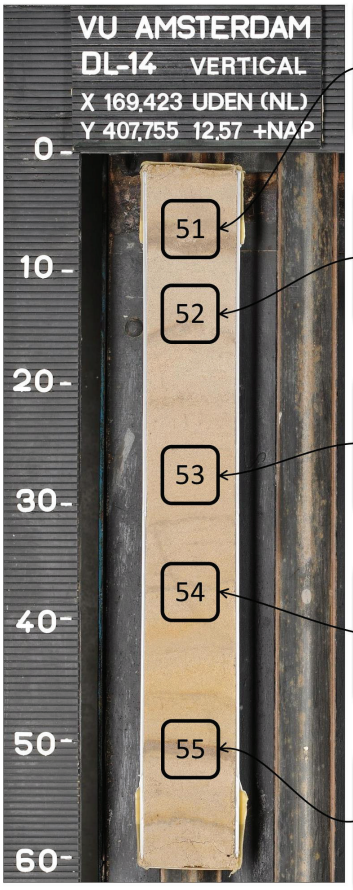

Laboratory sample **51** (4–9 cm - Appendix 1)
Attributed to trench sampling **section 1**

1. General lithology (USDA): fine sand
2. Median grain size: 206 µm
3. Total organic matter: 0.32%
4. Total carbonate ($CaCO_3$): 0.17%
5. Total porosity: 35.8%
6. **Hydraulic conductivity (*K*):** **0.3 m d^{-1} (K_v)** with permeameter
7. Remark(s): thin silty band

Laboratory sample **52** (11–16 cm - Appendix 1)
Attributed to trench sampling **section 1**

1. General lithology (USDA): fine sand
2. Median grain size: 202 µm
3. Total organic matter: 0.26%
4. Total carbonate ($CaCO_3$): 0.19%
5. Total porosity: 36.1%
6. **Hydraulic conductivity (*K*):** **2.7 m d^{-1} (K_h)** with permeameter
7. Remark(s): thin silty band

Laboratory sample **53** (25–30 cm - Appendix 1)
Attributed to trench sampling **section 1**

1. General lithology (USDA): fine sand
2. Median grain size: 174 µm
3. Total organic matter: 0.25%
4. Total carbonate ($CaCO_3$): 0.17%
5. Total porosity: 37.4%
6. **Hydraulic conductivity (*K*):** **3.4 m d^{-1} (K_v)** with permeameter
7. Remark(s): -

Laboratory sample **54** (35–40 cm - Appendix 1)
Attributed to trench sampling **section 1**

1. General lithology (USDA): fine sand
2. Median grain size: 232 µm
3. Total organic matter: 0.26%
4. Total carbonate ($CaCO_3$): 0.18%
5. Total porosity: 36.0%
6. **Hydraulic conductivity (*K*):** **5.6 m d^{-1} (K_h)** with permeameter
7. Remark(s): -

Laboratory sample **55** (48–53 cm - Appendix 1)
Attributed to trench sampling **section 1**

1. General lithology (USDA): fine sand
2. Median grain size: 204 µm
3. Total organic matter: 0.34%
4. Total carbonate ($CaCO_3$): 0.20%
5. Total porosity: 36.5%
6. **Hydraulic conductivity (*K*):** **1.1 m d^{-1} (K_v)** with permeameter
7. Remark(s): thin silty band

Field sample **DL15**

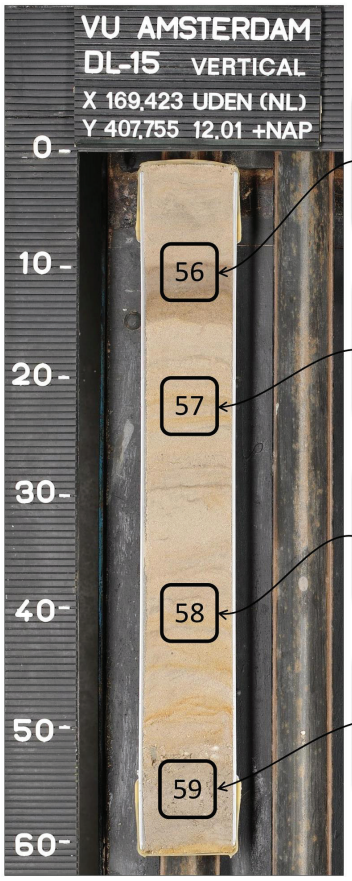

Laboratory sample **56** (8–13 cm - Appendix 1)
Attributed to trench sampling **section 1**

1. General lithology (USDA): fine sand
2. Median grain size: 179 µm
3. Total organic matter: 0.57%
4. Total carbonate ($CaCO_3$): 0.23%
5. Total porosity: 35.4%
6. **Hydraulic conductivity (*K*):** **0.02 m d^{-1} (K_v)** with permeameter
7. Remark(s): thin silty band in sample

Laboratory sample **57** (20–25 cm - Appendix 1)
Attributed to trench sampling **section 1**

1. General lithology (USDA): fine sand
2. Median grain size: 204 µm
3. Total organic matter: 0.21%
4. Total carbonate ($CaCO_3$): 0.17%
5. Total porosity: 35.1%
6. **Hydraulic conductivity (*K*):** **6.6 m d^{-1} (K_h)** with permeameter
7. Remark(s): -

Laboratory sample **58** (38–43 cm - Appendix 1)
Attributed to trench sampling **section 1**

1. General lithology (USDA): fine sand
2. Median grain size: 223 µm
3. Total organic matter: 0.23%
4. Total carbonate ($CaCO_3$): 0.17%
5. Total porosity: 35.4%
6. **Hydraulic conductivity (*K*):** **5.4 m d^{-1} (K_v)** with permeameter
7. Remark(s): -

Laboratory sample **59** (53–58 cm - Appendix 1)
Attributed to trench sampling **section 1**

1. General lithology (USDA): fine sand
2. Median grain size: 203 µm
3. Total organic matter: 0.23%
4. Total carbonate ($CaCO_3$): 0.19%
5. Total porosity: 30.0%
6. **Hydraulic conductivity (*K*):** **3.9 m d^{-1} (K_h)** with permeameter
7. Remark(s): coarser sediments with gravel

https://doi.org/10.70712/NJG.v105.12686

Field sample **DL16**

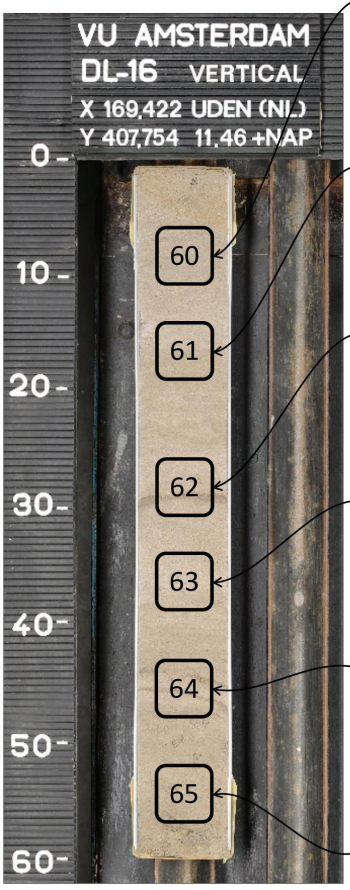

Laboratory sample **60** (6–11 cm - Appendix 1)
Attributed to trench sampling **section 1**

1.	General lithology (USDA):	fine sand
2.	Median grain size:	173 µm
3.	Total organic matter:	0.27%
4.	Total carbonate ($CaCO_3$):	0.23%
5.	Total porosity:	34.7%
6.	**Hydraulic conductivity (K):**	**3.4 m d^{-1} (K_h)** with permeameter
7.	Remark(s):	gravel in sample

Laboratory sample **61** (14–19 cm - Appendix 1)
Attributed to trench sampling **section 1**

1.	General lithology (USDA):	fine sand
2.	Median grain size:	166 µm
3.	Total organic matter:	0.31%
4.	Total carbonate ($CaCO_3$):	0.23%
5.	Total porosity:	35.9%
6.	**Hydraulic conductivity (K):**	**3.1 m d^{-1} (K_h)** with permeameter
7.	Remark(s):	gravel in sample

Laboratory sample **62** (26–31 cm - Appendix 1)
Attributed to trench sampling **section 1**

1.	General lithology (USDA):	fine sand
2.	Median grain size:	179 µm
3.	Total organic matter:	0.37%
4.	Total carbonate ($CaCO_3$):	0.26%
5.	Total porosity:	36.9%
6.	**Hydraulic conductivity (K):**	**0.1 m d^{-1} (K_h)** with permeameter
7.	Remark(s):	thin silty band

Laboratory sample **63** (34–39 cm - Appendix 1)
Attributed to trench sampling **section 1**

1.	General lithology (USDA):	fine sand
2.	Median grain size:	211 µm
3.	Total organic matter:	0.24%
4.	Total carbonate ($CaCO_3$):	0.17%
5.	Total porosity:	34.3%
6.	**Hydraulic conductivity (*K*):**	**5.7 m d^{-1} (K_h)** with permeameter
7.	Remark(s):	-

Laboratory sample **64** (43–48 cm - Appendix 1)
Attributed to trench sampling **section 1**

1.	General lithology (USDA):	fine sand
2.	Median grain size:	183 µm
3.	Total organic matter:	0.35%
4.	Total carbonate ($CaCO_3$):	0.22%
5.	Total porosity:	36.7%
6.	**Hydraulic conductivity (*K*):**	**0.9 m d^{-1} (K_v)** with permeameter
7.	Remark(s):	multiple thin silty bands and gravel

Laboratory sample **65** (52–57 cm - Appendix 1)
Attributed to trench sampling **section 1**

1.	General lithology (USDA):	fine sand
2.	Median grain size:	187 µm
3.	Total organic matter:	0.24%
4.	Total carbonate ($CaCO_3$):	0.17%
5.	Total porosity:	34.1%
6.	**Hydraulic conductivity (*K*):**	**3.5 m d^{-1} (K_h)** with permeameter
7.	Remark(s):	gravel

Field sample **DL17**

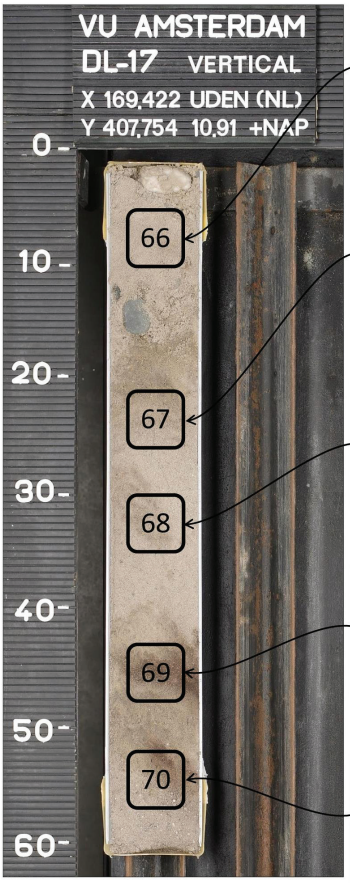

Laboratory sample **66** (5–10 cm - Appendix 1)
Attributed to trench sampling **section 1**

1.	General lithology (USDA):	medium sand
2.	Median grain size:	353 µm
3.	Total organic matter:	0.22%
4.	Total carbonate ($CaCO_3$):	0.14%
5.	Total porosity:	27.4%
6.	**Hydraulic conductivity (K):**	**5.7 m d^{-1} (K_h)** with permeameter
7.	Remark(s):	gravel

Laboratory sample **67** (21–26 cm - Appendix 1)
Attributed to trench sampling **section 1**

1.	General lithology (USDA):	medium sand
2.	Median grain size:	405 µm
3.	Total organic matter:	0.22%
4.	Total carbonate ($CaCO_3$):	0.16%
5.	Total porosity:	31.2%
6.	**Hydraulic conductivity (K):**	**11.6 m d^{-1} (K_v)** with permeameter
7.	Remark(s):	gravel

Laboratory sample **68** (30–35 cm - Appendix 1)
Attributed to trench sampling **section 1**

1.	General lithology (USDA):	medium sand
2.	Median grain size:	384 µm
3.	Total organic matter:	0.21%
4.	Total carbonate ($CaCO_3$):	0.14%
5.	Total porosity:	31.8%
6.	**Hydraulic conductivity (*K*):**	**14.4 m d^{-1} (K_h)** with permeameter
7.	Remark(s):	gravel

Laboratory sample **69** (43–48 cm - Appendix 1)
Attributed to trench sampling **section 1**

1.	General lithology (USDA):	fine sand
2.	Median grain size:	244 µm
3.	Total organic matter:	0.57%
4.	Total carbonate ($CaCO_3$):	0.25%
5.	Total porosity:	32.5%
6.	**Hydraulic conductivity (*K*):**	**2.3 m d^{-1} (K_v)** with permeameter
7.	Remark(s):	diffuse organic matter and gravel

Laboratory sample **70** (52–57 cm - Appendix 1)
Attributed to trench sampling **section 1**

1.	General lithology (USDA):	medium sand
2.	Median grain size:	389 µm
3.	Total organic matter:	0.33%
4.	Total carbonate ($CaCO_3$):	0.05%
5.	Total porosity:	30.9%
6.	**Hydraulic conductivity (*K*):**	**10.0 m d^{-1} (K_h)** with permeameter
7.	Remark(s):	diffuse organic matter and gravel

https://doi.org/10.70712/NJG.v105.12686

Field sample **DL18**

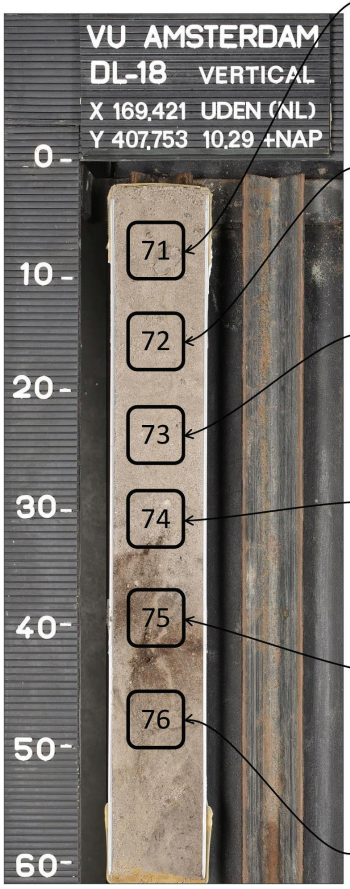

Laboratory sample **71** (5–10 cm - Appendix 1)
Attributed to trench sampling **section 1**

1.	General lithology (USDA):	medium sand
2.	Median grain size:	322 µm
3.	Total organic matter:	0.23%
4.	Total carbonate ($CaCO_3$):	0.18%
5.	Total porosity:	32.5%
6.	**Hydraulic conductivity (*K*):**	**13.7 m d^{-1} (K_v)** with permeameter
7.	Remark(s):	gravel

Laboratory sample **72** (13–18 cm - Appendix 1)
Attributed to trench sampling **section 1**

1.	General lithology (USDA):	medium sand
2.	Median grain size:	394 µm
3.	Total organic matter:	0.20%
4.	Total carbonate ($CaCO_3$):	0.15%
5.	Total porosity:	33.0%
6.	**Hydraulic conductivity (*K*):**	**10.4 m d^{-1} (K_h)** with permeameter
7.	Remark(s):	gravel

Laboratory sample **73** (21–26 cm - Appendix 1)
Attributed to trench sampling **section 1**

1.	General lithology (USDA):	medium sand
2.	Median grain size:	400 µm
3.	Total organic matter:	0.21%
4.	Total carbonate ($CaCO_3$):	0.15%
5.	Total porosity:	33.6%
6.	**Hydraulic conductivity (*K*):**	**16.6 m d^{-1} (K_v)** with permeameter
7.	Remark(s):	thin silty band in sample

Laboratory sample **74** (28–33 cm - Appendix 1)
Attributed to trench sampling **section 1**

1.	General lithology (USDA):	medium sand
2.	Median grain size:	362 µm
3.	Total organic matter:	0.26%
4.	Total carbonate ($CaCO_3$):	0.17%
5.	Total porosity:	31.0%
6.	**Hydraulic conductivity (*K*):**	**13.6 m d^{-1} (K_h)** with permeameter
7.	Remark(s):	gravel

Laboratory sample **75** (37–42 cm - Appendix 1)
Attributed to trench sampling **section 1**

1.	General lithology (USDA):	medium sand
2.	Median grain size:	321 µm
3.	Total organic matter:	0.97%
4.	Total carbonate ($CaCO_3$):	0.45%
5.	Total porosity:	30.0%
6.	**Hydraulic conductivity (*K*):**	**2.1 m d^{-1} (K_v)** with permeameter
7.	Remark(s):	diffuse organic matter and gravel

Laboratory sample **76** (45–50 cm - Appendix 1)
Attributed to trench sampling **section 1**

1.	General lithology (USDA):	medium sand
2.	Median grain size:	269 µm
3.	Total organic matter:	0.26%
4.	Total carbonate ($CaCO_3$):	0.16%
5.	Total porosity:	32.9%
6.	**Hydraulic conductivity (*K*):**	**3.3 m d^{-1} (K_h)** with permeameter
7.	Remark(s):	gravel

Field sample **DL19**

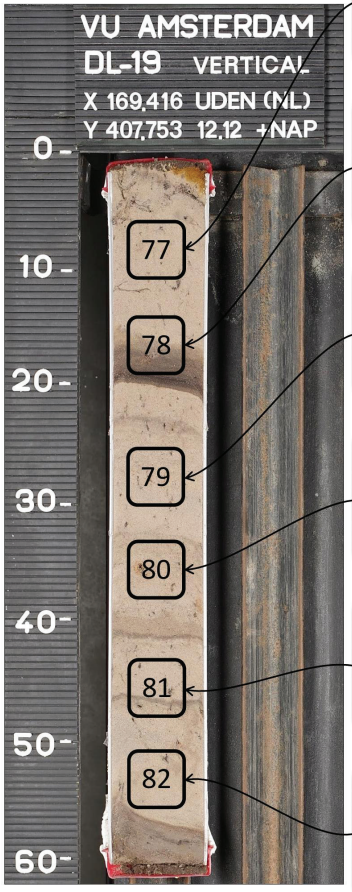

Laboratory sample **77** (6–11 cm - Appendix 1)
Attributed to trench sampling **section 2**

1.	General lithology (USDA):	fine sand
2.	Median grain size:	191 µm
3.	Total organic matter:	0.37%
4.	Total carbonate ($CaCO_3$):	0.20%
5.	Total porosity:	37.0%
6.	**Hydraulic conductivity (*K*):**	**2.9 m d^{-1} (K_v)** with permeameter
7.	Remark(s):	fine root remnants

Laboratory sample **78** (14–19 cm - Appendix 1)
Attributed to trench sampling **section 2**

1.	General lithology (USDA):	fine sand
2.	Median grain size:	184 µm
3.	Total organic matter:	0.79%
4.	Total carbonate ($CaCO_3$):	0.36%
5.	Total porosity:	36.1%
6.	**Hydraulic conductivity (*K*):**	**0.1 m d^{-1} (K_v)** with permeameter
7.	Remark(s):	accumulation of organic matter

Laboratory sample **79** (25–30 cm - Appendix 1)
Attributed to trench sampling **section 2**

1.	General lithology (USDA):	fine sand
2.	Median grain size:	221 µm
3.	Total organic matter:	0.30%
4.	Total carbonate ($CaCO_3$):	0.23%
5.	Total porosity:	34.5%
6.	**Hydraulic conductivity (*K*):**	**4.0 m d^{-1} (K_h)** with permeameter
7.	Remark(s):	fine root remnants

Laboratory sample **80** (33–38 cm - Appendix 1)
Attributed to trench sampling **section 2**

1.	General lithology (USDA):	fine sand
2.	Median grain size:	216 µm
3.	Total organic matter:	0.52%
4.	Total carbonate ($CaCO_3$):	0.24%
5.	Total porosity:	37.4%
6.	**Hydraulic conductivity (*K*):**	**4.0 m d^{-1} (K_h)** with permeameter
7.	Remark(s):	fine root remnants

Laboratory sample **81** (43–48 cm - Appendix 1)
Attributed to trench sampling **section 2**

1.	General lithology (USDA):	fine sand
2.	Median grain size:	183 µm
3.	Total organic matter:	0.40%
4.	Total carbonate ($CaCO_3$):	0.23%
5.	Total porosity:	34.6%
6.	**Hydraulic conductivity (*K*):**	**2.7 m d^{-1} (K_h)** with permeameter
7.	Remark(s):	fine root remnants

Laboratory sample **82** (51–56 cm - Appendix 1)
Attributed to trench sampling **section 2**

1.	General lithology (USDA):	fine sand
2.	Median grain size:	196 µm
3.	Total organic matter:	0.32%
4.	Total carbonate ($CaCO_3$):	0.23%
5.	Total porosity:	37.3%
6.	**Hydraulic conductivity (*K*):**	**4.6 m d^{-1} (K_h)** with permeameter
7.	Remark(s):	fine root remnants

https://doi.org/10.70712/NJG.v105.12686

Field sample **DL20**

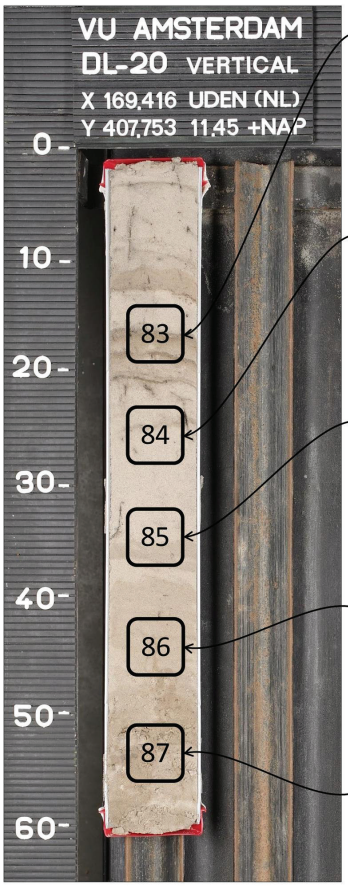

Laboratory sample **83** (14–19 cm - Appendix 1)
Attributed to trench sampling **section 2**

1.	General lithology (USDA):	fine sand
2.	Median grain size:	201 µm
3.	Total organic matter:	0.43%
4.	Total carbonate ($CaCO_3$):	0.24%
5.	Total porosity:	38.8%
6.	**Hydraulic conductivity (*K*):**	**3.6 m d^{-1} (K_v)** with permeameter
7.	Remark(s):	multiple accumulation bands organic matter and root remnants

Laboratory sample **84** (23–28 cm - Appendix 1)
Attributed to trench sampling **section 2**

1.	General lithology (USDA):	fine sand
2.	Median grain size:	204 µm
3.	Total organic matter:	0.24%
4.	Total carbonate ($CaCO_3$):	0.19%
5.	Total porosity:	37.7%
6.	**Hydraulic conductivity (*K*):**	**5.3 m d^{-1} (K_h)** with permeameter
7.	Remark(s):	fine root remnants

Laboratory sample **85** (32–37 cm - Appendix 1)
Attributed to trench sampling **section 2**

1.	General lithology (USDA):	fine sand
2.	Median grain size:	195 µm
3.	Total organic matter:	0.26%
4.	Total carbonate ($CaCO_3$):	0.17%
5.	Total porosity:	35.8%
6.	**Hydraulic conductivity (*K*):**	**4.0 m d^{-1} (K_v)** with permeameter
7.	Remark(s):	fine root remnants and gravel

Laboratory sample **86** (42–47 cm - Appendix 1)
Attributed to trench sampling **section 2**

1.	General lithology (USDA):	fine sand
2.	Median grain size:	180 µm
3.	Total organic matter:	0.27%
4.	Total carbonate ($CaCO_3$):	0.19%
5.	Total porosity:	32.4%
6.	**Hydraulic conductivity (*K*):**	**2.5 m d^{-1} (K_v)** with permeameter
7.	Remark(s):	fine root remnants and gravel

Laboratory sample **87** (51–56 cm - Appendix 1)
Attributed to trench sampling **section 2**

1.	General lithology (USDA):	fine sand
2.	Median grain size:	194 µm
3.	Total organic matter:	0.29%
4.	Total carbonate ($CaCO_3$):	0.17%
5.	Total porosity:	32.5%
6.	**Hydraulic conductivity (*K*):**	**3.3 m d^{-1} (K_h)** with permeameter
7.	Remark(s):	fine root remnants and gravel

Field sample **DL21**

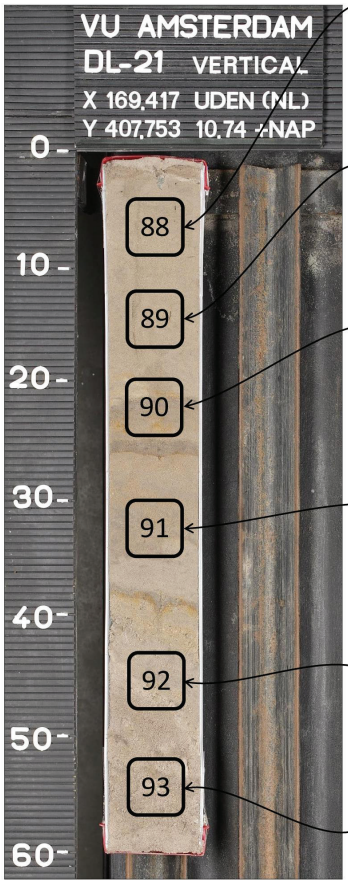

Laboratory sample **88** (4–9 cm - Appendix 1)
Attributed to trench sampling **section 2**

1.	General lithology (USDA):	fine sand
2.	Median grain size:	147 µm
3.	Total organic matter:	0.47%
4.	Total carbonate ($CaCO_3$):	0.21%
5.	Total porosity:	37.0%
6.	**Hydraulic conductivity (*K*):**	**1.4 m d^{-1} (K_v)** with permeameter
7.	Remark(s):	-

Laboratory sample **89** (12–17 cm - Appendix 1)
Attributed to trench sampling **section 2**

1.	General lithology (USDA):	fine sand
2.	Median grain size:	146 µm
3.	Total organic matter:	0.46%
4.	Total carbonate ($CaCO_3$):	0.20%
5.	Total porosity:	35.1%
6.	**Hydraulic conductivity (*K*):**	**1.4 m d^{-1} (K_h)** with permeameter
7.	Remark(s):	-

Laboratory sample **90** (20–25 cm - Appendix 1)
Attributed to trench sampling **section 2**

1.	General lithology (USDA):	fine sand
2.	Median grain size:	178 µm
3.	Total organic matter:	0.48%
4.	Total carbonate ($CaCO_3$):	0.20%
5.	Total porosity:	35.2%
6.	**Hydraulic conductivity (*K*):**	**0.2 m d^{-1} (K_v)** with permeameter
7.	Remark(s):	thin silty band and iron discolorations

Laboratory sample **91** (30–35 cm - Appendix 1)
Attributed to trench sampling **section 2**

1.	General lithology (USDA):	fine sand
2.	Median grain size:	164 µm
3.	Total organic matter:	0.40%
4.	Total carbonate ($CaCO_3$):	0.18%
5.	Total porosity:	35.8%
6.	**Hydraulic conductivity (*K*):**	**2.2 m d^{-1} (K_h)** with permeameter
7.	Remark(s):	-

Laboratory sample **92** (43–48 cm - Appendix 1)
Attributed to trench sampling **section 2**

1.	General lithology (USDA):	medium sand
2.	Median grain size:	307 µm
3.	Total organic matter:	0.22%
4.	Total carbonate ($CaCO_3$):	0.10%
5.	Total porosity:	31.8%
6.	**Hydraulic conductivity (*K*):**	**10.6 m d^{-1} (K_h)** with permeameter
7.	Remark(s):	coarser sediments with gravel

Laboratory sample **93** (52–57 cm - Appendix 1)
Attributed to trench sampling **section 2**

1.	General lithology (USDA):	medium sand
2.	Median grain size:	311 µm
3.	Total organic matter:	0.21%
4.	Total carbonate ($CaCO_3$):	0.08%
5.	Total porosity:	31.1%
6.	**Hydraulic conductivity (*K*):**	**11.9 m d^{-1} (K_v)** with permeameter
7.	Remark(s):	coarser sediments with gravel

https://doi.org/10.70712/NJG.v105.12686

Field sample **DL22**

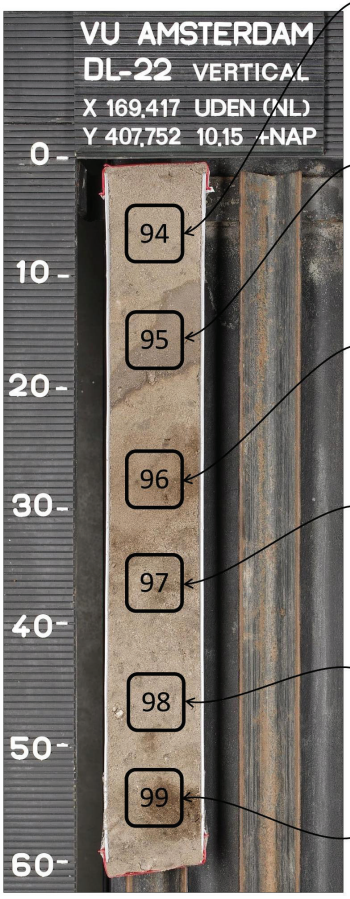

Laboratory sample **94** (4–9 cm - Appendix 1)
Attributed to trench sampling **section 2**

1. General lithology (USDA): medium sand
2. Median grain size: 299 µm
3. Total organic matter: 0.26%
4. Total carbonate ($CaCO_3$): 0.11%
5. Total porosity: 32.2%
6. **Hydraulic conductivity (*K*):** **10.0 m d^{-1} (K_h)** with permeameter
7. Remark(s): gravel

Laboratory sample **95** (13–18 cm - Appendix 1)
Attributed to trench sampling **section 2**

1. General lithology (USDA): medium sand
2. Median grain size: 299 µm
3. Total organic matter: 0.33%
4. Total carbonate ($CaCO_3$): 0.12%
5. Total porosity: 33.0%
6. **Hydraulic conductivity (*K*):** **3.8 m d^{-1} (K_v)** with permeameter
7. Remark(s): thin silty band, traces of iron discolorations and gravel

Laboratory sample **96** (25–30 cm - Appendix 1)
Attributed to trench sampling **section 2**

1. General lithology (USDA): medium sand
2. Median grain size: 348 µm
3. Total organic matter: 0.25%
4. Total carbonate ($CaCO_3$): 0.12%
5. Total porosity: 32.9%
6. **Hydraulic conductivity (*K*):** **12.3 m d^{-1} (K_h)** with permeameter
7. Remark(s): gravel

Laboratory sample **97** (34–39 cm - Appendix 1)
Attributed to trench sampling **section 2**

1. General lithology (USDA): medium sand
2. Median grain size: 374 µm
3. Total organic matter: 0.25%
4. Total carbonate ($CaCO_3$): 0.17%
5. Total porosity: 30.1%
6. **Hydraulic conductivity (*K*):** **10.4 m d^{-1} (K_h)** with permeameter
7. Remark(s): gravel

Laboratory sample **98** (44–49 cm - Appendix 1)
Attributed to trench sampling **section 2**

1. General lithology (USDA): medium sand
2. Median grain size: 350 µm
3. Total organic matter: 0.20%
4. Total carbonate ($CaCO_3$): 0.14%
5. Total porosity: 31.9%
6. **Hydraulic conductivity (*K*):** **12.3 m d^{-1} (K_h)** with permeameter
7. Remark(s): gravel

Laboratory sample **99** (52–57 cm - Appendix 1)
Attributed to trench sampling **section 2**

1. General lithology (USDA): medium sand
2. Median grain size: 352 µm
3. Total organic matter: 0.52%
4. Total carbonate ($CaCO_3$): 0.21%
5. Total porosity: 30.2%
6. **Hydraulic conductivity (*K*):** **4.5 m d^{-1} (K_v)** with permeameter
7. Remark(s): diffuse organic matter and gravel

Field sample **DL23**

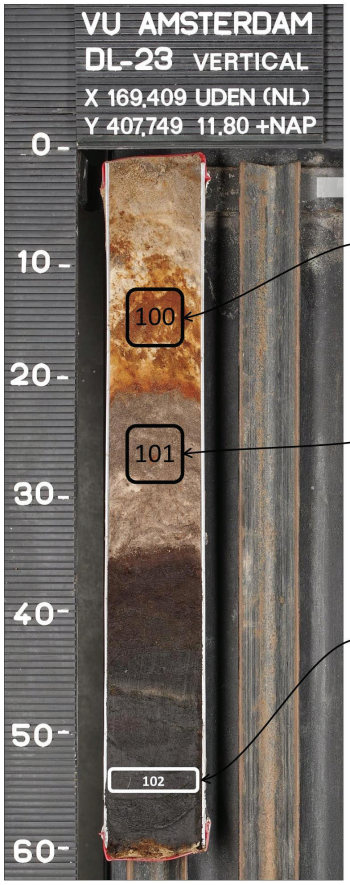

Laboratory sample **100** (12–17 cm - Appendix 1)
Excluded from analyses

1. General lithology (USDA): fine sand
2. Median grain size: 204 µm
3. Total organic matter: 1.13%
4. Total carbonate ($CaCO_3$): 0.24%
5. Total porosity: 39.1%
6. **Hydraulic conductivity (*K*):** **1.8 m d^{-1} (K_v)** with permeameter
7. Remark(s): iron precipitation in reworked top layer (man-made channel)

Laboratory sample **101** (24–29 cm - Appendix 1)
Excluded from analyses

1. General lithology (USDA): fine sand
2. Median grain size: 201 µm
3. Total organic matter: 1.97%
4. Total carbonate ($CaCO_3$): 0.26%
5. Total porosity: 43.1%
6. **Hydraulic conductivity (*K*):** **0.3 m d^{-1} (K_v)** with permeameter
7. Remark(s): reworked layer (man-made channel)

Laboratory sample **102** (53–55 cm - Appendix 1)
Excluded from analyses

1. General lithology (USDA): organic layer
2. Median grain size: 34 µm
3. Total organic matter: 43.19%
4. Total carbonate ($CaCO_3$): 10.70%
5. Total porosity: 79.5%
6. **Hydraulic conductivity (*K*):** **0.1 m d^{-1} (*Kv*)** with mod. oedometer
7. Remark(s): layer with organic matter, clay and silt (man-made channel)

https://doi.org/10.70712/NJG.v105.12686

Field sample **DL24**

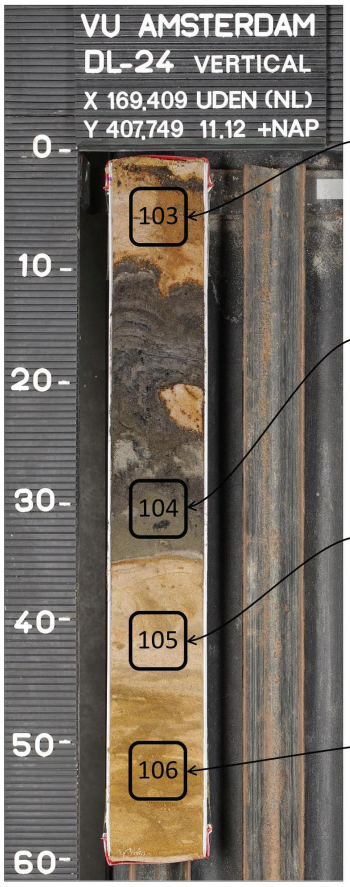

Laboratory sample **103** (3–8 cm - Appendix 1)
Excluded from analyses

1.	General lithology (USDA):	fine sand
2.	Median grain size:	228 µm
3.	Total organic matter:	0.72%
4.	Total carbonate ($CaCO_3$):	0.37%
5.	Total porosity:	39.5%
6.	**Hydraulic conductivity (*K*):**	**2.5 m d^{-1} (K_v)** with permeameter
7.	Remark(s):	diffuse iron precipitation (man-made channel)

Laboratory sample **104** (28–33 cm - Appendix 1)
Excluded from analyses

1.	General lithology (USDA):	fine sand
2.	Median grain size:	205 µm
3.	Total organic matter:	1.11%
4.	Total carbonate ($CaCO_3$):	0.50%
5.	Total porosity:	36.7%
6.	**Hydraulic conductivity (*K*):**	**0.01 m d^{-1} (K_h)** with permeameter
7.	Remark(s):	reworked layer with organic matter (man-made channel)

Laboratory sample **105** (39–44 cm - Appendix 1)
Excluded from analyses

1.	General lithology (USDA):	fine sand
2.	Median grain size:	210 µm
3.	Total organic matter:	0.29%
4.	Total carbonate ($CaCO_3$):	0.18%
5.	Total porosity:	36.2%
6.	**Hydraulic conductivity (*K*):**	**1.2 m d^{-1} (K_h)** with permeameter
7.	Remark(s):	reworked bottom with iron precipitation (man-made channel)

Laboratory sample **106** (50–55 cm - Appendix 1)
Attributed to trench sampling **section 5**

1.	General lithology (USDA):	fine sand
2.	Median grain size:	203 µm
3.	Total organic matter:	0.38%
4.	Total carbonate ($CaCO_3$):	0.18%
5.	Total porosity:	39.4%
6.	**Hydraulic conductivity (*K*):**	**0.7 m d^{-1} (K_v)** with permeameter
7.	Remark(s):	diffuse iron precipitation below reworked bottom

Field sample **DL25**

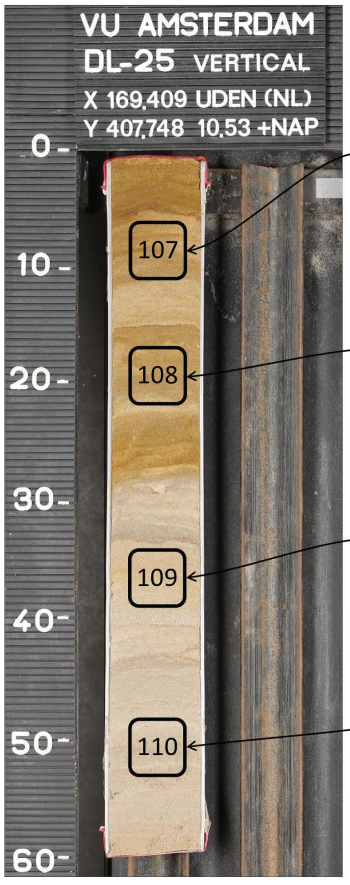

Laboratory sample **107** (6–11 cm - Appendix 1)
Attributed to trench sampling **section 5**

1.	General lithology (USDA):	fine sand
2.	Median grain size:	186 µm
3.	Total organic matter:	0.34%
4.	Total carbonate ($CaCO_3$):	0.19%
5.	Total porosity:	38.2%
6.	**Hydraulic conductivity (*K*):**	**1.1 m d^{-1} (K_h)** with permeameter
7.	Remark(s):	diffuse iron precipitation

Laboratory sample **108** (17–22 cm - Appendix 1)
Attributed to trench sampling **section 5**

1.	General lithology (USDA):	fine sand
2.	Median grain size:	213 µm
3.	Total organic matter:	0.33%
4.	Total carbonate ($CaCO_3$):	0.15%
5.	Total porosity:	38.5%
6.	**Hydraulic conductivity (*K*):**	**0.3 m d^{-1} (K_v)** with permeameter
7.	Remark(s):	diffuse iron precipitation

Laboratory sample **109** (34–39 cm - Appendix 1)
Attributed to trench sampling **section 5**

1.	General lithology (USDA):	fine sand
2.	Median grain size:	227 µm
3.	Total organic matter:	0.19%
4.	Total carbonate ($CaCO_3$):	0.16%
5.	Total porosity:	39.4%
6.	**Hydraulic conductivity (*K*):**	**5.8 m d^{-1} (K_v)** with permeameter
7.	Remark(s):	little iron precipitation

Laboratory sample **110** (48–53 cm - Appendix 1)
Attributed to trench sampling **section 5**

1.	General lithology (USDA):	fine sand
2.	Median grain size:	169 µm
3.	Total organic matter:	0.21%
4.	Total carbonate ($CaCO_3$):	0.18%
5.	Total porosity:	37.1%
6.	**Hydraulic conductivity (*K*):**	**3.2 m d^{-1} (K_h)** with permeameter
7.	Remark(s):	-

https://doi.org/10.70712/NJG.v105.12686

Field sample **DL26**

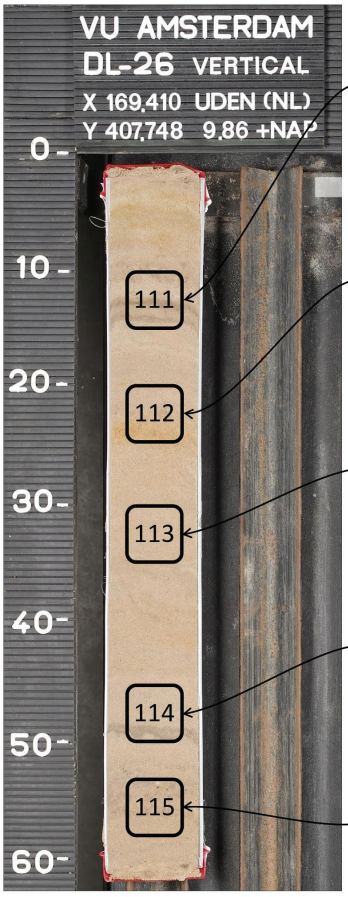

Laboratory sample **111** (10–15 cm - Appendix 1)
Attributed to trench sampling **section 5**

1.	General lithology (USDA):	fine sand
2.	Median grain size:	148 µm
3.	Total organic matter:	0.32%
4.	Total carbonate ($CaCO_3$):	0.23%
5.	Total porosity:	36.2%
6.	**Hydraulic conductivity (*K*):**	**0.9 m d^{-1} (K_v)** with permeameter
7.	Remark(s):	thin silty band and gravel

Laboratory sample **112** (20–25 cm - Appendix 1)
Attributed to trench sampling **section 5**

1.	General lithology (USDA):	medium sand
2.	Median grain size:	265 µm
3.	Total organic matter:	0.22%
4.	Total carbonate ($CaCO_3$):	0.24%
5.	Total porosity:	34.8%
6.	**Hydraulic conductivity (*K*):**	**32.1 m d^{-1} (K_h)** with permeameter
7.	Remark(s):	traces of iron discolorations

Laboratory sample **113** (30–35 cm - Appendix 1)
Attributed to trench sampling **section 5**

1.	General lithology (USDA):	fine sand
2.	Median grain size:	184 µm
3.	Total organic matter:	0.24%
4.	Total carbonate ($CaCO_3$):	0.24%
5.	Total porosity:	36.6%
6.	**Hydraulic conductivity (*K*):**	**2.7 m d^{-1} (K_v)** with permeameter
7.	Remark(s):	gravel

Laboratory sample **114** (45–50 cm - Appendix 1)
Attributed to trench sampling **section 5**

1.	General lithology (USDA):	fine sand
2.	Median grain size:	152 µm
3.	Total organic matter:	0.25%
4.	Total carbonate ($CaCO_3$):	0.25%
5.	Total porosity:	36.3%
6.	**Hydraulic conductivity (*K*):**	**3.1 m d^{-1} (K_h)** with permeameter
7.	Remark(s):	thin silty band

Laboratory sample **115** (53–58 cm - Appendix 1)
Attributed to trench sampling **section 5**

1.	General lithology (USDA):	fine sand
2.	Median grain size:	197 µm
3.	Total organic matter:	0.24%
4.	Total carbonate ($CaCO_3$):	0.23%
5.	Total porosity:	35.2%
6.	**Hydraulic conductivity (*K*):**	**3.2 m d^{-1} (K_h)** with permeameter
7.	Remark(s):	gravel

Field sample **DL27**

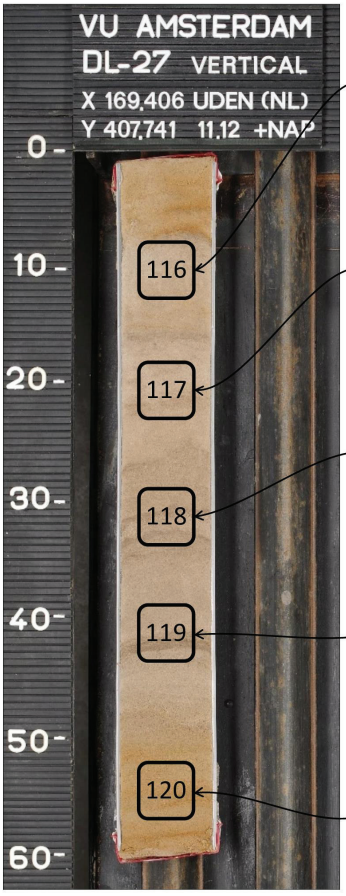

Laboratory sample **116** (7–12 cm - Appendix 1)
Attributed to trench sampling **section 5**

1.	General lithology (USDA):	fine sand
2.	Median grain size:	191 µm
3.	Total organic matter:	0.27%
4.	Total carbonate ($CaCO_3$):	0.17%
5.	Total porosity:	36.6%
6.	**Hydraulic conductivity (*K*):**	**4.5 m d^{-1} (K_h)** with permeameter
7.	Remark(s):	traces of iron discolorations and gravel

Laboratory sample **117** (18–23 cm - Appendix 1)
Attributed to trench sampling **section 5**

1.	General lithology (USDA):	fine sand
2.	Median grain size:	242 µm
3.	Total organic matter:	0.26%
4.	Total carbonate ($CaCO_3$):	0.15%
5.	Total porosity:	37.2%
6.	**Hydraulic conductivity (*K*):**	**6.6 m d^{-1} (K_h)** with permeameter
7.	Remark(s):	-

Laboratory sample **118** (29–34 cm - Appendix 1)
Attributed to trench sampling **section 5**

1.	General lithology (USDA):	fine sand
2.	Median grain size:	218 µm
3.	Total organic matter:	0.34%
4.	Total carbonate ($CaCO_3$):	0.19%
5.	Total porosity:	35.6%
6.	**Hydraulic conductivity (*K*):**	**1.9 m d^{-1} (K_v)** with permeameter
7.	Remark(s):	multiple thin silty bands and gravel

Laboratory sample **119** (39–44 cm - Appendix 1)
Attributed to trench sampling **section 5**

1.	General lithology (USDA):	fine sand
2.	Median grain size:	241 µm
3.	Total organic matter:	0.33%
4.	Total carbonate ($CaCO_3$):	0.18%
5.	Total porosity:	35.6%
6.	**Hydraulic conductivity (*K*):**	**1.6 m d^{-1} (K_v)** with permeameter
7.	Remark(s):	multiple thin silty bands

Laboratory sample **120** (52–57 cm - Appendix 1)
Attributed to trench sampling **section 5**

1.	General lithology (USDA):	fine sand
2.	Median grain size:	219 µm
3.	Total organic matter:	0.25%
4.	Total carbonate ($CaCO_3$):	0.15%
5.	Total porosity:	36.3%
6.	**Hydraulic conductivity (*K*):**	**5.2 m d^{-1} (K_h)** with permeameter
7.	Remark(s):	diffuse iron precipitation

https://doi.org/10.70712/NJG.v105.12686

Field sample **DL28**

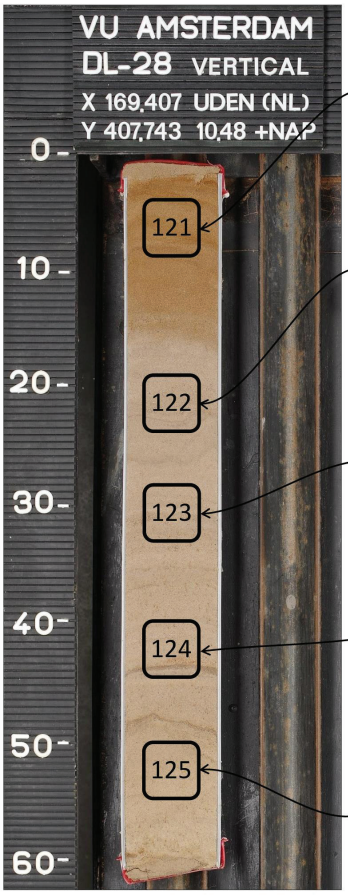

Laboratory sample **121** (4–9 cm - Appendix 1)
Attributed to trench sampling **section 5**

1.	General lithology (USDA):	fine sand
2.	Median grain size:	189 µm
3.	Total organic matter:	0.30%
4.	Total carbonate ($CaCO_3$):	0.18%
5.	Total porosity:	37.4%
6.	**Hydraulic conductivity (*K*):**	**2.9 m d^{-1} (K_v)** with permeameter
7.	Remark(s):	diffuse iron precipitation and gravel

Laboratory sample **122** (19–24 cm - Appendix 1)
Attributed to trench sampling **section 5**

1.	General lithology (USDA):	fine sand
2.	Median grain size:	213 µm
3.	Total organic matter:	0.25%
4.	Total carbonate ($CaCO_3$):	0.21%
5.	Total porosity:	34.4%
6.	**Hydraulic conductivity (*K*):**	**1.8 m d^{-1} (K_v)** with permeameter
7.	Remark(s):	gravel

Laboratory sample **123** (28–33 cm - Appendix 1)
Attributed to trench sampling **section 5**

1.	General lithology (USDA):	fine sand
2.	Median grain size:	212 µm
3.	Total organic matter:	0.24%
4.	Total carbonate ($CaCO_3$):	0.22%
5.	Total porosity:	33.3%
6.	**Hydraulic conductivity (*K*):**	**2.9 m d^{-1} (K_h)** with permeameter
7.	Remark(s):	gravel in sample

Laboratory sample **124** (40–45 cm - Appendix 1)
Attributed to trench sampling **section 5**

1.	General lithology (USDA):	fine sand
2.	Median grain size:	207 µm
3.	Total organic matter:	0.24%
4.	Total carbonate ($CaCO_3$):	0.18%
5.	Total porosity:	34.4%
6.	**Hydraulic conductivity (*K*):**	**0.7 m d^{-1} (K_v)** with permeameter
7.	Remark(s):	thin silty band

Laboratory sample **125** (50–55 cm - Appendix 1)
Attributed to trench sampling **section 5**

1.	General lithology (USDA):	fine sand
2.	Median grain size:	195 µm
3.	Total organic matter:	0.19%
4.	Total carbonate ($CaCO_3$):	0.13%
5.	Total porosity:	37.8%
6.	**Hydraulic conductivity (*K*):**	**3.9 m d^{-1} (K_h)** with permeameter
7.	Remark(s):	-

Field sample **DL29**

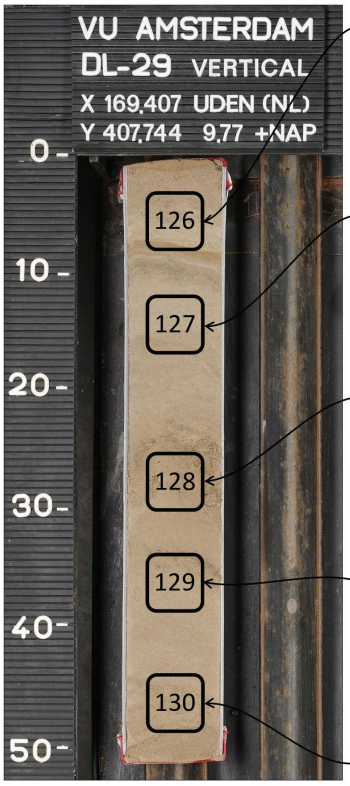

Laboratory sample **126** (3–8 cm - Appendix 1)
Attributed to trench sampling **section 5**

1.	General lithology (USDA):	fine sand
2.	Median grain size:	208 µm
3.	Total organic matter:	0.18%
4.	Total carbonate ($CaCO_3$):	0.14%
5.	Total porosity:	35.0%
6.	**Hydraulic conductivity (*K*):**	**1.8 m d^{-1} (K_v)** with permeameter
7.	Remark(s):	traces of iron discolorations and gravel

Laboratory sample **127** (12–17 cm - Appendix 1)
Attributed to trench sampling **section 5**

1.	General lithology (USDA):	fine sand
2.	Median grain size:	181 µm
3.	Total organic matter:	0.20%
4.	Total carbonate ($CaCO_3$):	0.13%
5.	Total porosity:	37.4%
6.	**Hydraulic conductivity (*K*):**	**2.0 m d^{-1} (K_h)** with permeameter
7.	Remark(s):	-

Laboratory sample **128** (25–30 cm - Appendix 1)
Attributed to trench sampling **section 5**

1.	General lithology (USDA):	fine sand
2.	Median grain size:	187 µm
3.	Total organic matter:	0.26%
4.	Total carbonate ($CaCO_3$):	0.17%
5.	Total porosity:	34.7%
6.	**Hydraulic conductivity (*K*):**	**3.3 m d^{-1} (K_h)** with permeameter
7.	Remark(s):	gravel

Laboratory sample **129** (34–39 cm - Appendix 1)
Attributed to trench sampling **section 5**

1.	General lithology (USDA):	fine sand
2.	Median grain size:	201 µm
3.	Total organic matter:	0.19%
4.	Total carbonate ($CaCO_3$):	0.12%
5.	Total porosity:	35.1%
6.	**Hydraulic conductivity (*K*):**	**5.1 m d^{-1} (K_v)** with permeameter
7.	Remark(s):	gravel

Laboratory sample **130** (44–49 cm - Appendix 1)
Attributed to trench sampling **section 5**

1.	General lithology (USDA):	fine sand
2.	Median grain size:	204 µm
3.	Total organic matter:	0.21%
4.	Total carbonate ($CaCO_3$):	0.10%
5.	Total porosity:	36.0%
6.	**Hydraulic conductivity (*K*):**	**5.8 m d^{-1} (K_h)** with permeameter
7.	Remark(s):	-

https://doi.org/10.70712/NJG.v105.12686

Field sample **DL30**

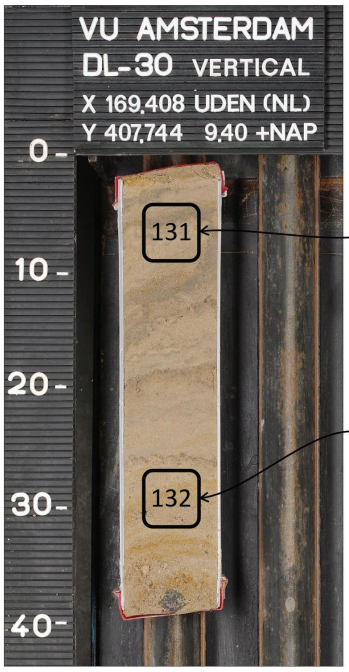

Laboratory sample **131** (4–9 cm - Appendix 1)
Attributed to trench sampling **section 5**

1.	General lithology (USDA):	fine sand
2.	Median grain size:	157 µm
3.	Total organic matter:	0.29%
4.	Total carbonate ($CaCO_3$):	0.16%
5.	Total porosity:	36.5%
6.	**Hydraulic conductivity (*K*):**	**1.9 m d^{-1} (K_n)** with permeameter
7.	Remark(s):	multiple silty bands

Laboratory sample **132** (27–32 cm - Appendix 1)
Attributed to trench sampling **section 5**

1.	General lithology (USDA):	fine sand
2.	Median grain size:	225 µm
3.	Total organic matter:	0.19%
4.	Total carbonate ($CaCO_3$):	0.14%
5.	Total porosity:	34.9%
6.	**Hydraulic conductivity (*K*):**	**5.0 m d^{-1} (K_n)** with permeameter
7.	Remark(s):	traces of iron discolorations and gravel

Field sample **DL32**

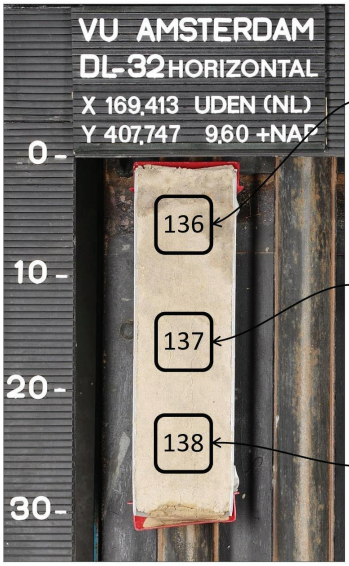

Laboratory sample **136** (3–8 cm - Appendix 1)
Attributed to trench sampling **section 5**

1.	General lithology (USDA):	fine sand
2.	Median grain size:	152 µm
3.	Total organic matter:	0.26%
4.	Total carbonate ($CaCO_3$):	0.19%
5.	Total porosity:	37.6%
6.	**Hydraulic conductivity (*K*):**	**3.7 m d^{-1} (K_h)** with permeameter
7.	Remark(s):	silt and gravel

Laboratory sample **137** (13–18 cm - Appendix 1)
Attributed to trench sampling **section 5**

1.	General lithology (USDA):	fine sand
2.	Median grain size:	146 µm
3.	Total organic matter:	0.35%
4.	Total carbonate ($CaCO_3$):	0.22%
5.	Total porosity:	37.9%
6.	**Hydraulic conductivity (*K*):**	**1.8 m d^{-1} (K_h)** with permeameter
7.	Remark(s):	silt and gravel

Laboratory sample **138** (22–27 cm - Appendix 1)
Attributed to trench sampling **section 5**

1.	General lithology (USDA):	fine sand
2.	Median grain size:	156 µm
3.	Total organic matter:	0.31%
4.	Total carbonate ($CaCO_3$):	0.22%
5.	Total porosity:	37.1%
6.	**Hydraulic conductivity (*K*):**	**0.5 m d^{-1} (K_n)** with permeameter
7.	Remark(s):	silt and gravel

Field sample **DL31**

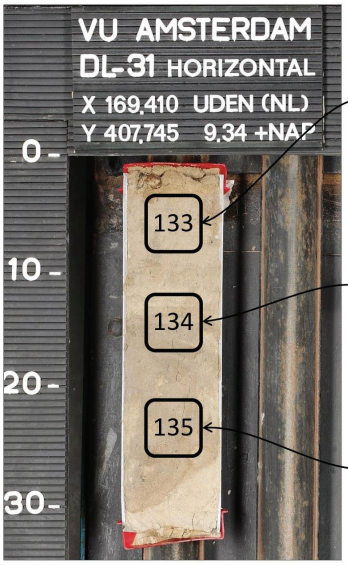

Laboratory sample **133** (3–8 cm - Appendix 1)
Attributed to trench sampling **section 5**

1.	General lithology (USDA):	fine sand
2.	Median grain size:	186 µm
3.	Total organic matter:	0.23%
4.	Total carbonate ($CaCO_3$):	0.15%
5.	Total porosity:	35.9%
6.	**Hydraulic conductivity (*K*):**	**5.6 m d^{-1} (K_h)** with permeameter
7.	Remark(s):	gravel

Laboratory sample **134** (12–17 cm - Appendix 1)
Attributed to trench sampling **section 5**

1.	General lithology (USDA):	fine sand
2.	Median grain size:	179 µm
3.	Total organic matter:	0.24%
4.	Total carbonate ($CaCO_3$):	0.13%
5.	Total porosity:	35.3%
6.	**Hydraulic conductivity (*K*):**	**5.2 m d^{-1} (K_h)** with permeameter
7.	Remark(s):	gravel in sample

Laboratory sample **135** (21–26 cm - Appendix 1)
Attributed to trench sampling **section 5**

1.	General lithology (USDA):	fine sand
2.	Median grain size:	163 µm
3.	Total organic matter:	0.26%
4.	Total carbonate ($CaCO_3$):	0.20%
5.	Total porosity:	36.5%
6.	**Hydraulic conductivity (*K*):**	**3.7 m d^{-1} (K_h)** with permeameter
7.	Remark(s):	gravel in sample

https://doi.org/10.70712/NJG.v105.12686

Field sample **DL33A**

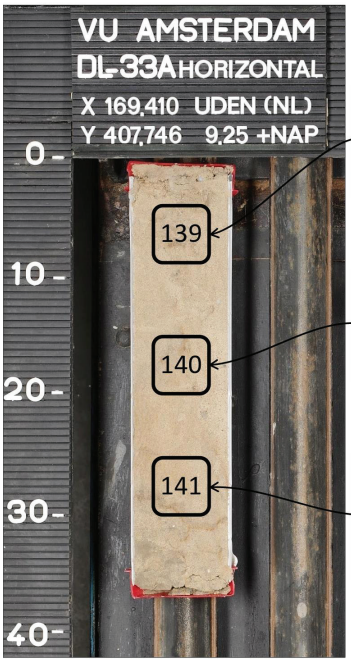

Laboratory sample **139** (4–9 cm - Appendix 1)
Attributed to trench sampling **section 5**

1.	General lithology (USDA):	fine sand
2.	Median grain size:	173 µm
3.	Total organic matter:	0.24%
4.	Total carbonate ($CaCO_3$):	0.20%
5.	Total porosity:	36.4%
6.	**Hydraulic conductivity (*K*):**	**4.2 m d^{-1} (K_v)** with permeameter
7.	Remark(s):	gravel

Laboratory sample **140** (15–20 cm - Appendix 1)
Attributed to trench sampling **section 5**

1.	General lithology (USDA):	fine sand
2.	Median grain size:	181 µm
3.	Total organic matter:	0.22%
4.	Total carbonate ($CaCO_3$):	0.16%
5.	Total porosity:	36.5%
6.	**Hydraulic conductivity (*K*):**	**4.1 m d^{-1} (K_v)** with permeameter
7.	Remark(s):	gravel

Laboratory sample **141** (25–30 cm - Appendix 1)
Attributed to trench sampling **section 5**

1.	General lithology (USDA):	fine sand
2.	Median grain size:	191 µm
3.	Total organic matter:	0.27%
4.	Total carbonate ($CaCO_3$):	0.17%
5.	Total porosity:	36.4%
6.	**Hydraulic conductivity (*K*):**	**2.7 m d^{-1} (K_h)** with permeameter
7.	Remark(s):	traces of iron discolorations and gravel

Field sample **DL33B**

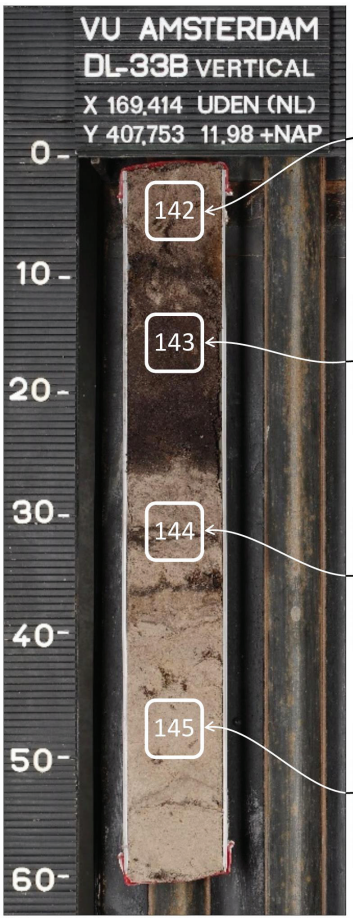

Laboratory sample **142** (2–7 cm - Appendix 1)
Excluded from analyses

1.	General lithology (USDA):	fine sand
2.	Median grain size:	199 µm
3.	Total organic matter:	2.86%
4.	Total carbonate ($CaCO_3$):	0.38%
5.	Total porosity:	48.1%
6.	**Hydraulic conductivity (*K*):**	**1.6 m d^{-1} (K_v)** with permeameter
7.	Remark(s):	root remains and organic matter in reworked top layer (man-made channel)

Laboratory sample **143** (13–18 cm - Appendix 1)
Excluded from analyses

1.	General lithology (USDA):	fine sand
2.	Median grain size:	196 µm
3.	Total organic matter:	4.53%
4.	Total carbonate ($CaCO_3$):	0.53%
5.	Total porosity:	55.9%
6.	**Hydraulic conductivity (*K*):**	**0.2 m d^{-1} (K_v)** with permeameter
7.	Remark(s):	root remains and organic matter in reworked top layer (man-made channel)

Laboratory sample **144** (29–34 cm - Appendix 1)
Excluded from analyses

1.	General lithology (USDA):	fine sand
2.	Median grain size:	218 µm
3.	Total organic matter:	1.68%
4.	Total carbonate ($CaCO_3$):	0.29%
5.	Total porosity:	43.9%
6.	**Hydraulic conductivity (*K*):**	**2.4 m d^{-1} (K_v)** with permeameter
8.	Remark(s):	root remains and organic matter in reworked layer (man-made channel)

Laboratory sample **145** (45–50 cm - Appendix 1)
Excluded from analyses

1.	General lithology (USDA):	fine sand
2.	Median grain size:	179 µm
3.	Total organic matter:	0.37%
4.	Total carbonate ($CaCO_3$):	0.27%
5.	Total porosity:	39.8%
6.	**Hydraulic conductivity (*K*):**	**3.8 m d^{-1} (K_h)** with permeameter
7.	Remark(s):	root remains and organic matter in reworked layer (man-made channel)

https://doi.org/10.70712/NJG.v105.12686

Field sample **DL34**

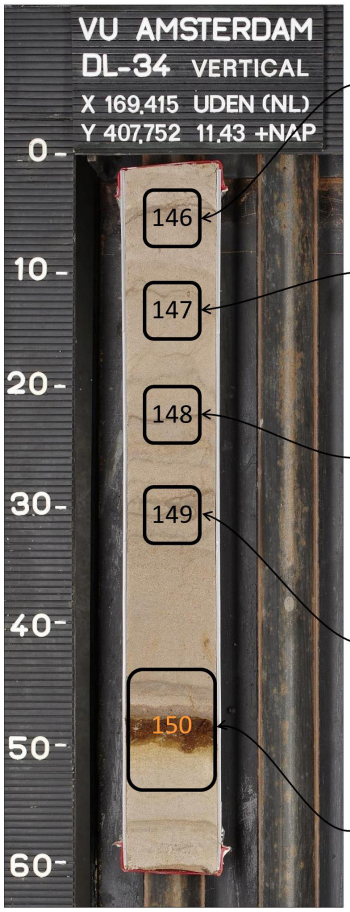

Laboratory sample **146** (3–8 cm - Appendix 1)
Attributed to trench sampling **section 4**

1.	General lithology (USDA):	fine sand
2.	Median grain size:	215 µm
3.	Total organic matter:	0.23%
4.	Total carbonate ($CaCO_3$):	0.16%
5.	Total porosity:	35.6%
6.	**Hydraulic conductivity (*K*):**	**5.6 m d^{-1} (K_h)** with permeameter
7.	Remark(s):	-

Laboratory sample **147** (11–16 cm - Appendix 1)
Attributed to trench sampling **section 4**

1.	General lithology (USDA):	fine sand
2.	Median grain size:	185 µm
3.	Total organic matter:	0.27%
4.	Total carbonate ($CaCO_3$):	0.17%
5.	Total porosity:	38.4%
6.	**Hydraulic conductivity (*K*):**	**3.8 m d^{-1} (K_v)** with permeameter
7.	Remark(s):	-

Laboratory sample **148** (20–25 cm - Appendix 1)
Attributed to trench sampling **section 4**

1.	General lithology (USDA):	fine sand
2.	Median grain size:	196 µm
3.	Total organic matter:	0.33%
4.	Total carbonate ($CaCO_3$):	0.20%
5.	Total porosity:	37.0%
6.	**Hydraulic conductivity (*K*):**	**2.6 m d^{-1} (K_h)** with permeameter
7.	Remark(s):	-

Laboratory sample **149** (28–33 cm - Appendix 1)
Attributed to trench sampling **section 4**

1.	General lithology (USDA):	fine sand
2.	Median grain size:	209 µm
3.	Total organic matter:	0.26%
4.	Total carbonate ($CaCO_3$):	0.17%
5.	Total porosity:	34.7%
6.	**Hydraulic conductivity (*K*):**	**2.8 m d^{-1} (K_v)** with permeameter
7.	Remark(s):	-

Laboratory sample **150** (44–54 cm - Appendix 1)
Attributed to trench sampling **section 3**

1.	General lithology (USDA):	fine sand
2.	Median grain size:	205 µm
3.	Total organic matter:	0.67%
4.	Total carbonate ($CaCO_3$):	0.19%
5.	Total porosity:	measurement failed
6.	**Hydraulic conductivity (*K*):**	**measurement failed** with triaxial
7.	Remark(s):	thin silt layers (1-2 cm) and compact (cemented) iron layer

Field sample **DL35**

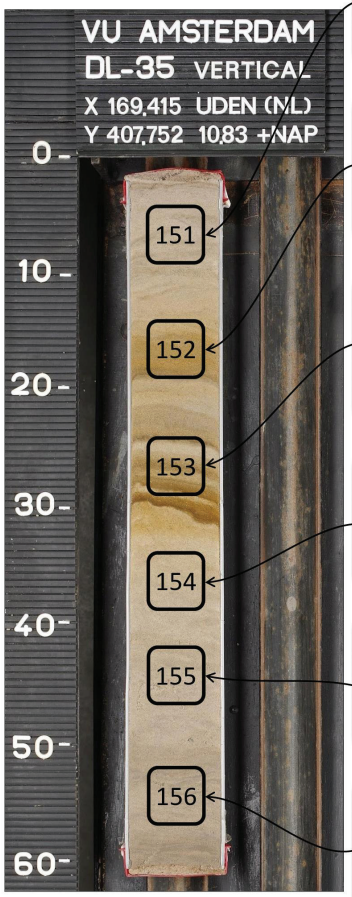

Laboratory sample **151** (4–9 cm - Appendix 1)
Attributed to trench sampling **section 4**

1.	General lithology (USDA):	fine sand
2.	Median grain size:	183 µm
3.	Total organic matter:	0.22%
4.	Total carbonate ($CaCO_3$):	0.15%
5.	Total porosity:	37.5%
6.	**Hydraulic conductivity (*K*):**	**2.0 m d^{-1} (K_h)** with permeameter
7.	Remark(s):	-

Laboratory sample **152** (14–19 cm - Appendix 1)
Attributed to trench sampling **section 3**

1.	General lithology (USDA):	fine sand
2.	Median grain size:	201 µm
3.	Total organic matter:	0.31%
4.	Total carbonate ($CaCO_3$):	0.16%
5.	Total porosity:	37.9%
6.	**Hydraulic conductivity (*K*):**	**2.3 m d^{-1} (K_h)** with permeameter
7.	Remark(s):	compact iron precipitation layer in sample

Laboratory sample **153** (24–29 cm - Appendix 1)
Attributed to trench sampling **section 3**

1.	General lithology (USDA):	fine sand
2.	Median grain size:	194 µm
3.	Total organic matter:	0.37%
4.	Total carbonate ($CaCO_3$):	0.14%
5.	Total porosity:	39.4%
6.	**Hydraulic conductivity (*K*):**	**0.2 m d^{-1} (K_v)** with permeameter
7.	Remark(s):	compact iron precipitation layer in sample

Laboratory sample **154** (34–39 cm - Appendix 1)
Attributed to trench sampling **section 4**

1.	General lithology (USDA):	fine sand
2.	Median grain size:	214 µm
3.	Total organic matter:	0.16%
4.	Total carbonate ($CaCO_3$):	0.17%
5.	Total porosity:	37.7%
6.	**Hydraulic conductivity (*K*):**	**4.3 m d^{-1} (K_h)** with permeameter
7.	Remark(s):	gravel in sample

Laboratory sample **155** (42–47 cm - Appendix 1)
Attributed to trench sampling **section 4**

1.	General lithology (USDA):	fine sand
2.	Median grain size:	198 µm
3.	Total organic matter:	0.19%
4.	Total carbonate ($CaCO_3$):	0.17%
5.	Total porosity:	37.4%
6.	**Hydraulic conductivity (*K*):**	**3.7 m d^{-1} (K_v)** with permeameter
7.	Remark(s):	gravel in sample

Laboratory sample **156** (52–57 cm - Appendix 1)
Attributed to trench sampling **section 4**

1.	General lithology (USDA):	fine sand
2.	Median grain size:	165 µm
3.	Total organic matter:	0.23%
4.	Total carbonate ($CaCO_3$):	0.22%
5.	Total porosity:	37.2%
6.	**Hydraulic conductivity (*K*):**	**2.2 m d^{-1} (K_v)** with permeameter
7.	Remark(s):	gravel in sample

https://doi.org/10.70712/NJG.v105.12686

Field sample **DL36**

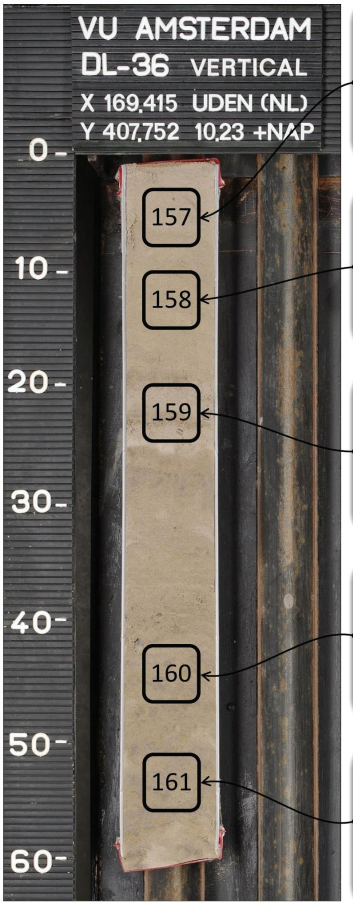

Laboratory sample **157** (3–8 cm - Appendix 1)
Attributed to trench sampling **section 4**

1. General lithology (USDA): fine sand
2. Median grain size: 165 µm
3. Total organic matter: 0.25%
4. Total carbonate ($CaCO_3$): 0.21%
5. Total porosity: 37.0%
6. **Hydraulic conductivity (*K*):** **2.4 m d^{-1} (K_h)** with permeameter
7. Remark(s): gravel in sample

Laboratory sample **158** (10–15 cm - Appendix 1)
Attributed to trench sampling **section 4**

1. General lithology (USDA): fine sand
2. Median grain size: 167 µm
3. Total organic matter: 0.25%
4. Total carbonate ($CaCO_3$): 0.21%
5. Total porosity: 36.9%
6. **Hydraulic conductivity (*K*):** **1.8 m d^{-1} (K_v)** with permeameter
7. Remark(s): gravel and thin compact layer in sample

Laboratory sample **159** (20–25 cm - Appendix 1)
Attributed to trench sampling **section 4**

1. General lithology (USDA): fine sand
2. Median grain size: 199 µm
3. Total organic matter: 0.25%
4. Total carbonate ($CaCO_3$): 0.22%
5. Total porosity: 34.0%
6. **Hydraulic conductivity (*K*):** **4.5 m d^{-1} (K_h)** with permeameter
7. Remark(s): gravel in sample

Laboratory sample **160** (42–47 cm - Appendix 1)
Attributed to trench sampling **section 4**

1. General lithology (USDA): fine sand
2. Median grain size: 146 µm
3. Total organic matter: 0.35%
4. Total carbonate ($CaCO_3$): 0.24%
5. Total porosity: 37.1%
6. **Hydraulic conductivity (*K*):** **2.7 m d^{-1} (K_h)** with permeameter
7. Remark(s): gravel in sample

Laboratory sample **161** (51–56 cm - Appendix 1)
Attributed to trench sampling **section 4**

1. General lithology (USDA): fine sand
2. Median grain size: 149 µm
3. Total organic matter: 0.34%
4. Total carbonate ($CaCO_3$): 0.22%
5. Total porosity: 36.0%
6. **Hydraulic conductivity (*K*):** **2.6 m d^{-1} (K_v)** with permeameter
7. Remark(s): -

https://doi.org/10.70712/NJG.v105.12686